arXiv:1401.6691v2 [nucl-th] 28 Jan 2014

Tensor interaction in mean-field and density functional theory approaches to nuclear structure

Hiroyuki Sagawa,[1,2] Gianluca Colò,[3,4]
[1]Center for Mathematics and Physics, University of Aizu
Aizu-Wakamatsu, Fukushima 965-8560, Japan
[2]Nishina Center, RIKEN, Wako, Japan
[3]Dipartimento di Fisica, Università degli Studi di Milano,
via Celoria 16, 20133 Milano, Italy
[4]INFN, Sezione di Milano, via Celoria 16, 20133 Milano, Italy

January 29, 2014

Abstract

The importance of the tensor force for nuclear structure has been recognized long ago. Recently, the interest for this topic has been revived by the study of the evolution of nuclear properties far from the stability line. However, in the context of the effective theories that describe medium-heavy nuclei, the role of the tensor force is still debated. This review focuses on ground-state properties like masses and deformation, on single-particle states, and on excited vibrational and rotational modes. The goal is to assess which properties, if any, can bring clear signatures of the tensor force within the mean-field or density functional theory framework. It will be concluded that, while evidences for a clear neutron-proton tensor force exist despite quantitative uncertainties, the role of the tensor force among equal particles is less well established.

1 Introduction

As discussed in all nuclear physics textbooks, the tensor force is one of the important components of the nucleon-nucleon (NN) interaction. The long-range part of this interaction is associated with the exchange of the lightest meson, namely the pion, and it has a tensor character; the one pion exchange potential (OPEP) is the most well known part of the NN interaction yet at the same time it is not strong enough to bind two nucleons, because its expectation value is of the same order of magnitude of the kinetic energy associated with the relative motion. However, the tensor force is of paramount importance for the nuclear binding since the exchange of two pions, i.e., the second order effect of the tensor force, is providing a strong central attraction in the isospin zero ($T = 0$) channel which is responsible for the deuteron binding. At the same time, the electric quadrupole moment of the deuteron is a signature of the pure tensor component. The introduction of the tensor force dates back to the early 1940s [1, 2, 3], not so long after the birth of nuclear physics (see also [4]).

All this belongs to conventional nuclear physics wisdom. More qualitative and especially quantitative understanding has been obtained later concerning the role of tensor terms in the bare NN interaction, since sophisticated interactions have been built that can explain at the same time the deuteron and

many high-precision scattering data with a χ^2/datum of the order of ≈ 1. This can be done within the traditional picture of the NN force and, to some extent, also within effective field theories (EFTs) based on the chiral symmetry and its breaking (see, e.g., [5] for recent reviews).

However, our focus is different and concerns the role of tensor terms when the interaction in the nuclear medium is considered, in particular within the framework of those models that can be applied throughout the whole periodic table like self-consistent mean-field or density functional theory (DFT) based methods [6]. There is a new blooming of studies of the possible tensor terms, in general because of the tremendous progress achieved by these theoretical methods in the last decades but also for specific reasons that we shall briefly illustrate.

A very important motivation to revive the study of the tensor force in nuclear physics is related to the new domain of exotic, unstable nuclei. Generally speaking, nuclei far from the stability valley open a new test ground for nuclear models. Recently, many experimental and theoretical efforts have been devoted to the study of the structure and the reaction mechanisms in nuclei near the drip lines. Modern radioactive ion beam facilities (RIBFs) and experimental detectors reveal several unexpected phenomena in unstable nuclei such as the existence of haloes and skins [7], the modifications of shell closures [8] and the so-called pygmy resonances in electric dipole transitions [9]. The tensor force plays a role, in particular, in the shell evolution of nuclei far from the stability line [10]. This fact has motivated thoroughly studies of the effect of the tensor force on the shell structure of both stable and unstable nuclei, with emphasis also on masses, single-particle states and sometimes on the onset of deformation.

Another context in which the tensor force is expected to be crucial are the properties of spin and spin-isospin states. Such modes of nuclear excitation, like the Gamow-Teller or spin-dipole states, are not only of interest for nuclear structure but also for nuclear astrophysics and particle physics (in connection with β and $\beta\beta$ decays, neutrino mass and its possible Majorana nature). Review papers have been devoted to this topic [11, 12]. Many of the currently employed mean-field or DFT-based methods are not well calibrated in the spin-isospin channel and/or suffer from spin and spin-isospin instabilities (i.e., spontaneous magnetization) above some critical density (see, e.g., [13] and references therein). There is obviously a strong need to improve the predictive power of the models as far as the spin-isospin states are concerned, and it must be established to which extent the tensor terms are important in this channel.

Our review is somehow timely because most of this discussion concerning the tensor force in stable and unstable nuclei, and its role for collective excitations (mainly spin and spin-isospin modes but also density modes and rotations of deformed nuclei), has already produced a considerable number of results, and yet some of the key questions are not completely solved.

One of the fundamental issues is related to whether the effective tensor force that governs shell evolution and excited states in complex nuclei keeps a close resemblance with the original bare tensor force or not. In some of the works that we shall discuss, the adopted point of view is that at least the proton-neutron tensor force is only slightly renormalized in the nuclear medium because of its long-range character; in other words, some authors believe that finite nuclei still bear signatures of the tail of the OPEP. In other cases it is assumed that the potential is actually renormalized but the bare OPEP (together with the tensor components associated with exchange of other mesons) still must be taken as guideline. Another, complementary point of view is that in the mean-field or DFT description the effective interaction does not need to bear any connection with the interaction in the vacuum. When its parameters are fitted, the effect of the bare tensor force is likely to be reabsorbed by the central force parameters because, as we recalled at the start of this Introduction, the second order effect of the tensor interaction gives rise to central terms. In this context, the search for an appropriate "remnant" of the tensor force in nuclei (or nuclear matter, or neutron stars) is mainly driven by a careful attempt to reproduce the data.

Using these arguments as a red thread throughout our paper, we will review the recent attempts to implement tensor terms and compare with experimental data. In particular, the outline of our paper is

as follows. In Sec. 2 we will discuss the formal aspects related to the tensor force, starting from a brief summary of the origin of the bare tensor force. We first discuss relativistic theories like Relativistic Mean Field (RMF) or Relativistic Hartree-Fock (RHF) based on the meson-exchange picture, and move then to nonrelativistic models by distinguishing the zero-range Skyrme interactions and the finite-range ones. In Sec. 3 we analyze the results obtained by the various groups, starting from ground-state properties and moving then to excited states. A specific section (Sec. 4) will be devoted to the role of the tensor force to drive instabilities (mainly the ferromagnetic instability we have mentioned above, but not only) in nuclear matter. Since instabilities are not present in realistic calculations one should remove them or push them to high densities, but at present the main effort is devoted to identifying these instabilities and the role of the tensor force in producing them. We will draw some conclusions in Sec. 5.

2 Bare and effective tensor forces

2.1 Discussion of the bare meson exchange potentials

One of the first experimental facts that suggested the presence of a tensor component in the NN interaction is the quadrupole moment of the deuteron. More generally, it is known that the tensor force plays an essential role to produce the binding for systems like the deuteron. As is shown schematically in Fig. 1, the tensor interaction acts on the spin triplet state ($S = 1$) of a two nucleon system. When the relative distance vector of a proton and a neutron is aligned in the direction of the two spins, the deuteron gets an extra binding energy through the action of the tensor interaction,

$$V_T = f(r)S_{12}, \tag{1}$$

since $f(r)$ is negative and $S_{12} = 3(\vec{\sigma}_1 \cdot \hat{r})(\vec{\sigma}_2 \cdot \hat{r}) - \vec{\sigma}_1 \cdot \vec{\sigma}_2 = 2$. On the other hand, if the relative distance vector of a proton and a neutron is perpendicular to the spins direction, the deuteron will loose its binding energy since $S_{12} = -1$. Thus, the deuteron assumes a deformed prolate shape and makes a bound system only when the tensor correlations are taken into account.

The main origin of tensor interactions stems from the $\pi-$nucleon coupling and the tensor part of the $\rho-$nucleon couplings: these are spin and isospin dependent. The isoscalar tensor coupling arises from the tensor $\omega-$nucleon coupling. In momentum space, the one-pion exchange reads [14]

$$V_{OPEP}(\vec{k}) = -\frac{4\pi f_\pi^2}{m_\pi^2}\vec{\tau}_1 \cdot \vec{\tau}_2 \frac{(\vec{\sigma}_1 \cdot \vec{k})(\vec{\sigma}_2 \cdot \vec{k})}{k^2 + m_\pi^2}. \tag{2}$$

Eq. (2) is decomposed into a central and a tensor part as

$$V_{OPEP}(\vec{k}) = -\frac{4\pi f_\pi^2}{3m_\pi^2}\vec{\tau}_1 \cdot \vec{\tau}_2 \left[\frac{3(\vec{\sigma}_1 \cdot \vec{k})\ (\vec{\sigma}_2 \cdot \vec{k}) - \vec{\sigma}_1 \cdot \vec{\sigma}_2 k^2}{k^2 + m_\pi^2} + \vec{\sigma}_1 \cdot \vec{\sigma}_2 \left(1 - \frac{m_\pi^2}{k^2 + m_\pi^2}\right)\right], \tag{3}$$

where the pseudo-vector $\pi-$nucleon coupling constant is f_π^2=0.08, the pion mass is m_π=138 MeV and $\vec{k}$ is the momentum transfer. The first term in the bracket of Eq. (3) is a tensor interaction and the second term is a central interaction. The momentum-indpendent part of the $\vec{\sigma}_1 \cdot \vec{\sigma}_2$ term of the central part (the term 1 in the round bracket) will become $\delta(\vec{r}_1 - \vec{r}_2)$ in the Fourier transform to the coordinate space, and can be dropped because it is overcome by the short-range NN repulsion. V_{OPEP} is transformed to the coordinate space as follows,

$$V_{OPEP}(\vec{r}) = f_\pi^2 m_\pi \vec{\tau}_1 \cdot \vec{\tau}_2 \left[\left(\frac{1}{3m_\pi r} + \frac{1}{(m_\pi r)^2} + \frac{1}{(m_\pi r)^3}\right) e^{-m_\pi r} S_{12} + \frac{1}{3}\vec{\sigma}_1 \cdot \vec{\sigma}_2 \frac{e^{-m_\pi r}}{m_\pi r}\right]. \tag{4}$$

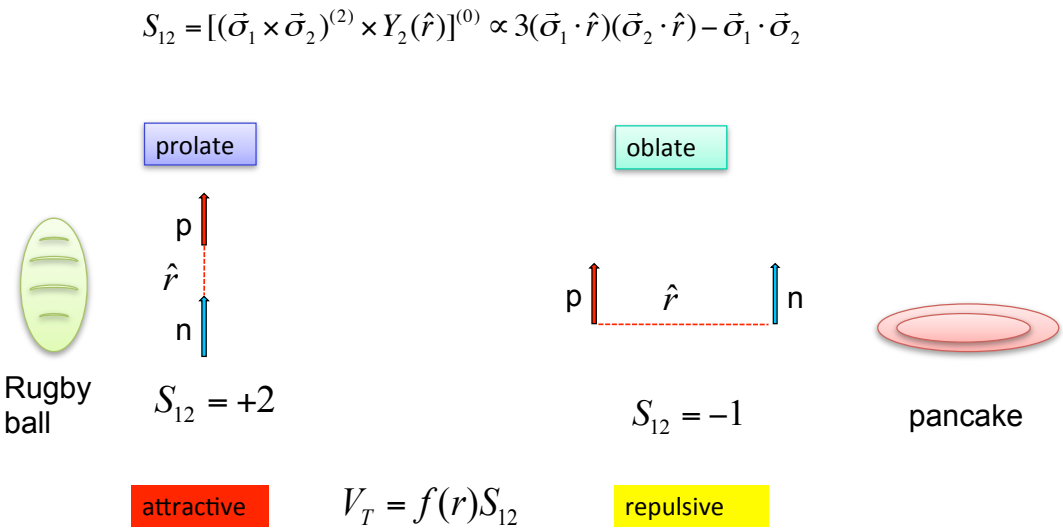

Figure 1: Schematic picture of the expectation values of the tensor operator S_{12} when the spins are either aligned with (prolate configuration) or perpendicular to (oblate configuration) the relative distance vector $\vec{r}$. The function $f(r)$ is negative, favouring a prolate shape for the deuteron [4].

The $\rho-$meson exchange potential resulting from the tensor $\rho-$nucleon coupling reads in the momentum space

$$V_\rho(\vec{k}) = -\frac{4\pi f_\rho^2}{m_\rho^2}\vec{\tau}_1\cdot\vec{\tau}_2\frac{(\vec{\sigma}_1\times\vec{k})(\vec{\sigma}_2\times\vec{k})}{k^2+m_\rho^2}. \tag{5}$$

This potential has a very similar structure to the $\pi-$exchange one,

$$V_\rho(\vec{r}) = f_\rho^2 m_\rho \vec{\tau}_1\cdot\vec{\tau}_2\left[-\left(\frac{1}{3m_\rho r}+\frac{1}{(m_\rho r)^2}+\frac{1}{(m_\rho r)^3}\right)e^{-m_\rho r}S_{12}+\frac{2}{3}\vec{\sigma}_1\cdot\vec{\sigma}_2\left(\frac{e^{-m_\rho r}}{m_\rho r}-\frac{4\pi}{m_\rho^3}\delta(\vec{r})\right)\right], \tag{6}$$

where m_ρ=770 MeV and f_ρ^2=4.86. One should notice that the tensor part of the potential has the opposite sign compared to the $\pi-$exchange one. In general, the tensor part of the $\rho-$exchange potential has a much shorter range character and gives a smaller contribution to the matrix elements than the $\pi-$ exchange one, because of the much larger ρ meson mass compared with the pion mass.

The $\omega-$tensor exchange potential is written as

$$V_\omega(\vec{k}) = -\frac{4\pi f_\omega^2}{m_\omega^2}\frac{(\vec{\sigma}_1\times\vec{k})(\vec{\sigma}_2\times\vec{k})}{k^2+m_\rho^2} \tag{7}$$

in the momentum space. This tensor potential has no isospin dependence. The $\omega-$tensor potential in the coordinate space becomes

$$V_\omega(\vec{r}) = f_\omega^2 m_\omega\left[-\left(\frac{1}{3m_\omega r}+\frac{1}{(m_\omega r)^2}+\frac{1}{(m_\omega r)^3}\right)e^{-m_\omega r}S_{12}+\frac{2}{3}\vec{\sigma}_1\cdot\vec{\sigma}_2\left(\frac{e^{-m_\omega r}}{m_\omega r}-\frac{4\pi}{m_\omega^3}\delta(\vec{r})\right)\right], \tag{8}$$

where the mass of the omega meson is $m_\omega = 783$ MeV.

2.2 Tensor interactions in relativistic Hartree-Fock model

The relativistic mean field (RMF) model was originally based on the Hartree theory and involved only the scalar-isoscalar and vector-isoscalar mesons, namely the σ and ω mesons with $(J^\pi,T) = (0^+,0)$ and $(1^-,0)$ respectively. Then the vector-isovector ρ meson with $(J^\pi,T) = (1^-,1)$ was also introduced to get reasonable agreement with the experimental systematics of masses and radii. Within the Hartree model, the π meson$-$ and $\rho-$ and $\omega-$ tensor couplings do not give any contributions in the static mean field calculations. In the 1980s, there were several attempts to extend the RMF model including the Fock term, which can accommodate the $\pi-$N coupling, as well as the ρ-tensor and also ω-tensor interactions. A. Bouyssy *et al.* [15] did the first attempt to perform relativistic Hartree-Fock (RHF) calculations. The effective Hamiltonian density in the covariant relativistic model can be obtained from the Lagrangian density $\mathcal{L}$ through the general Legendre transformation

$$H = \frac{\partial\mathcal{L}}{\partial\dot{\phi}_i}\dot{\phi}_i - \mathcal{L}, \tag{9}$$

where ϕ_i is the field operator. This leads to the general form for the effective Hamiltonian in the nucleon space:

$$H = \bar{\psi}(x_1)(-i\gamma\cdot\partial+M)\psi(x_1)+\frac{1}{2}\int d^4x_2\sum_{i=\sigma,\omega,\rho,\pi,A}\bar{\psi}(x_1)\bar{\psi}(x_2)\Gamma_i D_i(x_1,x_2)\psi(x_2)\psi(x_1), \tag{10}$$

where $\psi(x)$ is the nucleon field operator and $D_i(x_1, x_2)$ represents the corresponding meson propagators. The interaction vertices Γ_i for mesons are defined as

$$\Gamma_\sigma(1,2) = -g_\sigma(1)g_\sigma(2), \tag{11}$$

$$\Gamma_\omega(1,2) = +g_\omega(1)\gamma_\mu(1)g_\omega(2)\gamma^\mu(2), \tag{12}$$

$$\Gamma_\rho(1,2) = +g_\rho(1)\gamma_\mu(1)\vec{\tau}(1)\cdot g_\omega(2)\gamma^\mu(2)\vec{\tau}(2), \tag{13}$$

$$\Gamma_\pi(1,2) = -\left[\frac{f_\pi}{m_\pi}\vec{\tau}\gamma_5\gamma_\mu\partial^\mu\right]_1 \cdot \left[\frac{f_\pi}{m_\pi}\vec{\tau}\gamma_5\gamma_\mu\partial^\mu\right]_2 . \tag{14}$$

In the point coupling models, the meson-nucleon couplings $g_\sigma, g_\omega, g_\rho$ and f_π are taken to be constants. In the density dependent coupling model, these couplings are assumed to be a function of the baryonic density. In the RHF model of Ref. [15], the authors took the bare point coupling for the $\pi-$N vertex, and also for the $\rho-$N and $\omega-$N tensor couplings. Their coupling constants were adjusted to obtain good fits of both nuclear matter and finite nuclear properties. While the charge distributions are described well by this pioneering RHF method, nuclei were underbound due to the missing meson self-interactions. Some improvements were obtained by taking into account the non-linear $\sigma-$couplings, but the RHF model based on the point couplings was not comparable with the RMF model in the quantitative description of nuclear observables.

Twenty years after the introduction of the point-coupling RHF model, W.H. Long *et al.* [16] introduced a RHF model with density dependent couplings between mesons and nucleons. The tensor coupling due to the pion exchange, and the vector coupling associated with the $\rho-$exchange, were introduced in the effective Lagrangian. The $\pi-$ and $\rho-$ couplings in the model are the bare couplings in the free space, but they are very much quenched in the nuclear medium. The authors of Ref. [16] obtained good agreement with the experimental data for the ground state properties (masses and radii of several closed shell nuclei), at the same level or even better than the RMF models. Moreover, the description of the nuclear effective mass and of its isospin and energy dependence have been improved by the RHF model. More recently [17], it was shown that the RHF model can remove the problem of artificial shell closures at N, Z = 58 and 92 existing in some RMF calculations, by taking into account the Fock term associated with the pion and the $\rho-$tensor interactions (cf. Fig. 2). The RHF+RPA model has also been developed for the change-exchange excitations, and it has provided a good description of Gamow-Teller and spin-dipole states [23].

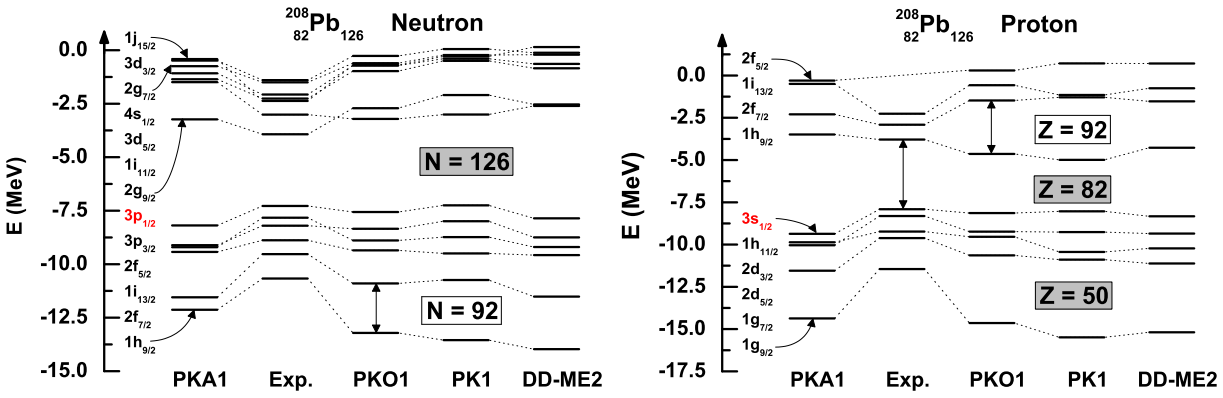

Figure 2: Single-particle energies of ^{208}Pb [18]. The calculations are performed using the RHF model with the Lagrangians PKA1 [17] and PKO1 [19], and using the RMF model with PK1 [20] and DD-ME2 [21]. The experimental data are taken from Ref. [22].

2.3 From bare tensor to Skyrme tensor

In the first paper by T.H.R. Skyrme [24], the central part of the effective interaction was introduced in a simplified form for the case of finite nuclei in the same spirit of Bruckner's self-consistent nuclear model. The simplified interaction has all the terms proportional to a zero-range $\delta-$function, but includes quadratic momentum-dependent terms that mimick a finite-range interaction. In the subsequent paper by J.S. Bell and T.H.R. Skyrme [25], the spin-orbit coupling was introduced and the resultant potential has a radial dependence of the type $\sim r^{-1}d\rho/dr$, with a reasonable magnitude required to explain the empirical spin-orbit splitting of nuclei with mass A=16±1. The tensor terms were introduced in 1959 by T.H.R. Skyrme [26] under the requirement of making a complete parametrization of zero-range, momentum-dependent effective interactions. But nothing was mentioned about the role of these tensor terms in the mean field calculations. These tensor terms have been neglected in the seminal paper by D. Vautherin and D.M. Brink [27], and also in most of the Skyrme parameter sets that have been fitted in the next 20 years.

There have been a few exceptions. In fact, the effect of the tensor interactions was first discussed for the single-particle energies in the Hartree-Fock (HF) calculations by Fl. Stancu *et al.* [28]. We will discuss their findings in Sec. 3.2. In a somewhat different context, the tensor effect on the spin-orbit splittings were discussed in the papers by J. Dudek *et al.* [29], and also by M. Ploszajczak and M.E. Faber [30]. F. Tondeur [31] included the spin-orbit densities $\vec{J}$ (see below) in his construction of the Skyrme energy density functional for HF+Bardeen-Cooper-Schrieffer (HF+BCS) calculations. He chose the value of the parameters giving the dependence of the energy density on $\vec{J}$ to fit the spin-orbit splittings of ^{16}O, ^{48}Ca and ^{208}Pb, and implicitly included the tensor effects on the spin-orbit splitting. K.-F. Liu *et al.* [32] worked out the energy-weighted and non-energy weighted sum rules of the electromagnetic transitions, Fermi transitions and Gamow-Teller transitions including the tensor interactions. However, these authors never performed any practical calculation of the sum rule values including the tensor correlations. In summary, we can say that serious attempts to clarify the role of the tensor correlations have never been performed until very recently, when such studies have been started with the aim of clarifying the shell evolutions in the exotic nuclei (cf. Sec. 3.2).

We provide now the basic formulas for the tensor force within the Skyrme framework. The Skyrme tensor interaction is the sum of the triplet-even and triplet-odd tensor zero-range tensor parts, namely

$$\begin{aligned} v_T &= \frac{T}{2}\left\{\left[(\vec{\sigma}_1\cdot k')(\vec{\sigma}_2\cdot k') - \frac{1}{3}(\vec{\sigma}_1\cdot\vec{\sigma}_2)k'^2\right]\delta(\vec{r}_1-\vec{r}_2)\right. \\ &+ \left.\delta(\vec{r}_1-\vec{r}_2)\left[(\vec{\sigma}_1\cdot k)(\vec{\sigma}_2\cdot k) - \frac{1}{3}(\vec{\sigma}_1\cdot\vec{\sigma}_2)k^2\right]\right\} \\ &+ U\left\{(\vec{\sigma}_1\cdot k')\delta(\vec{r}_1-\vec{r}_2)(\vec{\sigma}_2\cdot k) - \frac{1}{3}(\vec{\sigma}_1\cdot\vec{\sigma}_2)\left[k'\cdot\delta(\vec{r}_1-\vec{r}_2)k\right]\right\}, \end{aligned} \tag{15}$$

where the operator $k = (\overrightarrow{\nabla}_1 - \overrightarrow{\nabla}_2)/2i$ acts on the right and $k' = -(\overleftarrow{\nabla}_1 - \overleftarrow{\nabla}_2)/2i$ on the left. The coupling constants T and U denote the strength of the triplet-even and triplet-odd tensor interactions, respectively. The tensor terms (15) give contributions to the binding energy and to the spin-orbit splitting that are proportional to the spin-orbit density $\vec{J}$. In spherical nuclei only the radial component of this vector does not vanish and its expression reads [27]

$$J_q(r) = \frac{1}{4\pi r^3}\sum_i v_i^2(2j_i+1)\left[j_i(j_i+1) - l_i(l_i+1) - \frac{3}{4}\right]R_i^2(r), \tag{16}$$

where $i = n, l, j$ runs over all states and $q = 0(1)$ is the quantum number $(1-t_z)/2$ (t_z being the third isospin component) for neutrons (protons). The quantity v_i^2 is the occupation probability of each

orbit determined by the BCS approximation and $R_i(r)$ is the radial part of the HF single-particle wave function (cf. Fig. 3). In the HF-Bogolyubov (HFB) approximation, $v_i R_i(r)$ will be replaced by the lower component of the HFB wave fucntion $V_i(r)$. It should be noticed that the exchange part of the central Skyrme interaction gives the same kind of contributions to the total energy density. The central exchange and tensor contributions give extra terms to the energy density that read

$$\delta E = \frac{1}{2}\alpha(J_n^2 + J_p^2) + \beta J_n J_p. \tag{17}$$

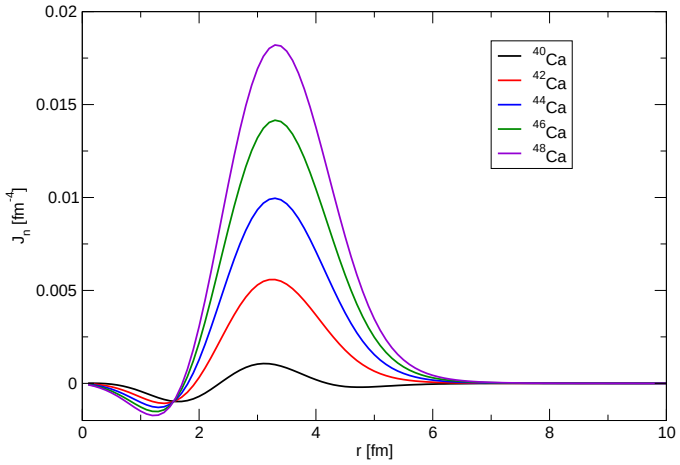

Figure 3: Neutron spin-orbit density J_n of the Ca isotopes. Since ^{40}Ca is a $\vec{l}\cdot\vec{s}$-saturated nucleus the spin-orbit density is negligible. In the heavier isotopes, the contribution of the $f_{7/2}$ orbit is making the spin-orbit density non-negligible.

.

The spin-orbit potential is expressed as

$$V_{s.o.}^{(q)}(r) = U_{s.o.}^{(q)}(r)\vec{l}\cdot\vec{s} \tag{18}$$

with

$$U_{s.o.}^{(q)}(r) = \frac{W_0}{2r}\left(2\frac{d\rho_q}{dr} + \frac{d\rho_{1-q}}{dr}\right) + \left(\alpha\frac{J_q}{r} + \beta\frac{J_{1-q}}{r}\right). \tag{19}$$

In Eq. (19), the first term on the r.h.s comes from the Skyrme spin-orbit interaction and the second term include contributions both from the exchange part of the central force and from the tensor terms, that is, $\alpha = \alpha_C + \alpha_T$ and $\beta = \beta_C + \beta_T$. The central exchange contributions are given by

$$\begin{aligned} \alpha_C &= \frac{1}{8}(t_1 - t_2) - \frac{1}{8}(t_1 x_1 + t_2 x_2), \\ \beta_C &= -\frac{1}{8}(t_1 x_1 + t_2 x_2), \end{aligned} \tag{20}$$

in terms of the parameters of the Skyrme force as defined in Refs. [26, 27, 6]. The tensor contribution are expressed as

$$\begin{aligned} \alpha_T &= \frac{5}{12}U, \\ \beta_T &= \frac{5}{24}(T + U), \end{aligned} \tag{21}$$

in terms of the triplet-even and triplet-odd terms appearing in Eq. (15).

It is useful from the very beginning to stress that, at variance with the case of the standard central Skyrme force, the notation for the tensor parameters is not unique. Other authors write the tensor force as

$$\begin{aligned} v_T &= \frac{t_e}{2}\left\{\left[3(\vec{\sigma}_1\cdot k')(\vec{\sigma}_2\cdot k') - (\vec{\sigma}_1\cdot\vec{\sigma}_2)k'^2\right]\delta(\vec{r}_1-\vec{r}_2)\right. \\ &+ \left.\delta(\vec{r}_1-\vec{r}_2)\left[3(\vec{\sigma}_1\cdot k)(\vec{\sigma}_2\cdot k) - (\vec{\sigma}_1\cdot\vec{\sigma}_2)k^2\right]\right\} \\ &+ t_o\left\{3(\vec{\sigma}_1\cdot k')\delta(\vec{r}_1-\vec{r}_2)(\vec{\sigma}_2\cdot k) - (\vec{\sigma}_1\cdot\vec{\sigma}_2)\left[k'\cdot\delta(\vec{r}_1-\vec{r}_2)k\right]\right\}, \end{aligned} \tag{22}$$

and of course the following equations hold:

$$\begin{aligned} t_e &= \frac{U}{3}, \\ t_o &= \frac{T}{3}, \\ \alpha &= \frac{5}{4}t_o, \\ \beta &= \frac{5}{8}\left(t_e + t_o\right). \end{aligned} \tag{23}$$

We will now discuss some qualitative arguments that are very important to compare tensor forces defined within the Skyrme framework and in different contexts. In general, the tensor interaction can be divided into two parts, i.e., the isospin-independent and the isospin-dependent component,

$$V_T(r) = v_T^{IS}(r)S_{12} + v_T^{IV}(r)\tau_1\cdot\tau_2 S_{12}. \tag{24}$$

We will preferably call these two components isoscalar (IS) and isovector (IV) tensor force, respectively (other authors [33] use instead the terminology "pure tensor" and "isospin tensor"). In the HF mean field of spin-saturated nuclei, the direct term of the tensor interaction does not contribute whereas the exchange term gives a finite contribution. In the spirit of the density matrix expansion theory by J.W. Negele and D. Vautherin [34], one can look at the expectation value $\frac{1}{2}\sum_{ij}\langle ij|V|ij\rangle$ of the tensor interaction of Eq. (24). The isoscalar tensor $v_T^{IS}(r)S_{12}$ gives

$$\langle v_T^{IS}(\vec{r}_1-\vec{r}_2)S_{12}\rangle = -\frac{1}{2}\int d^3r_1 d^3r_2\ v_T^{IS}(\vec{r}_1-\vec{r}_2)\left(|\vec{s}_n(\vec{r}_1,\vec{r}_2)|^2 + |\vec{s}_p(\vec{r}_1,\vec{r}_2)|^2\right), \tag{25}$$

where the spin density matrix is defined as

$$\vec{s}(\vec{r}_1,\vec{r}_2) = \sum_{i,\sigma_1,\sigma_2}\phi_i^*(\vec{r}_1,\sigma_1)\langle\sigma_1|\vec{\sigma}|\sigma_2\rangle\phi_2(\vec{r}_2,\sigma_2). \tag{26}$$

The isovector part of the tensor interaction has a different dependence on the spin density matrix, namely

$$\langle v_T^{IV}(\vec{r}_1-\vec{r}_2)\vec{\tau}_1\cdot\vec{\tau}_2 S_{12}\rangle = -\frac{1}{2}\int d^3r_1 d^3r_2\ v_T^{IV}(\vec{r}_1-\vec{r}_2)\left(|\vec{s}_n(\vec{r}_1,\vec{r}_2)|^2 + |\vec{s}_p(\vec{r}_1,\vec{r}_2)|^2 + 2|\vec{s}_n(\vec{r}_1,\vec{r}_2)\cdot\vec{s}_p(\vec{r}_1,\vec{r}_2)|\right). \tag{27}$$

Let us look at this expectation value of the isovector tensor interaction in the neutron-proton (np) channel, that is,

$$\langle v_T^{np}(\vec{r}_1-\vec{r}_2)\vec{\tau}_1\cdot\vec{\tau}_2 S_{12}\rangle = -\int d^3r_1 d^3r_2\ v_T(\vec{r}_1-\vec{r}_2)|\vec{s}_n(\vec{r}_1,\vec{r}_2)\cdot\vec{s}_p(\vec{r}_1,\vec{r}_2)|. \tag{28}$$

The spin density matrix (26) for spherical nuclei can be factorized as [34]

$$\vec{s}(\vec{r}_1, \vec{r}_2) = i(\vec{r}_1 \times \vec{r}_2)\rho_1(\vec{r}_1, \vec{r}_2) \tag{29}$$

with

$$\rho_1(\vec{r}_1, \vec{r}_2) = \pm \sum_{nlj} \frac{1}{2\pi r_1^2 r_2^2} R_{nlj}(r_1) R_{nlj}(r_2) P_l'(cos\theta). \tag{30}$$

Here $P_l'(cos\theta)$ is the derivative of the Legendre polynomials $P_l(cos\theta)$, θ is the angle between $\vec{r}_1$ and $\vec{r}_2$ and the sign $\pm$ stands for $j = l \pm 1/2$. For a short-range interaction with $\theta \sim 0$, $P_l'(cos\theta \sim 1) \sim l(l+1)/2$. Then Eq. (30) gives a factor

$$\pm\, l(l+1) = \frac{1}{2}(2j+1)[j(j+1) - l(l+1) - 3/4] \quad \text{for} \quad j = l \pm 1/2, \tag{31}$$

which is the same factor in the spin-orbit density $J_q(r)$. If the radial wave function is the same for $j = l \pm 1/2$, the contribution to $\rho_1(\vec{r}_1, \vec{r}_2)$ vanishes if both orbits $j = l \pm 1/2$ are either completely occupied or completely empty. Accordingly, the tensor interaction can be represented by means of the spin-orbit densities in the short-range limit.

Based on the above picture, D.M. Brink and Fl. Stancu [35] have examined the validity of the Skyrme-type tensor interaction ansatz. They have shown that when the finite-range tensor force acts among Hartree-Fock wave functions, its matrix elements are to a good approximation proportional to those of the zero-range momentum-dependent force (15). Both for Gaussian and one-pion exchange potentials, the proportionality constant is almost the same for nuclei in the medium-heavy mass region with different A and also when the matrix elements involve different angular momenta l. In other words, the action of the long-range tensor can be recast in the form (15) without any significant error because of the momentum dependence and of the structure of HF wave functions. Therefeore, the reader should be advised to abandon the point of view that the Skyrme tensor force is truly zero-range.

Moreover, it is interesting to notice from Eqs. (25) and (27) that the IS tensor, if rewritten in the zero-range limit in terms of the spin-orbit densities, gives only a contribution to the total energy [cf. Eq (17)] proportional to α but no contribution proportional to β. On the other hand, the IV tensor gives two contributions such that $\beta = 2\alpha$ (cf. also [35]).

The necessity of having both IS and IV tensor terms can be seen through a comparison with bare tensor forces. The Skyrme-type tensor interaction (15) is essentially based on the short-range nature of the nuclear force. The one-pion exchange tensor interaction can be written as

$$V_T(r) = v_T(r)\vec{\tau}_1 \cdot \vec{\tau}_2[\frac{3}{r^2}(\vec{\sigma}_1 \cdot \vec{r})(\vec{\sigma}_2 \cdot \vec{r}) - \vec{\sigma}_1 \cdot \vec{\sigma}_2] \tag{32}$$

as was derived in Eq. (4). This one-pion exchange tensor interaction is attractive. The ρ-meson exchange potential gives also rise to a tensor interaction as was shown in Eq. (6). Its range is much shorter than the pion-exchange one and the sign is positive (i.e., repulsive). This is due to the nature of the ρ-meson which is characterized by a pseudo-vector coupling and a mass which is about 6 times heavier than the pion mass. The tensor force due to the ρ-meson exchange tends to cancel that of the pion exchange. However, the net result is expected to be attractive. Thus, the tensor force is expected to give an attractive interaction in the np channel [that is, a positive value of β in keeping with the minus sign of Eq. (28)] in the deuteron-like configuration. As recalled above, the IS potential is instead coming from $\omega-$meson exchange.

In the mean-field and density functional theory (DFT) approaches, the tensor force is introduced as a phenomenological one in the framework of a Slater determinant description of the many-body system. There are, however, alternative approaches adopting a bare tensor force. In the unitary correlation

operator (UCOM) approaches in Refs. [36], a careful attempt has been undertaken to study how tensor correlations evolve as the model space employed for the calculations is changed. In this study, it was pointed out that strong bare tensor correlations become much weaker in the transformed potential which should be used in a smaller model space such as shell model or HF, when the high momentum components of the tensor force are taken into account in the correlated wave functions. Another interesting approach is the one introduced by T. Myo and co-workers [37], in which the tensor force is considered in the framework of a charge- and parity-breaking shell model approach. This approach allows a strong mixing of odd and even parity states by the tensor correlations and nuclear states are eventually obtained by the projection techniques. We shall not discuss further these approaches that can not be easily related with the present mean field or DFT approaches.

2.4 Skyrme force and Skyrme energy functional

In this subsection we discuss an important aspect related to the introduction of the tensor force in the Skyrme framework. Let us assume that we start from the standard expression of the central Skyrme force. This expression does not include any tensor term: however, as discussed above, the central exchange terms generate in the energy functional some terms that look the same as those generated through a tensor force, although the coefficients are fixed [α_C and β_C, cf. Eqs. (20)]. When tensor terms are introduced, they give the same kind of contribution to the energy functional, so that α_T and β_T are summed, respectively, to α_C and β_C [cf. Eq. (21)]. In short, we can say that the central and tensor terms are not decoupled at all in the Skyrme framework. Moreover, there have been attempts in the last decade to go beyond the picture of the Skyrme *force* and fit directly a Skyrme *functional*. When this is done, at least in the spherical nuclei, there is no way of discussing separately the tensor and central exchange terms. Therefore, when we discuss the Skyrme results in the following of our paper, we will try to distinguish carefully the two cases (either force or functional) because the way in which the parameters are defined and affect the results is different. We shall refer to self-consistent mean-field (SCMF) calculations in the case in which an effective force, that is, an Hamiltonian picture, is assumed as a starting point, and we shall refer instead to density functional theory (DFT) in the case in which the functional is taken as a starting point. In the following of the subsection we shall define the quantities related to the energy density functional (EDF) picture and we shall discuss the difference between spherical and deformed case.

The Skyrme energy functional is discussed at length in many papers (see, e.g., Ref. [6]). It is the prototype of any conceivable local energy functional (*viz.*, a functional of local densities only). To define local densities, we start from the (non-local) density matrix

$$\rho_q(\vec{r}\sigma,\vec{r}'\sigma') \equiv \langle\Phi|\psi_q^\dagger(\vec{r}'\sigma')\psi_q(\vec{r},\sigma)|\Phi\rangle = \sum_i \phi_{i,q}^*(\vec{r}'\sigma')\phi_{i,q}(\vec{r},\sigma), \tag{33}$$

where $|\Phi\rangle$ is the Slater determinant made up with the single-particle wave functions $\phi_{i,q}$ labelled by a set of quantum numbers i. From this density matrix we can extract the scalar density matrix and the spin density matrix as

$$\rho_q(\vec{r}\sigma,\vec{r}'\sigma') = \frac{1}{2}\rho_q(\vec{r},\vec{r}')\delta_{\sigma\sigma'} + \frac{1}{2}\vec{s}_q(\vec{r},\vec{r}')\langle\sigma'|\vec{\sigma}|\sigma\rangle. \tag{34}$$

In turn, from these non-local densities we extract the local quantities

$$\begin{aligned}
\rho_q(\vec{r}) &= \rho_q(\vec{r},\vec{r}')|_{\vec{r}=\vec{r}'}, \\
\tau_q(\vec{r}) &= \vec{\nabla}\cdot\vec{\nabla}'\rho_q(\vec{r},\vec{r}')|_{\vec{r}=\vec{r}'}, \\
J_{q,\mu\nu}(\vec{r}) &= -\frac{i}{2}\left(\nabla_\mu - \nabla'_\mu\right) s_{q,\nu}(\vec{r},\vec{r}')|_{\vec{r}=\vec{r}'},
\end{aligned} \tag{35}$$

that are called, respectively, density, kinetic energy density and spin-current density. These densities are enough if we restrict ourselves to the time-even part of the energy functional. If one is concerned also with the time-odd part of the energy functional, then the following densities need to be considered:

$$\begin{aligned}
\vec{j}_q(\vec{r}) &= \frac{1}{2i}\left(\vec{\nabla}-\vec{\nabla}'\right)\rho_q(\vec{r},\vec{r}')|_{\vec{r}=\vec{r}'}, \\
\vec{s}_q(\vec{r}) &= \vec{s}_q(\vec{r},\vec{r}')|_{\vec{r}=\vec{r}'}, \\
\vec{T}_q(\vec{r}) &= \nabla\cdot\nabla'\vec{s}_q(\vec{r},\vec{r}')|_{\vec{r}=\vec{r}'}, \\
F_{\mu,q}(\vec{r}) &= \frac{1}{2}\sum_\nu\left(\nabla_\mu\nabla'_\nu+\nabla'_\mu\nabla_\nu\right)s_{q,\nu}(\vec{r},\vec{r}')|_{\vec{r}=\vec{r}'}.
\end{aligned} \tag{36}$$

These quantities are called, respectively, current density, spin density, spin-kinetic density and tensor-kinetic density. All these proton/neutron densities can be re-expressed in terms of isoscalar ($t=0$) and isovector ($t=1$) densities in the standard way. We drop the label q in what follows, since the same formulas hold for the $t=0,1$ components as well.

We can decompose the (pseudo-tensor) spin-current density that appears in (35) into

$$J_{\mu\nu}(\vec{r}) = \frac{1}{3}\delta_{\mu\nu}J^{(0)}(\vec{r}) + \frac{1}{2}\sum_\kappa \epsilon_{\mu\nu\kappa}J^{(1)}_\kappa(\vec{r}) + J^{(2)}_{\mu\nu}(\vec{r}), \tag{37}$$

where the three terms are pseudo-scalar, vector and pseudo-tensor, and read

$$\begin{aligned}
J^{(0)}(\vec{r}) &= \sum_\mu J_{\mu\mu}(\vec{r}), \\
J^{(1)}_\kappa(\vec{r}) &= \sum_{\mu\nu}\epsilon_{\kappa\mu\nu}J_{\mu\nu}(\vec{r}), \\
J^{(2)}_{\mu\nu}(\vec{r}) &= \frac{1}{2}\left[J_{\mu\nu}(\vec{r})+J_{\nu\mu}(\vec{r})\right] - \frac{1}{3}\delta_{\mu\nu}\sum_\kappa J_{\kappa\kappa}(\vec{r}).
\end{aligned} \tag{38}$$

The time-even part of the energy density functional that is obtained when a tensor force of the type (15) is introduced is

$$\mathcal{E}_{\rm tensor} = \sum_{t=0,1}\mathcal{E}_t, \tag{39}$$

where

$$\begin{aligned}
\mathcal{E}_t = \; & -C^T_t \sum_{\mu\nu} J_{t,\mu\nu}J_{t,\mu\nu} \\
& -C^F_t \left[\frac{1}{2}\left(\sum_\mu J_{t,\mu\mu}\right)^2 + \frac{1}{2}\sum_{\mu\nu}J_{t,\mu\nu}J_{t,\mu\nu}\right].
\end{aligned} \tag{40}$$

We follow here the notation of [38, 39]. The notation T and F will become more transparent by looking at Eq. (45) below. To deal with the spherical limit more clearly, we can transform Eq. (40) into

$$\mathcal{E}_t = C^{(J0)}_t\left(J^{(0)}_t\right)^2 + C^{(J1)}_t\vec{J}^2_t + C^{(J2)}_t\sum_{\mu\nu}J^{(2)}_{t,\mu\nu}J^{(2)}_{t,\mu\nu}. \tag{41}$$

As above, the coefficients C are actually sums of terms coming from the exchange part of the central Skyrme force and terms associated with the tensor force. In fact,

$$C^T_t = A^T_t + B^T_t,$$

$$
\begin{aligned}
C_t^F &= A_t^F + B_f^T, \\
A_0^T &= -\frac{1}{8}t_1\left(\frac{1}{2}-x_1\right)+\frac{1}{8}t_2\left(\frac{1}{2}+x_2\right), \\
A_1^T &= -\frac{1}{16}t_1+\frac{1}{16}t_2, \\
A_0^F &= 0, \\
A_1^F &= 0, \\
B_0^T &= \frac{1}{8}\left(t_e+3t_o\right), \\
B_1^T &= \frac{1}{8}\left(t_e-t_o\right), \\
B_0^F &= \frac{3}{8}\left(t_e+3t_o\right), \\
B_1^F &= \frac{3}{8}\left(t_e-t_o\right),
\end{aligned} \tag{42}
$$

and the following relations hold

$$
\begin{aligned}
C_t^{(J0)} &= -\frac{1}{3}C_t^T-\frac{2}{3}C_t^F, \\
C_t^{(J1)} &= -\frac{1}{2}C_t^T+\frac{1}{4}C_t^F, \\
C_t^{(J2)} &= -C_t^T-\frac{1}{2}C_t^F.
\end{aligned} \tag{43}
$$

From Eq. (41), one can deduce that in the EDF picture one could introduce in principle six independent coupling constants. However, even in the deformed case, the pseudo-scalar density is zero if the parity is conserved and then only four independent coupling constants can be introduced in this case for deformed nuclei. These reduce to two in the spherical case as discussed above. The four constants $C^{(J1)}$ and $C^{(J2)}$ are non-zero in the static calculations of deformed nuclei and they reduce to the two constants $C^{(J1)}$ in static calculations of spherical nuclei. As we did at the start of the subsection, we stress once more the difference between the Hamiltonian and EDF schemes: if the starting point is the Skyrme Hamiltonian with tensor-even and tensor-odd terms, the independent constants are in any case only two. If the energy functional strategy is enforced, the independent constants can be more. The same holds in case of non-static, e.g. RPA calculations. If one starts from the Hamiltonian, automatically one sticks to two independent constants.

We now briefly discuss what happens when time-odd terms have to be taken into account. We remind that our discussion takes care of Galilean invariance, which is needed since the results ought not to depend on the reference frame, and that time-odd terms are to be included in odd (or odd-odd) nuclei as well as in dynamical calculations of even-even ones. Following Ref. [39], the terms generated by the inclusion of tensor terms in the Skyrme force in both the time-even and time-odd sectors of the EDF are

$$
\mathcal{E}_{\rm tensor} = \sum_{t=0,1}\mathcal{E}_t, \tag{44}
$$

where

$$
\begin{aligned}
\mathcal{E}_t &= B_t^T\left(\vec{s}_t\cdot\vec{T}_t-\sum_{\mu\nu}J_{t,\mu\nu}J_{t,\mu\nu}\right) \\
&+ B_t^{\Delta s}\vec{s}_t\cdot\nabla\vec{s}_t+C_t^{\nabla s}\left(\vec{\nabla}\cdot\vec{s}_t\right)^2
\end{aligned}
$$

$$+ \quad C_t^F \left[\vec{s}_t \cdot \vec{F}_t - \frac{1}{2} \left(\sum_\mu J_{t,\mu\mu} \right)^2 - \frac{1}{2} \sum_{\mu\nu} J_{t,\mu\nu} J_{t,\mu\nu} \right] . \tag{45}$$

The new constants that appear in this expression are

$$\begin{aligned}
C_0^{\nabla s} &= A_0^{\nabla s} + B_0^{\nabla s}, \\
C_1^{\nabla s} &= A_1^{\nabla s} + B_1^{\nabla s}, \\
A_0^{\nabla s} &= 0, \\
A_1^{\nabla s} &= 0, \\
B_0^{\nabla s} &= \frac{9}{8} (t_e - t_o) , \\
B_1^{\nabla s} &= -\frac{3}{8} (3t_e + t_o) , \\
C_0^{\Delta s} &= A_0^{\Delta s} + B_0^{\Delta s}, \\
C_1^{\Delta s} &= A_1^{\nabla s} + B_1^{\Delta s}, \\
A_0^{\Delta s} &= \frac{3}{192} (3t_1 - 6t_1 x_1 + t_2 + 2t_2 x_2) , \\
A_1^{\Delta s} &= \frac{3}{192} (3t_1 + t_2) , \\
B_0^{\Delta s} &= \frac{3}{32} (t_e - t_o) , \\
B_1^{\Delta s} &= \frac{1}{27} (3t_e - t_o) .
\end{aligned} \tag{46}$$

We refer to [40] for these and other general formulas related to the Skyrme energy functional.

2.5 Gogny plus tensor

The standard calculations performed using the finite-range Gogny force, starting from the paper by J. Dechargè and D. Gogny [41], do not include any tensor term. It should be mentioned that most of these calculations are performed in the harmonic oscillator basis, and the formulas to calculate the matrix elements of central, two-body spin-orbit but also tensor forces on that basis can be actually found in the earlier paper by D. Gogny [42]. Despite this, early attempts to complement the Gogny force with tensor terms are scarce. In Ref. [43], one-pion and one-rho tensor terms have been added pertubatively to the D1 Gogny set. Unfortunately, this study is only devoted to some hypothetic states in N=Z nuclei where a non-zero expectation value of $\langle \sigma\sigma\tau\tau \rangle$ might show up. The authors are interested in finding a sort of ferromagnetic structure (called "spin-isospin lattice") in which proton spins are aligned along one direction and neutron spins are aligned in opposite direction, at variance with the normal shell model configurations. This study, focused on low-lying states in ^{32}S, remains to some extent speculative. More or less at the same time, another type of finite-range (Gaussian) force that includes tensor terms has been introduced in Ref. [44]. The strengths of these terms have been determined through a fitting procedure, but the results are very sensitive to the choice of the observables that enter the fit (that can be either bulk nuclear properties, single-particle states or shell-model p-h matrix elements). Surprisingly, in most of the cases the tensor strength seems to be dominated by the isoscalar term at variance with almost all the tensor parametrizations. No clear conclusion can be extracted from these studies.

However, these early attempts suggest that a tensor force of the type (1), namely

$$V_T(r) = f_G(r) S_{12} \tag{47}$$

with a Gaussian form factor f_G, would fit appropriately the Gogny ansatz. Such kind of force has been introduced only much later in Ref. [45]. Following the spirit of Ref. [10], the tensor term added to the Gogny force is written

$$V_T(r) = f_G(r) S_{12}\ \vec{\tau}_1 \cdot \vec{\tau}_2, \tag{48}$$

(and, for practical reasons, turned into $V_T(r) = g_G(r) \left[[\vec{r} \otimes \vec{r}]^{(2)} \otimes [\vec{\sigma}_1 \otimes \vec{\sigma}_2]^{(2)} \right]^{(0)}$ by using standard recoupling). This Gaussian function has the largest among the ranges associated with the Gogny terms, namely 1.2 fm (in agreement with the long-range nature of the pion exchange). The strength is adjusted so that the volume integral is the same as that of AV8' [46]. The other (central and spin-orbit terms) of the new force introduced in [45] are the same as in D1S [47] but their strengths have been refitted and the new force is called GT2. This force has been constructed with the goal of including the specific attraction between protons and neutrons respectively in the $j_<$ and $j_>$ (or $j_>$ and $j_>$) orbits, that we will discuss in detail in 3.2 below. However, GT2 has not been systematically applied to many other nuclear properties later.

There have been many applications of Gogny plus tensor performed by the groups of Granada and Lecce, as we shall discuss below. However, they have at times employed hybrid approaches. A tensor force derived by the Argonne V18 potential and multiplied by a correlation function that includes short-range effects [48],

$$v_{\rm T}(r) = v_{6,\rm AV18}(r) \left(1 - e^{-br^2}\right), \tag{49}$$

where $v_{6,\rm AV18}(r)$ is the radial function of the Argonne potential, has been introduced in [49]. We show in Fig. 4 the Fourier tranform of the bare tensor component of the Argonne potential and of the IV tensor force introduced in Ref. [49]. Although there is a clear resemblance between the effective and bare tensor forces, the quenching is not negligible.

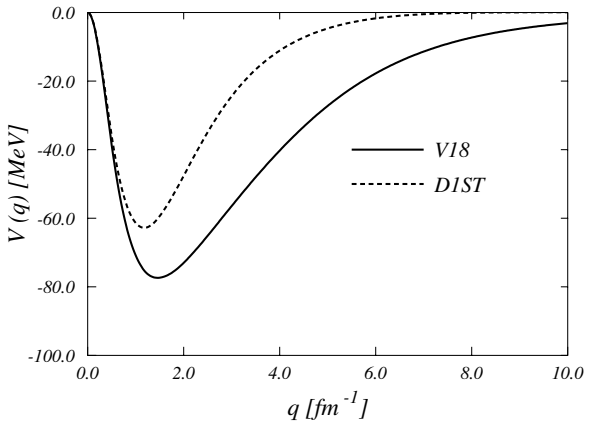

Figure 4: Tensor component of the Argonne potential and screening due to short-range correlations. [49, 50]

We end this Section by mentioning another class of finite-range tensor forces. In the papers by H. Nakada [51, 52, 53], semi-realistic interactions derived from the original M3Y interaction [54] have been introduced. By adding a density-dependent term to the M3Y ansatz, saturation of uniform matter can be achieved and HF calculations in finite nuclei can be performed with reasonable success. The parameters have been refitted at different levels of approximation, and the resulting sets are named M3Y-Pn. They include tensor terms (although not big effort is done to single out the specific effect of these terms). Starting from the set M3Y-P2 [51], these sets take care of the experimental systematics

of single-particle states: in fact, the quenching factor of the tensor force with respect to the original M3Y interaction is obtained by considering the ordering of states in ^{208}Pb.

3 Results

3.1 Masses

The question whether the tensor terms can improve the agreement of theoretical binding energies with experiment has been analyzed mainly within the Skyrme framework. It should be said that some accurately calibrated Skyrme functionals have achieved great success in reproducing experimental masses, yet with a few *ad hoc* additional parameters associated with correlations. When the term δE of Eq. (17) coming from the tensor force is added to the binding energy, the effect is not huge. For instance, in ^{208}Pb, when the tensor force SLy5$_{\rm T}$ introduced in Ref. [55] is employed the total binding energy is changed only by about 0.5%. However, recently there has been ample discussion whether a fine agreement with the experimental masses can be reached at the level of less than $\approx$ 1 MeV, or several hundreds of keV. In this respect, the tensor terms of the force can play a role.

In particular, it can be seen from Fig. 3 that the spin-orbit densities J have a specific isotope dependence: they are negligible in $\vec{l}\cdot\vec{s}$ saturated nuclei, i.e., in the magic nuclei of the light or medium mass region (like in ^{40}Ca), whereas they are large in the middle of the shell where $j_>$ orbits are filled and $j_<$ orbits are empty (like in ^{48}Ca). The associated binding energy δE of Eq. (17),

$$\delta E = \frac{1}{2}\alpha(J_n^2 + J_p^2) + \beta J_n J_p,$$

is also likely to display "arches", namely to be minimal for magic nuclei and maximal in the middle of the shell. This argument has been raised first in Ref. [56] (cf. also Fig. 4 of that work), where also the hope was expressed that these arches can remedy some open theoretical problem in the reproduction of experimental masses by theoretical models. In fact, it is known that when a functional is designed with the goal of reproducing accurately the binding energies, often double-magic nuclei turn out to be underbound (see, e.g., the review paper [57]). It should be added, though, that this deficiency is more often ascribed either (i) to the fact that a large-scale fit of any functional is dominated by open-shell nuclei, and pairing gives a strong bias to the results of the fit so that the errors are larger when pairing is absent, or (ii) to the fact that correlation energies are systematically different in open-shell and closed-shell nuclei.

The conclusion of the systematic study of Ref. [58], about the possible improvement of the agreement with the data when tensor is included in a Skyrme functional, is rather on the negative side. As is well known, masses and charge radii are among the quantities that are fitted in the protocol to determine a Skyrme functional. In the fit of Ref. [58], the value of χ^2 is minimum when β is equal to zero, so that masses and charge radii seem to discard the proton-neutron tensor force to some extent. This is at variance with the conclusion obtained from the study of single-particle states (cf. Sec. 3.2 below) and, more generally, with the overall conclusions of many works and of the current review. Within the specific ansatz made in [58], the analysis of the difference between theoretical and experimental binding energies would suggest that the best parameter sets for the binding energies give unrealistic single-particle spectra. Even the analysis of the charge radii brings in some contradiction: for instance, the difference between the charge radii of ^{40}Ca and ^{48}Ca is controlled by the position of proton 1d$_{3/2}$ level, and the parameter sets that would fit the radii at best make the overall single-particle spectra worse. In conclusion, there seems to be little room to accommodate within the chosen framework an overall agreement between theory and experiment at the same time for single-particle states, binding energies and radii.

Interestingly, the same conclusion can be drawn within the framework of relativistic functionals. The authors of Ref. [59] have started from conventional RMF and extended it by including pion coupling in the RHF framework. They also point out that the pion tensor is important for single-particle states but the fit of masses would instead "prefer" not to have the pion-coupling included.

It would be interesting to compare these conclusions with analogous ones coming from extensive studies performed with finite-range nonrelativistic interactions like the Gogny force. We do not dispose yet of such studies in which we can compare e.g. the results of D1M (the Gogny set which is the best suited for masses [60]), and an analogous study by including the tensor. As we have discussed in Sec. 2.5, another type of finite-range force has been introduced by H. Nakada [51, 52]. In the case of his M3Y-P* forces, the results for binding energies of specific nuclei do not seem to deteriorate if the tensor force is included. At this stage, we may conclude that the deterioration of the results for masses when some realistic tensor terms are included seems to be (only) the outcome of large scale fits.

3.2 Single-particle states

3.2.1 Early attempts and general considerations

Even before the advent of modern self-consistent calculations, there have been pioneering attempts to relate the behaviour of the spin-orbit splittings, in both $\vec{l}\cdot\vec{s}$ saturated and unsaturated nuclei, to some kind of effective tensor force (cf., e.g., [61, 62, 63]). The mass dependence of the l=5 spin-orbit splitting has been explained, within the HF-BCS framework, in terms of the tensor force in Ref. [64]. The main difference between non self-consistent calculations, and self-consistent Hartree or Hartree-Fock ones, is that in the latter case the tensor terms affect directly the spin-orbit splittings but affect indirectly other features of the spectrum as well.

Within the Skyrme-HF framework, the role of the tensor interactions was firstly discussed in Ref. [28]. In this work, the authors added tensor terms on top of the SIII parameter set [65]. They favored values of α and β in the "triangle" defined by -80 MeV·fm^5 $< \beta < 0$, $0 < \alpha <$ 80 MeV·fm^5, and $|\alpha| < |\beta|$. Thus, they have been the first to note that the signs of β and α agree and disagree, respectively, with what extracted from G-matrix calculations. However, their conclusion was based on the analysis of few examples of spin-orbit splittings. It did not focus on the trend of spin-orbit splittings with the mass number which, as discussed in Sec. 2.3, is the main effect of tensor terms. Also the conclusion of Ref. [28] did not point to a clear improvement in the comparison of theory and experiment after the inclusion of the tensor force. Therefore, such kind of research has been for some time abandoned. There were some exceptions [31, 32] that have been mentioned in Sec. 2.3, but still we can state that the tensor force was essentially dropped in most Skyrme parameter sets which have been used widely in nuclear structure calculations in the 1980s and 1990s. Serious and systematic attempts to assess the impact of the tensor force on single-particle states have been performed only in the last decade [56, 66, 55, 35, 58, 67].

This interest for the tensor force has been revived indeed by the paper by T. Otsuka and collaborators [10] (cf. also Ref. [68]). In this work, a specific and strong effect induced by the proton-neutron tensor force on the evolution of the single-particle states as a function of the neutron excess has been pointed out. If a proton and a neutron lie in spin-orbit partner orbitals, $j_<$ and $j_>$ respectively, the $S = 1$ component of the relative motion (the only one sensitive to the tensor force) corresponds in a semiclassical picture to orbits having opposite direction and large relative momenta; consequently, the wave function is spatially confined and in this deuteron-like configuration the tensor force is known to give attraction (cf. Fig. 1 in this review and Fig. 5.1 of Ref. [4] in case of the deuteron). The complementary case is that in which both particles are in either ($j_<$, $j_<$) or in ($j_>$, $j_>$) configuration. Here, the orbits have aligned orbital angular momenta, small relative momentum, and spread wave function on which the tensor force give a repulsive effect. These attractive or repulsive effects have been

shown to be relevant when looking at the evolution of s.p. states as a function of the neutron number, going far from stability.

This effect can be easily rephrased in the EDF language. So, before going to the discussion of the detailed studies performed so far in this domain, let us illustrate how the tensor (and the central exchange) produce the attractive and repulsive effects that have been just discussed. To this aim, we analyze their contributions to the Eq. (19) for the spin-orbit splitting. The first important point concerns the mass number dependence of the the first and second terms in Eq. (19). The Skyrme spin-orbit force proportional to W_0 gives rise to the first term of Eq. (19), that is, to a spin-orbit splitting which is proportional to the derivatives of the densities, whose mass number dependence is very moderate in heavy nuclei. We should nonetheless notice that this first term is negative because W_0 is positive and the derivatives $\frac{d\rho}{dr}$ are negative functions. On the other hand, the second term in Eq. (19) depends on the spin density J_q. This quantity is negligible for $\vec{l}\cdot\vec{s}$-saturated nuclei. Particles that occupy the $j_>$ orbit give a positive contribution to J_q, while particles that occupy the $j_<$ orbit give a negative contribution to J_q. Thus, if β is positive and the $j_>$ orbit for q is occupied, the second term of Eq. (19) is opposite to the first term and the spin-orbit splitting for $1-q$ is reduced; in other words, the occupation of the $j_>$ orbit for q pushes the $j_>$ orbit for $1-q$ up and brings the $j_<$ orbit for $1-q$ down, exactly along the line of the previous discussion. The occupation of the $j_<$ orbit for q changes the sign of J_q, and therefore enlarges the spin-orbit splitting for $1-q$; this pushes the $j_<$ orbit for $1-q$ up and brings the $j_>$ orbit for $1-q$ down, again following the same pattern. In conclusion a positive β corresponds to the findings of Ref. [10].

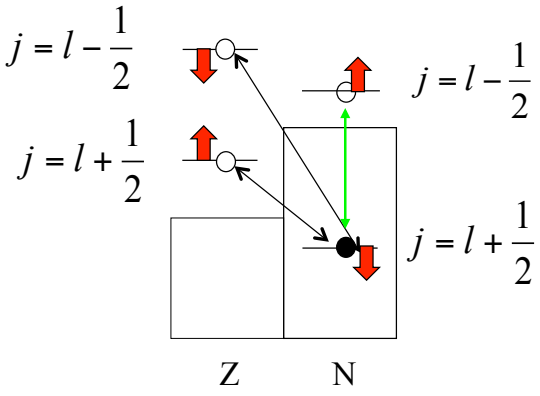

Figure 5: Effect of a neutron in the $j_>$ orbit on the proton and neutron spin-orbit splittings, in the case in which β is positive and α is negative. See the text for the corresponding discussion.

A positive (negative) value of α would produce the same (opposite) result on the orbits for q when J_q is varied. This is illustrated in Fig. 5, in which we consider a nucleus where the last occupied orbit is a neutron $j_>$ orbit (like, for instance, ^{90}Zr or ^{48}Ca). A negative value for α (which may be preferable according to [28] and to our discussion below, albeit with many warnings) increases the spin-orbit splitting for neutrons because of the positive contribution to $J_{q=0}$ from the $j_>$ orbit, whereas a positive value for β decreases the spin-orbit splitting for protons.

A first evidence for a positive value of β in modern Skyrme functional calculations was obtained in Ref. [56]. In this work, the study of single-particle states has been motivated by experiments in neutron-rich Ti isotopes [69, 70], that indicate a sort of sub-shell closure at N=32 although in an indirect way, that is, through the increase in energy and decrease in the electromagnetic transition probability of the 2^+ state in ^{54}Ti (similar to that observed in ^{50}Ti and associated with the N=28 sub-shell closure). It has been found that in the N=32 isotones the proton-neutron tensor force does not produce any effect on neutron levels at Z=20 (^{52}Ca) due to the $\vec{l}\cdot\vec{s}$ saturation and the vanishing of J_p. Then, as the proton $f_{7/2}$ orbital is filled, for positive values of β, the spin-orbit splittings of f and p orbit is reduced. For Z=22 the p orbit splitting is still large enough so that the N=32 sub-shell closure is visible, but this is not the case when increasing Z so that, e.g., in ^{60}Ni this sub-shell closure is gone.

The parameter α, namely the tensor force between equal particles, has not been considered in Refs. [10, 56]. This term comes purely from the triplet-odd tensor interaction [cf. Eq. (21)]. B.A. Brown and collaborators [66] have been the first to study how to complement a Skyrme type force with both isoscalar and isovector tensor terms. Their study is based on the Skyrme set SkX [71] and focused on single-particle states in ^{132}Sn and ^{114}Sn. Their starting point is a G-matrix tensor force [72]. If the strengths of the tensor terms added to SkX are calibrated on the G-matrix results, values of α_T = 60 MeV·fm^5 and β_T = 110 MeV·fm^5 are obtained. The force obtained by re-fitting the central and spin-orbit Skyrme parameters, named SkXa, is not very satisfactory. A re-fitting of the isoscalar tensor term, together with the central and spin-orbit parameters, leads to α_T = -118 MeV·fm^5 (the set is named SkXb). Their conclusion is that, because of the Skyrme ansatz and the resulting form of the one-body potential, there is a tendency for a good fit to lead to $\alpha_T \approx -\beta_T$. This conclusion is not based, however, on a very systematic study including different mass ragions and deformed nuclei.

In subsequent works, it has been shown that the inclusion of tensor terms in the Skyrme HF calculations (with positive values of β_T and negative values of α_T) can bring considerable success in explaining some features of the evolution of single-particle states along isotopic or isotonic chains [55, 35, 67]. The tensor terms were added perturbatively in Refs. [55, 67] and [35] to the existing standard parameterizations SLy5 [73] and SIII [65], respectively.

3.2.2 The Sn isotopes and the N=50 isotones

One of the main experimental benchmark for these kinds of studies is provided by the data on single-particle states in $N = 82$ isotones and $Z = 50$ isotopes [74]. In Ref. [55], the optimal parameters α_T and β_T are determined to be (α_T, β_T) = (-170,100) MeV·fm^5. The qualitative reasons why these values provide a quite reasonable fit to the experimental results can be understood by applying the arguments discussed in this subsection. In Fig. 6, the energy differences for the proton single-particle states $\Delta e(h_{11/2} - g_{7/2})$ in the Z=50 isotopes are shown as a function of the neutron excess N-Z. The original SLy5 interaction fails to reproduce the experimental trend qualitatively and quantitatively. Firstly, the energy differences of the HF results are much larger than the empirical data. Secondly, the experimental data decrease as the neutron excess decreases and reach about 0.5 MeV at the minimum value. On the other hand, the energy differences obtained with the original SLy5 force increase as the neutron excess decreases and attain the maximum at around N-Z=20 (several other Skyrme parameter sets show almost the same trends as those of SLy5). Then, when the tensor force is included, the results marked by open circles in Fig. 6 are obtained and the substantial improvement is clear. The force SLy5 plus tensor force parameters (α_T, β_T) = (-170,100) MeV·fm^5 will be denoted by SLy5$_\mathrm{T}$ in what follows.

The results can be qualitatively understood by the above general arguments. Firstly, introducing α changes the strength of the proton spin-orbit potential. In the Z=50 core, only the proton $g_{9/2}$ orbit gives a significant positive contribution to the spin density J_p in Eq. (16): consequently, with a negative α_T value the spin-orbit splittings are increased, in particular those associated with the $g_{9/2}$-$g_{7/2}$ orbits and $h_{13/2}$-$h_{11/2}$ orbits. As a net effect, the proton energy difference $\Delta e(h_{11/2} - g_{7/2})$ decreases substantially.

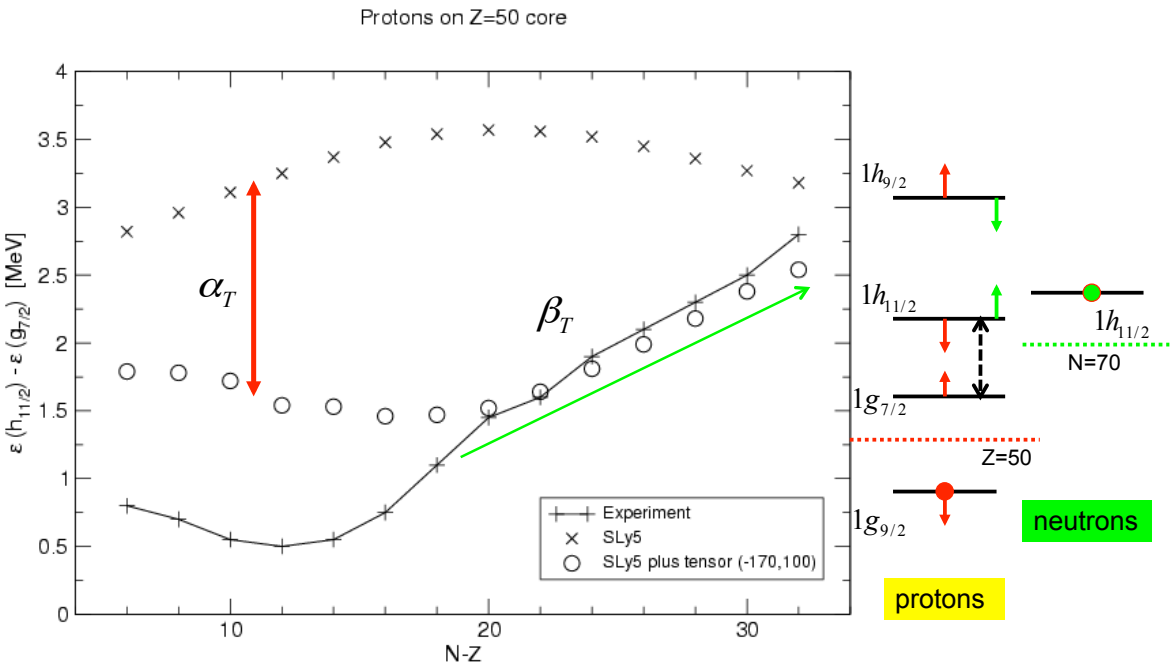

Figure 6: Energy difference between the single-particle $1g_{7/2}$ and $1h_{11/2}$ proton states along the Z=50 isotopes. The calculations are performed with and without tensor terms in the spin-orbit potential (19), on top of the SLy5 [73] parameter set. The experimental data are taken from Ref. [74]. See the text for details.

Let us now discuss the N-Z dependence of this energy difference, for which the isovector parameter β_T plays the essential role. From N-Z=6 to 14, the $g_{7/2}$ neutron orbit is gradually filled. Then the term associated with $\beta_T = 100$ MeV·fm^5 gives a negative contribution to the spin-orbit potential (19) and increases the spin-orbit splitting. Therefore, the energy difference $\Delta e(h_{11/2} - g_{7/2})$ is decreasing. From N-Z = 14 to 20, the $s_{1/2}$ and $d_{3/2}$ neutron orbits are occupied and in this region the spin density is not so much changed. For N-Z = 20 to 32, the $h_{11/2}$ orbit is gradually filled: this gives a positive contribution to the spin-orbit potential (19), that is, the the spin-orbit splitting is decreasing. This explains why the value of the energy difference $\Delta e(h_{11/2} - g_{7/2})$ increases. The magnitude of β determines the slope of the N-Z dependence, so that a larger value of β would give a steeper slope.

In Ref. [45] the force GT2, that includes an isovector tensor, produces the correct trend of the energy difference $\Delta e(h_{11/2} - g_{7/2})$ as a function of the neutron number at variance with D1S which is qualitatively and quantitatively in conflict with experiment, as is shown in Fig. 7. In the calculations the isoscalar tensor associated with α_T is not introduced; its effect is in fact not visible in Fig. 7 in which the energy difference is scaled so to set it at zero in ^{114}Sn. However, the fact that the trend as a function of the neutron excess of the GT2 results is very similar to that of the SLy5$_T$ results shown in Fig. 6 is quite remarkable and shows that the effective p-n tensor force (in other words, the values of β) is quantitatively rather close in the two cases.

A similar argument can be applied to (at least some of) the parameter sets M3Y-Pn that have been discussed at the end of Sec. 2.5. In Fig. 8 the energies of the proton orbits $1g_{7/2}$ and $1h_{11/2}$ have been

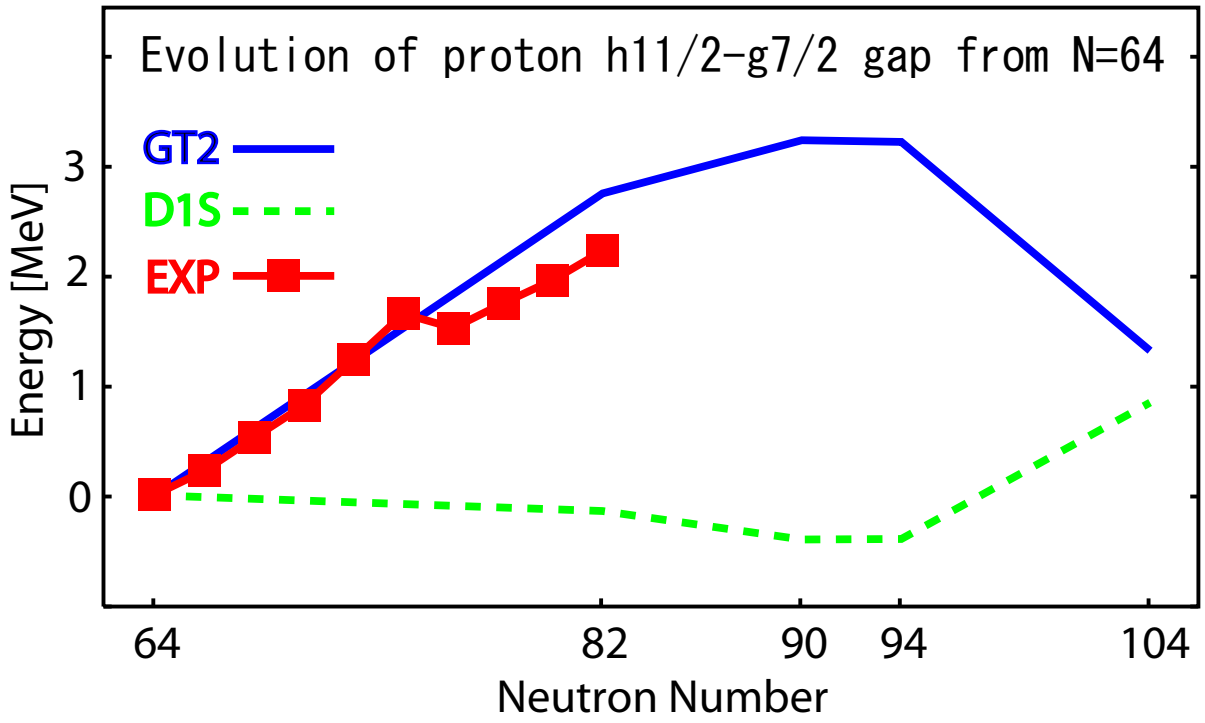

Figure 7: Energy difference between the single-particle $1g_{7/2}$ and $1h_{11/2}$ proton states along the Z=50 isotopes. The values are normalized to the difference in ^{114}Sn. The calculations are performed with the Gogny force D1S (without tensor) and GT2 (with tensor). The experimental data are taken from Ref. [74]. The figure is from Ref. [45]. See the text for details.

considered with respect to $1d_{5/2}$. The quantities $\Delta e_p(j) \equiv e_p(j) - e_p(1d_{5/2})$ have been calculated in Ref. [51] and in Fig. 8 they are plotted after a scaling to the value in ^{114}Sn like in the previous Fig. 7: in other words, $\delta\ \Delta e_p(j)$ is $\Delta e_p(j)$ minus its value in ^{114}Sn. As above, the trends show that effectively the p-n tensor force (i.e., the value of β) is not very different from the cases that we have already discussed.

We move back to the Skyrme case and analyze another case that has been object of the experimental investigation of Ref. [74]. In Fig. 9, the values of the energy difference $\Delta e(i_{13/2} - h_{9/2})$ on the N=82 core are plotted as a function of the neutron excess. Similar arguments as above can be applied. The last occupied $g_{7/2}$ level protons, because of the negative value of α_T, increase the neutron spin-orbit as compared as in the original SLy5 calculation, so that the energy difference $\Delta e(i_{13/2} - h_{9/2})$ becomes substantially smaller. The isotope dependence in the figure can again be explained by the effect of the positive value of β_T. The $1g_{7/2}$ and $2d_{5/2}$ are almost degenerate above the last occupied proton orbit $1g_{9/2}$ of the Z=50 core. These two $j_<$ and $j_>$ proton orbits have opposite effects on the spin-orbit potential but the occupancy is larger for the larger j orbit, so that the $1g_{7/2}$ orbit plays a more important role in the nuclei with N-Z from 32 to 18. That is, the neutron spin-orbit splitting becomes larger for these isotones so that the energy gap $\Delta e(i_{13/2} - h_{9/2})$ becomes smaller for the nuclei from N-Z = 32 (^{132}Sn) to N-Z = 18 (^{146}Gd).

3.2.3 Results for the medium-mass region

The work of Ref. [55] has been extended to a different mass region in [67], with a motivation coming from the experimental results of Ref. [76]. It has been concluded that the same tensor force employed in [55] can explain the trend of the proton single-particle states in Ca isotopes, and the reduction of the spin-orbit splittings going from ^{48}Ca to ^{46}Ar. The results of Ref. [35] are essentially along the same line, and it is remarkable that although the tensor force is added on top of a different Skyrme force

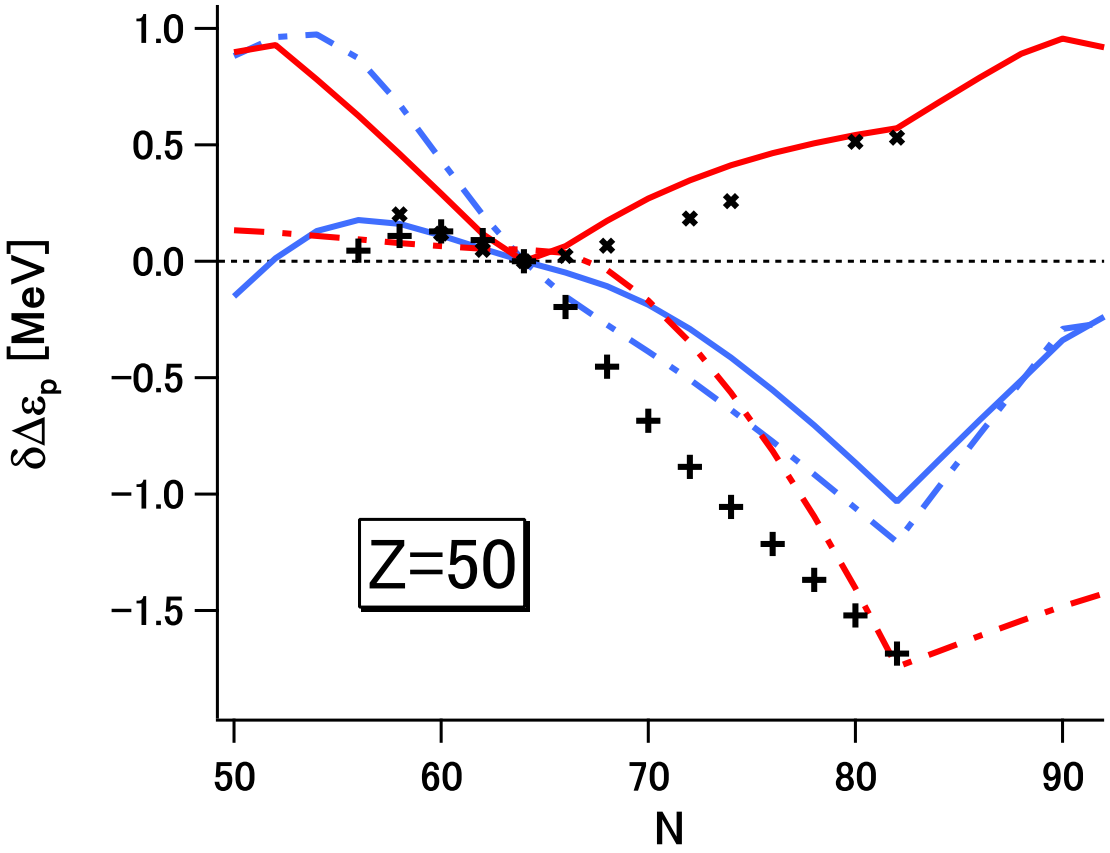

Figure 8: $\delta\ \Delta e_p(j)$ for j corresponding to the proton orbits $1g_{7/2}$ (dot-dashed lines) and $1h_{11/2}$ (solid lines) in the Z=50 isotopes. The calculations are performed with tensor terms (M3Y-P5, red lines) and without (D1S, blue lines). The experimental data (pluses for $1g_{7/2}$ and crosses for $1h_{11/2}$) are taken from Ref. [75]. See the text for details, including the definition of $\delta\ \Delta e_p(j)$.

the parameters are quite similar (α = -118.75 MeV·fm^5 and β = 120 MeV·fm^5). The evolution of the single-particle states in the Ca isotopes has been also analyzed in [77] and the role of the tensor force has been emphasized. Interestingly, in this work there has been also the attempt to study separately the evolution of all contributions (kinetic, central velocity-independent and velocity-dependent, and spin-orbit) to the s.p. energies. This is important in view of the global refitting of Skyrme forces including tensor that we discuss below.

We focus now on some experimental fact that may point to a specific effect of the equal-particle tensor force (i.e., non-vanishing value of α). The experimental evidence shows that the N=28 gap, or the difference between the $1f_{7/2}$ and $2p_{3/2}$ single-particle states, increases from ^{40}Ca to ^{48}Ca [78]. This fact is not reproduced by the Skyrme force SLy5 but it is reproduced by SLy5$_{\rm T}$ in keeping with the negative value of α [cf. panels (b) and (d) of Fig. 10]. The authors of Ref. [33] have used this and a few other experimental facts to claim that the IS tensor (or "pure tensor") should be included together with the IV tensor ("isospin tensor", present, e.g., in the GT2 set [45]) on top of the Gogny force. In Fig. 10 panels (a) and (c) display results obtained with Gogny forces that include both kinds of tensor terms. It can be seen that D1ST2b has the same trend as SLy5$_{\rm T}$. These results should be considered as a first step towards a fully refitted Gogny force with tensor terms [79], which should overcome the limits of the calculations of Ref. [33] that (in the case of the shell gaps of the Z = 8 isotopes, N = 8 isotones, Z = 20 isotopes, N = 20 isotones, Z = 28 isotopes and N = 28 isotones) do not agree well with experiment. One should also mention the work of Ref. [80]: the reduction of the proton $1d_{3/2}$-$1d_{5/2}$

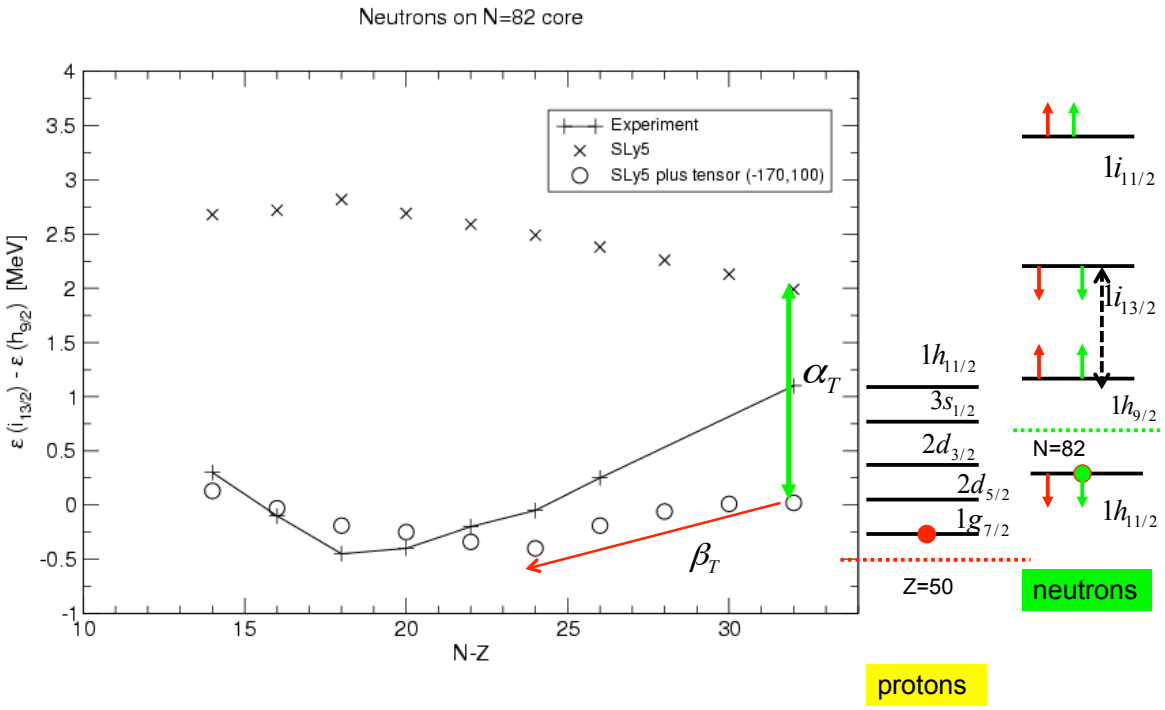

Figure 9: Energy difference between the single-particle $1i_{13/2}$ and $1h_{9/2}$ neutron states in the N=82 isotones. The calculations are performed with and without tensor terms in the spin-orbit potential (19), on top of the SLy5 parameter set. The experimental data are taken from Ref. [74]. See the text for details.

spin-orbit splitting going from ^{34}Si to ^{42}Si (that is, filling the $1f_{7/2}$ neutron orbital) is attributed to the effect of a tensor force. This is clear in the nonrelativistic approach but the authors also compare with the RHF case (cf. Sec. 3.2.5).

In conclusion, in the medium-mass region there are several examples of evolution of single-particle energies that cannot be explained without the introduction of a tensor force. We should keep in mind that in self-consistent studies all terms of the functionals are coupled and care must be taken before attributing effects to a single term or to a group of terms.

3.2.4 Attempts of global fittings of single-particle states

In Ref. [81] the emphasis is put on a global fitting of Skyrme functionals by considering also, or mainly, single-particle states functionals. In this respect, tensor force plays a role. At variance with the works discussed in the last paragraphs, the tensor force is fitted not on isotopic or isotonic trends but rather on $f_{5/2}$-$f_{7/2}$ spin-orbit splittings in ^{40}Ca, ^{56}Ni and ^{48}Ca. This fit is performed on top of existing SkP [82], SLy4 [73] and SkO [83], but the refit is performed at the same time on the spin-orbit parameter and on the tensor terms. For these latter terms, values of α around $\approx$ -100 MeV·fm^5 and β ranging from +15 to +55 MeV·fm^5 are obtained. The signs are consistent with our previous discussion, but the magnitude is affected by the concurrent 20-40% reduction of the spin-orbit strength W_0.

In Ref. [58] a very systematic study of the behaviour of the single-particle energies within the Skyrme

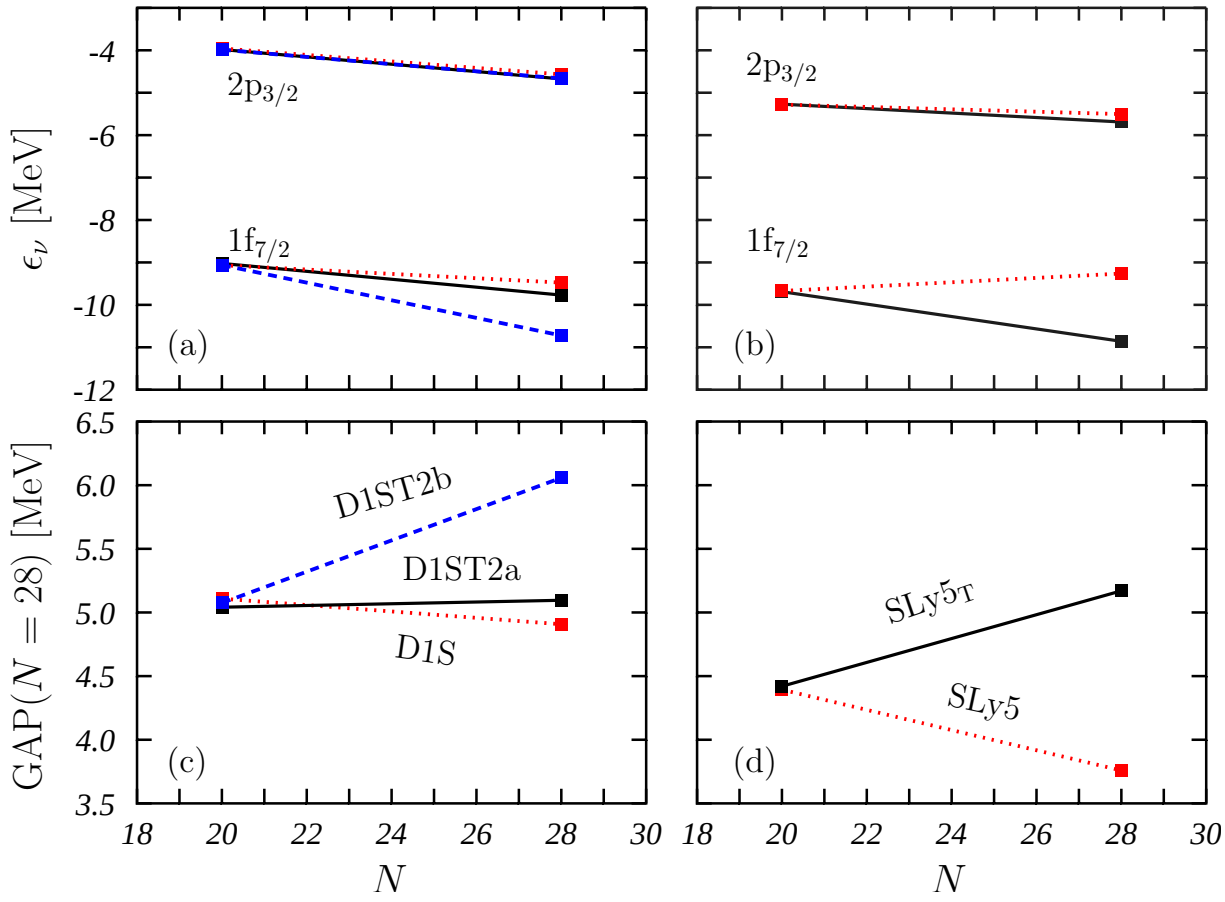

Figure 10: (a), (b): Single-particle energies of $2p_{3/2}$ and $1f_{7/2}$ states in Z=20 isotopes with Gogny D1S and SLy5 interactions, respectively. (c), (d): Energy difference between the two single-particle neutron states in the Z=20 isotopes with Gogny and SLy5 interactions, respectively. The calculations are performed with and without tensor terms in the spin-orbit potential (19), on top of the Gogny D1S and SLy5 parameter sets. The experimental data are taken from Ref. [78]. See the text for details.

HF framework, with and without the tensor interaction, has been performed. To this aim, new Skyrme sets have been built using basically the SLy protocol [73] aside from small differences. The emphasis is set on the J^2-terms, whose coefficients have been varied to a quite large extent. These new sets are named TIJ, and the indices I and J correspond to given values of the constants α and β that enter Eq. (21). In particular, the following relations hold

$$\begin{aligned} \alpha &= 60(J-2) \text{ MeV fm}^5, \\ \beta &= 60(I-2) \text{ MeV fm}^5. \end{aligned} \tag{50}$$

This choice allows to span the range of coupling constants associated with the interactions that had been previously used in this section and/or to scale their values up to a factor ≈ 2. The values of the coupling constants are shown in Fig. 11.

As expected, the inclusion of tensor terms gives rise to specific oscillations in the trend of s.p. states as a function of the neutron or proton numbers. The authors have looked at proton states as a function of the neutron number to fix the proton-neutron coupling constants, focusing in particular on the $1h_{11/2}$, $1g_{7/2}$, and $2d_{5/2}$ levels along the Sn isotopes and on the $1f_{5/2}$ and $2p_{3/2}$ levels along the Ni isotopes. In this way, they have extracted a positive value for β around 120 MeV fm^5. This value compares very well with the values we have already discussed: 110 MeV fm^5 from [66], 100 MeV fm^5 from [55, 67] and

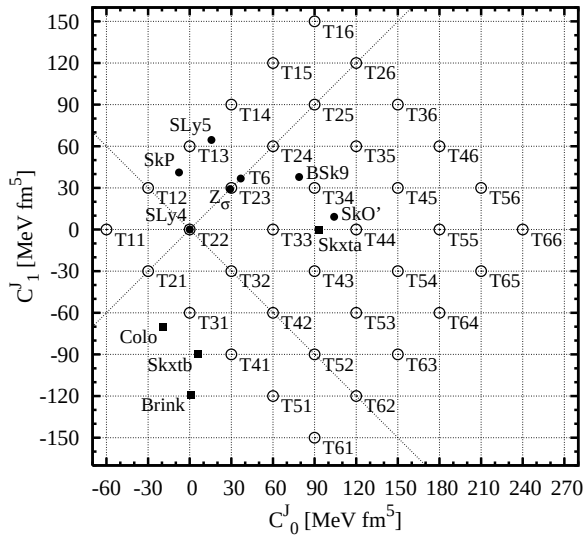

Figure 11: Values of the coupling constants C_t^J defined in Sec. 2.4 for the Skyrme sets introduced in [58] (circles). The diagonal lines indicate the loci for $C_0^J + C_1^J = 0$ (pure p-n tensor) and $C_0^J - C_1^J = 0$ (pure equal-particle tensor). Some other Skyrme sets are shown, and the original references can be found in [58], from which the figure is taken.

120 MeV fm^5 from [35]. This is quite comfortable albeit not surprising as similar data have been used as a reference. However, to fix the equal-particle coupling constant α, T. Lesinski *et al.* have used the evolution of $2s_{1/2}$ and $1d_{3/2}$ states between ^{40}Ca and ^{48}Ca: in this way, they have extracted a positive value for α, around 120 MeV fm^5 at variance with Refs. [66, 55, 67, 28, 35].

When they look directly at the spin-orbit splittings in several magic nuclei they find that, no matter which parameter set is used, the splittings between states belonging to the same shell (i.e., in-shell splittings) tend to be larger than the empirical findings, whereas the splittings between states belonging to different shells (i.e, out-shell splittings in which one intruder state is involved) tend to be too small. Discrepancies with respect to experiments are of the order of 40% (in absolute value). If they consider single-particle spectra as a whole, the systematics does not seem to single out any particular set that is satisfactory, in absolute or relative sense (cf. Figs. 12 and 13).

In this respect, the conclusions of the authors are pessimistic in an overall sense and do not put much emphasis on the aforementioned values of α and β. At the same time, it should be stressed that this conclusion seems to arise from a deficiency of the approach as a whole (i.e., the Skyrme ansatz plus a specific choice for the protocol fit), and not from a problem connected with the tensor in itself. The fact that in the fitting procedure the tensor and spin-orbit coupling constants are strongly dominated by the mass difference among ^{40}Ca, ^{48}Ca and ^{56}Ni is in this respect quite indicative.

3.2.5 RHF and Single-particle states

The single-particle states are studied by a RHF model with density-dependent coupling constants between mesons and nucleons in Refs. [16, 17] (cf. Sec. 2.2). The authors have included the tensor coupling due to the pion exchange and the vector coupling associated with the $\rho-$exchange in the effective Lagrangian. In order to obtain realistic values for the empirical observables in closed shell nuclei in their protocol, the $\pi-$ and $\rho-$ couplings in the model are the bare couplings in the free space, but they are very much quenched in the nuclear medium (cf. Fig. 14).

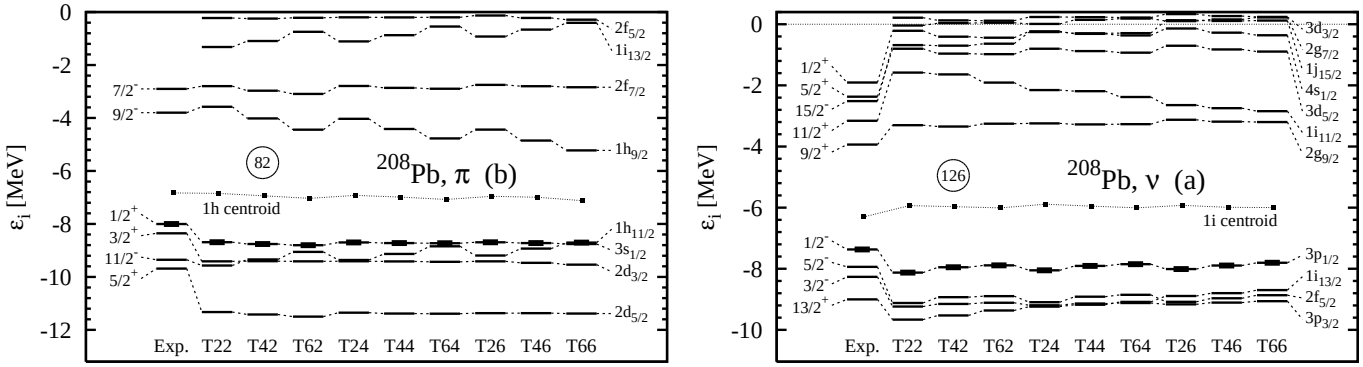

Figure 12: Single-particle energies in ^{208}Pb for some of the sets TIJ. In panel (a) the neutron levels are displayed while in panel (b) the proton levels are displayed. A thick mark indicates the Fermi level. Figure taken from Ref. [58].

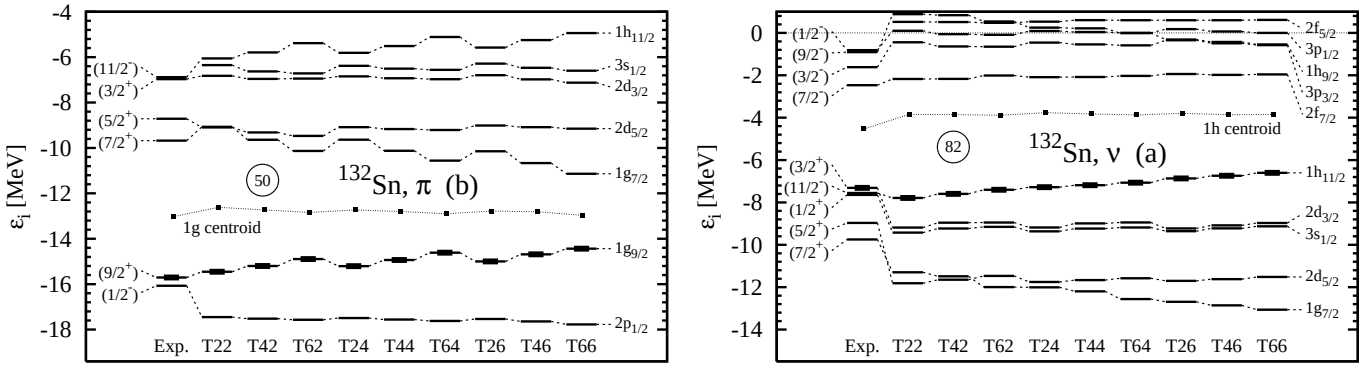

Figure 13: The same as Fig. 12 in the case of ^{132}Sn. Figure taken from Ref. [58].

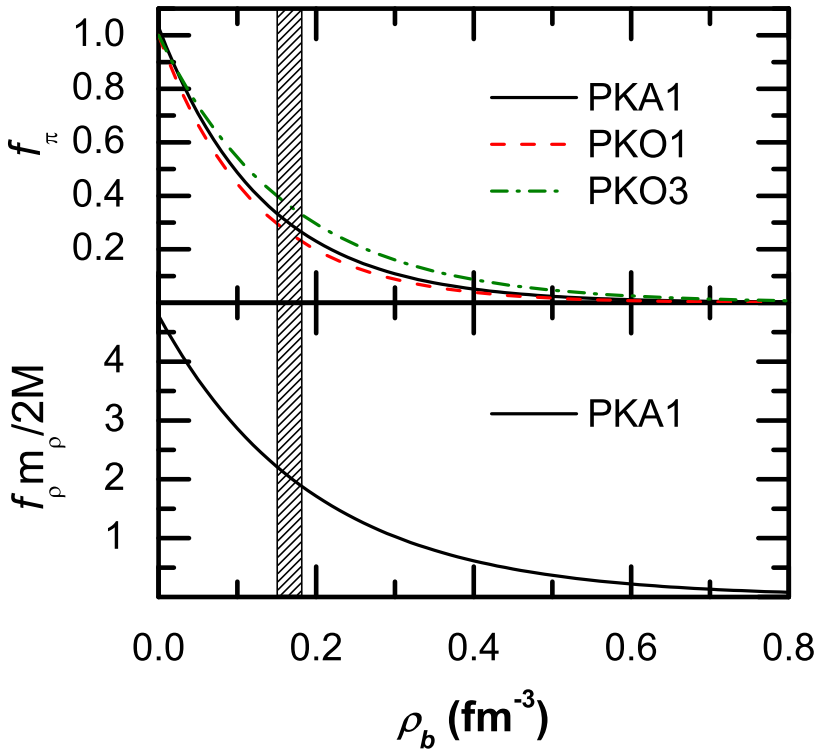

Figure 14: Density dependent meson-nucleon couplings in the isovector channels [18] as a function of density for the RHF effective interactions PKA1 [17] compared with PKO1 and PKO2 [19]. The shadowed area denotes the empirical saturation density region. See the text for details.

As already discussed above, the authors of Ref. [17] have shown that the RHF model can remove the problem of artificial shell closures at N,Z = 58 and 92 existing in some RMF calculations (cf. Fig. 2). In particular, it was pointed out that the spurious shell closure at 92 is related to the pairs of high-j states ($2f_{7/2}$, $1h_{9/2}$). This pair is the pseudospin partner $1\tilde{g}$ state. The spurious shell closure is then related to the conservation of pseudospin symmetry (PSS), i.e., the existing artificial shell structure in RMF breaks largely the PSS. As is seen in Fig. 2, PSS is successfully recovered for the $1\tilde{g}$ state. To improve this shell structure, the $\rho-$ tensor correlations play a crucial role. This is the reason why the PKA1 parameter set with the $\rho-$ tensor conserves PSS better than PKO1 that does not include the $\rho-$ tensor, and thus improves the shell structure in the single-particle states around the proton and neutron Fermi energies.

In Ref. [59], the role of the pion in covariant density functional theory was studied. Starting from conventional relativistic mean field (RMF) theory with a nonlinear coupling of the σ meson and without exchange terms, the pion$-N$ coupling with a pseudovector type in relativistic Hartree-Fock

approximation is added. In order to take into account the change of the pion field in the nuclear medium the effective coupling constant of the pion is treated as a free parameter and changed from 0 to the bare pion coupling in the free space. We have already discussed this work in Sec. 3.1.

It is found that the non-central contribution of the pion (tensor coupling) does have effects on single-particle energies and on binding energies of certain nuclei. To obtain better agreement with the experimental data for the binding energies and single-particle energies, a weak pion coupling is necessary. Moreover, the shell structure of closed shell nuclei is improved by the introduction of the pion field in the model. These conclusions of Ref. [59] are consistent with those of the RHF models of Refs. [16, 17]

3.2.6 Concluding remarks on single-particle states

Concerning single-particle states, a fundamental remark is that in principle one may argue whether they are indeed observable. Information about hole (particle) states is usually obtained by means of pickup (stripping) reactions on the corresponding core nucleus. As a rule, one compares the measured cross sections with Distorted Wave Born Approximation (DWBA) calculations performed with conventional assumptions. In particular, one usually assumes that the wave function of the transferred nucleon can be taken as an eigenfunction of a static mean field potential, by adjusting the depth of that potential so that the binding energy becomes equal to the experimental separation energy and the correct asymptotic dependence is guaranteed. Such a procedure is reasonable for levels which are concentrated in a single peak. This often happens around the Fermi energy. However, for states characterized by a broad distribution in energy, the comparison with a simple DWBA calculation is likely to be less reliable (cf., e.g., the discussion in Ref. [84]). These problems are still object of strong debates.

Even when single-particle states are not broad or fragmented, and their energies are associated with single peaks, they are believed not to belong to the DFT framework and are known to be significantly affected by dynamical correlations such as those associated with particle-vibration coupling (PVC) [85]. The authors of Ref. [58] are well aware of this fact, and try to argue that in some cases the PVC may not affect too much their conclusions. One of their arguments is that conventional wisdom may suggest that PVC just compresses the spectrum in the sense that particle (hole) states are pushed downward (upward) in energy, so that spin-orbit splittings between states that are either occupied or unoccupied may not be affected whereas spin-orbit splittings between states lying at opposite sides of the Fermi energy should be systematically reduced. This conventional wisdom may fail due to specific shell-effects, in particular in light or medium-mass nuclei. Easily the spin-orbit splittings can be changed by ≈ 500 keV or more, as an effect of the PVC, when they are calculated in a fully microscopic framework using Skyrme forces (see Ref. [86]). In particular, the $2f_{5/2}$-$2f_{7/2}$ spin-orbit splitting in ^{208}Pb is reduced by 1.07 MeV when PVC is implemented of top of RMF, and by 0.62 MeV if PVC is implemented on top of Skyrme-HF (see Table I of Ref. [87]). As a conclusion, one should not search for a fine-tuning agreement between theory and data in such cases. Particle-vibration coupling calculations that include the tensor force are currently underway [88].

3.3 Deformation

The subject of how tensor terms affect deformation properties has been thoroughly discussed in Ref. [38] with deformed HF calculations. The main purpose of this work has been to test the forces introduced in [58]. The strategy, in this case, has been to keep the coupling constants $C^{(J1)}$ associated with the TIJ sets and use them in deformed nuclei, by exploiting the relation between $C^{(J2)}$ and $C^{(J1)}$ that is implied by their relations with the coefficients of the central and tensor Skyrme forces. Other parameter sets have been considered, and also other ways to fix the coefficients $C^{(J2)}$ that are in principle unconstrained by calculations in spherical symmetry if the EDF strategy is adopted.

The authors have looked systematically at the total energy as a function of the quadrupole deformation parameter β_2. In general, for $\vec{\ell} \cdot \vec{s}$ saturated nuclei like ^{40}Ca the contribution of the tensor energy, which is close to zero at sphericity, increases with deformation, whereas in nuclei that are not $\vec{\ell} \cdot \vec{s}$ saturated (^{56,78}Ni, ^{100,132}Sn and ^{208}Pb) the tensor energy is largest at sphericity and decreases with deformation. The total energy, however, do not change as much as the tensor energy if the sets TIJ are employed. In other words, other terms of the energy functional compensate the change induced by the J^2 terms. Also in most of the nuclei that have been studied the differences among the predictions of the various sets are moderate ($\lesssim$ 2 MeV, yet with several exceptions). These two latter statements become less true if the self-consistency of the functional is broken, e.g., if one employs forces in which the tensor terms have been added pertubatively. This is a further argument, in the authors' viewpoint, to advise for consistently fitted Skyrme sets. The situation becomes very complicated in nuclei with open shells, where due to correlated effects from the various terms of the functional, no simple conclusion can be drawn about the role played by the coupling constants on the total energy curve.

In several cases, the authors have looked in detail at the Nilsson diagrams. Again, the conclusions are that the different tensor terms associated with the TIJ sets affect significantly the Nilsson levels around sphericity, while this is much less true at large deformations where the Nilsson levels tend to lie on top of each other. If other Skyrme sets are employed, the level structure is affected in a less obvious way.

Here we take one example, namely the nucleus ^{100}Zr with neutron open-shells, from Ref. [38] (cf. Fig. 15). A large set of experimental data demonstrate that ^{100}Zr is located in a region of deformed nuclei with possible shape coexistence [89]. The single-particle spectra at the spherical shape, the deformation energy curve and the variation of the tensor energy are plotted against quadrupole deformation in Fig. 15. The results obtained with the T44 and T62 parametrizations indicate a larger contribution from the isovector tensor terms. The positions of the neutron s.p. energies $2d_{3/2}$ and $2g_{7/2}$ are very much dependent on the sign and size of the isovector coupling constant C_1^J . For a positive value as in T26, the $2d_{3/2}$ level is close to the Fermi level and is occupied in such a way that it partially cancels the contribution from the $2d_{5/2}$ orbital. The isovector tensor terms are in this case strongly reduced. In contrast, for a negative C_1^J coefficient as in T62, the $2d_{3/2}$ level is pushed up and crosses the $1h_{11/2}$ level, increasing the neutron spin-current density. Results obtained with the SLy5$_{\rm T}$ interaction, for which C_1^J is also negative, are similar, although less pronounced. For even larger negative values of the tensor coupling constants, this feedback mechanism is suppressed by the reduced spin-orbit interaction. Most total deformation energy curves in Fig. 15 exhibit spherical, prolate, and oblate minima. The inclusion of beyond mean-field correlations should favor the prolate minima and create a 0^+ excitation exhibiting some amount of configuration mixing. Such results are consistent with experiment. The spherical minimum is too much below the deformed one to expect that additional correlations from the projection of $J = 0$ states will make ^{100}Zr deformed in its ground state. For T62, the deformation energy curve looks like that of a double magic nucleus. For SLy4T and SLy4Tself [38], it is the reduced spin-orbit interaction that reinforces the proton Z = 40 shell closure. The prolate minimum becomes a shoulder around 5 MeV, leading to the coexistence of spherical and oblate minima.

A different specific case that can illustrate the interplay of tensor correlations and deformation has been thoroughly discussed in Ref. [90], and concerns the tensor effect on the shape evolution of the Si isotopes. The basic questions in this case are: is the tensor-force-driven deformation present in other neutron-rich Si isotopes, especially ^{30}Si with a possible N = 16 subshell, since some models (e.g., the FRDM) predicted a spherical shape for this nuclei [91] while the large B(E2) value suggested its deformed nature [92]. For this purpose, the authors of Ref. [90] used the deformed Skyrme-Hartree-Fock model (DSHF) [93] with the BCS approximation for the nucleon pairing. For each nucleus the strength of the pairing force is fitted by taking care of the empirical data for the pairing gaps, as done in Refs. [94, 95, 96]. The parameter sets of Ref. [58] have been chosen, and they include: the Skyrme force T22 serving as a reference as it has vanishing J^2 terms, T24 with a substantial like-particle coupling

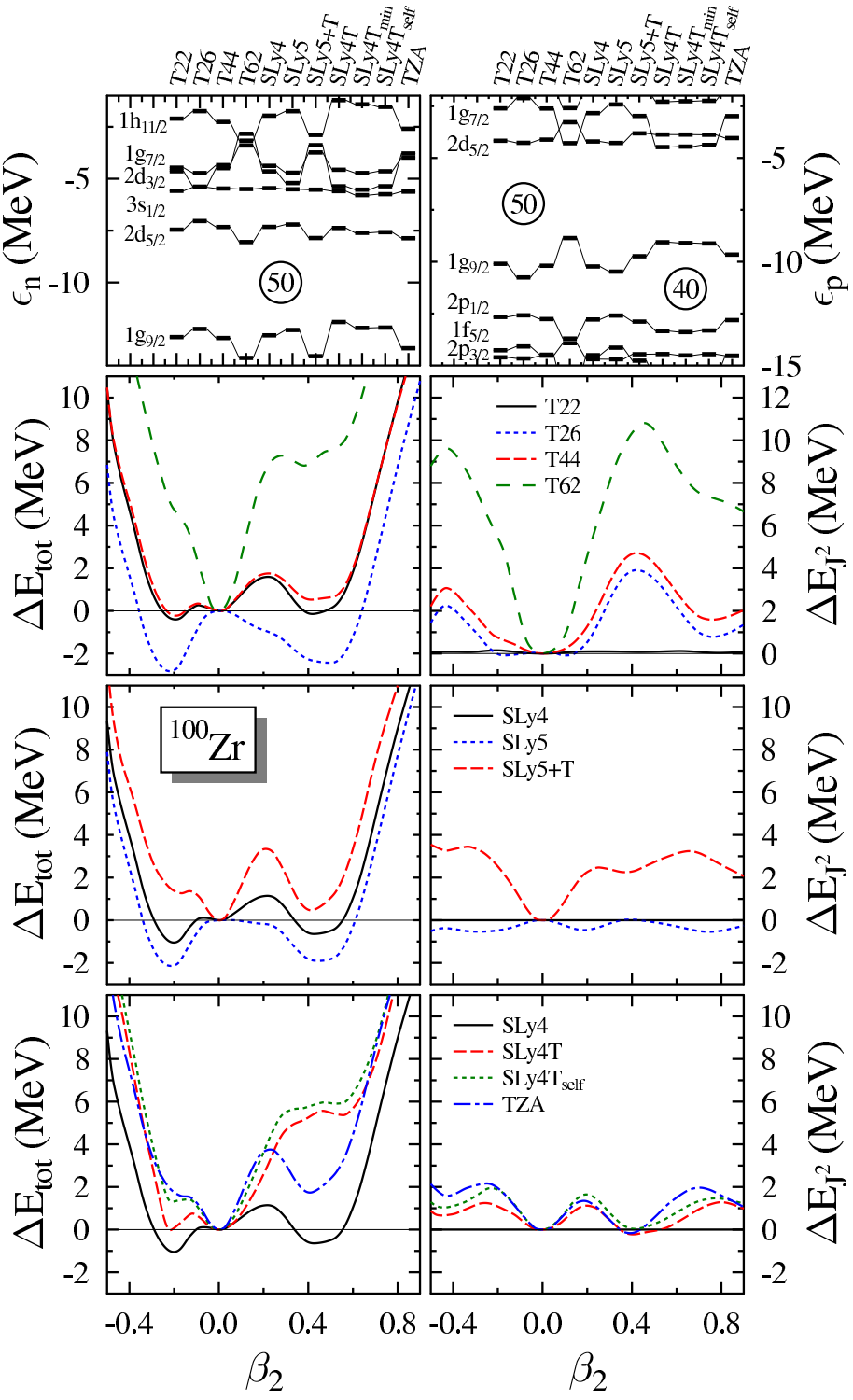

Figure 15: The single-particle spectra at spherical shape are shown in the upper panel for neutrons (left) and protons (right) The deformation energy (left) and the variation of the total tensor energy (right) are plotted on the lower panels for ^{100}Zr and different Skyrme parametrizations, as indicated. The protocols for the adopted Skyrme parameter sets can be found in Ref. [38]. This figure is taken from Ref. [38].

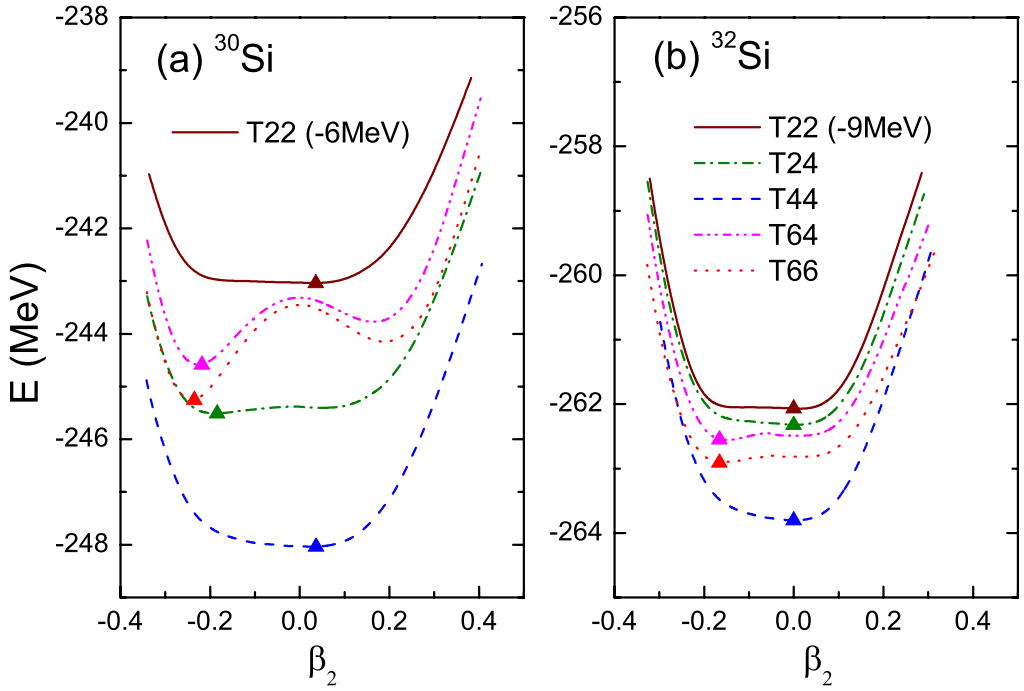

Figure 16: Energy surfaces of ^{30}Si (left panel) and ^{32}Si (right panel) as a function of the quadrupole deformation parameter β_2 using T22, T24, T44, T64, and T66. The results with T22 are shifted by -6 MeV and -9 MeV in ^{30}Si and ^{32}Si, respectively. The energy minima are indicated with triangles. This figure is taken from Ref. [90].

constant α and a vanishing proton-neutron coupling constant β; T44 with a mixture of like-particle and proton-neutron tensor terms, T62 with a large proton-neutron coupling constant β and a vanishing like-particle coupling constant α; and T66 with large and equal proton-neutron and like-particle tensor-term coupling constants. The coupling strengths of various parameter sets used in this study are collected in Tab. 1.

Table 1: Coupling strengths (in MeV·fm^5) of various parameter sets used in the work. α represents the strength of like-particle coupling between neutron-neutron or proton-proton, and β is that of the neutron-proton coupling. The subscripts T indicates the tensor contribution. See text for details.

	T22	T24	T44	T64	T66
α	0	120	120	120	240
β	0	0	120	240	240
α_T	-90.6	24.7	8.97	-0.246	113
β_T	73.9	19.4	113	218	204

We begin by showing in Fig. 16 the energy surfaces of ^{30}Si (left panel) and ^{32}Si (right panel) as a function of the quadrupole deformation parameter β_2. The energy minima are indicated with triangles. The nucleus ^{30}Si is suggested to be deformed as mentioned before, but T22 and T44 with relatively large pairing strengths ($\approx$ 1000 MeV·fm^3) fail to give deformed energy minima. On the contrary, deformed ground states can be achieved using the T24, T64 and T66 parametrizations with associated small pairing strengths ($\approx$ 800 MeV·fm^3). The predicted oblate shape of this nuclei is consistent with the recent RMF result [97]. The interesting performance of a weak nucleon pairing may stem from a well-known fact that the pairing interaction forms the $J = 0^+$ pairs of identical particles which have spherically symmetric wave functions, and as a result, nuclei tend to be more spherical with stronger

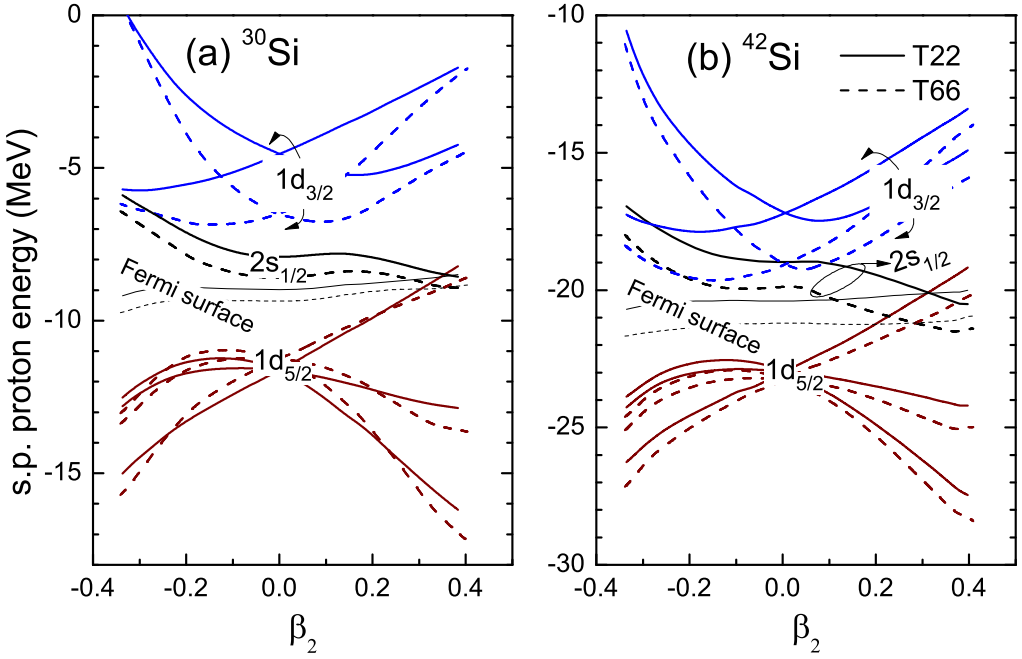

Figure 17: The s.p. orbits of protons for ^{30}Si (left panel) and ^{42}Si (right panel) are shown as a function of the quadrupole deformation parameter β_2 using T22 (solid lines) and T66 (dashed lines). The Fermi surface is also shown between the $2s_{1/2}$ and $1d_{5/2}$ orbits in the spherical limit. This figure is taken from Ref. [90].

pairing couplings. We also notice that large tensor terms present in T64 and T66 tend to make the energy surface deep, namely the tensor force affects dramatically to create a well-deformed ground state for ^{30}Si. The importance of tensor force will be seen also in ^{32}Si as shown in the right panel of the same figure. Its shape is predicted to be spherical with T22, T24 and T44, but oblate with T64 and T66 with large tensor terms.

To clarify the effect of tensor correlations on deformation, through the HF fields, we plot in Fig. 17 the single proton levels in ^{30}Si (left panel) and ^{42}Si (right panel) as a function of the quadrupole deformation parameter β_2 using T22 (solid lines) and T66 (dashed lines). The Fermi surface is also shown between the $2s_{1/2}$ and $1d_{5/2}$ orbits in the spherical limit. One can see that there are two main features indicating the tensor effect to compare the results between T22 and T66 for ^{30}Si: a narrower $1d_{3/2}$-$1d_{5/2}$ gap and a steeper $1d_{5/2}$ orbits downward in the oblate side. Then, in the case of T66, more mixing between $1d_{3/2}$ and $1d_{5/2}$ results in an oblate shape for this nuclei in comparison with the case of T22. The shell gap by T66 interaction is narrower also in ^{42}Si, but both T22 and T66 give oblate deformations, since the tensor effect in this nuclei is not as evident as the case of ^{30}Si regarding the $1d_{5/2}$ orbits.

The effect of the tensor interaction on the stability of superheavy elements (SHEs) was studied in Ref. [98] with the spherical Skyrme HF model. In Ref. [99], the deformed HF model with the tensor and the pairing correlations was adopted to study the stability of SHEs. It was pointed out in Ref. [99] that the shell gaps at Z=114 and N=164 are more stabilized by the tensor correlations of the SLy5$_{\rm T}$ interaction.

3.4 Vibrational states

It can be expected that spin-flip excitations are quite sensitive to the tensor force, while non spin-flip excitations are less sensitive. At the unperturbed level, this is schematically illustrated in Fig. 18: as

the tensor force mainly changes the spin-orbit splittings, particle-hole (p-h) transitions between spin-orbit partners $j_>$ and $j_<$ are more affected than transitions between $j_>$ and $j_>$ states (or between $j_<$ and $j_<$). This argument remains true at the level of residual interaction since the tensor force is only active between the $S = 1$ component of the p-h configurations. In fact, in Ref. [100] the response of nuclear matter has been studied and the effect of the tensor force is clearly much stronger in the $S = 1$ than in the $S = 0$ channel.

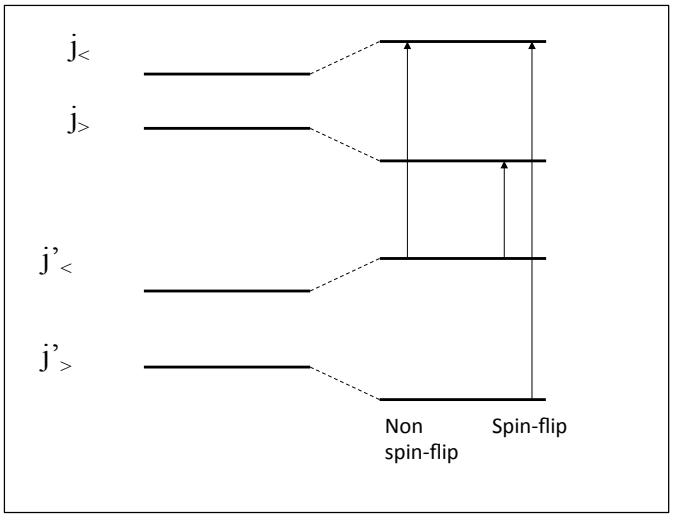

Figure 18: Schematic view of the effect of the tensor force on the mean-field responses to different operators. The levels displayed on the left side evolve to those depicted on the right side due to the effect of the tensor force. The arrows show the transitions that are excited mainly by either non spin-flip (the single arrow in the left part) or spin-flip (the two arrows in the right part) external fields.

Nevertheless, this $S = 1$ component is not completely absent in the natural parity states. Therefore, a careful study of the effect of the tensor force on the natural parity vibrational states has been carried out in Ref. [101] by using self-consistent Skyrme-RPA [102] with and without the tensor force. It has been found that the effects of the tensor force are small, especially in the high-lying giant resonance region. The low-lying 2^+ and 3^- states, that have been considered in the nuclei ^{40,48}Ca and ^{208}Pb, are shifted in energy by the tensor force: these shifts can range from very small values to several hundreds of keV (reaching at most ≈ 700 keV in the case of 2^+ and ≈ 1.3 MeV in the case of 3^-). The electromagnetic transition probabilities are affected in a less significant way. The energy shifts induced by the tensor force can be written approximately as

$$\Delta E_{\rm RPA} \approx \Delta E_{\rm HF} + \langle V_{\rm tensor} \rangle, \tag{51}$$

where the first term in the r.h.s. denotes the average change of the p-h energies with and without the tensor force and the second term is an average value of the tensor force. The average value of the tensor force can be numerically calculated, but also estimated with within the framework of a separable approximation (see Appendix B of [101]). When forces having negative values of α and positive values of β are employed, with $\alpha \approx -\beta$, the tensor force is attractive in the natural parity isoscalar channel and the second term in the r.h.s. of Eq. (51) is as a rule negative; however, the sign of the first term turns out to depend on the nucleus and on the specific states involved in the 2^+ and 3^- transitions. In summary, these low-lying states cannot be a good constraint for the tensor force because of their dependence on shell effects. Despite this, a more systematic study of the effects of the tensor force on

the low-lying states in ^{40}Ca and ^{208}Pb has been carried out in Ref. [103]. It has been found that these states are reasonably described by the sets T44, T45 and SGII [104] plus a perturbative tensor force.

There exist pioneering attempts to relate the low-lying spin excitations to the tensor force. One of the first papers to point out the sensitivity of the 0^- states in ^{16}O to the tensor interaction is Ref. [105]. In the work of Ref. [106] the authors had already noticed that the single-particle states in a $\vec{\ell}\cdot\vec{s}$-saturated nucleus like ^{16}O are insensitive to the tensor force. On top of this, they have made attempts to understand the effects of the spin-orbit and the tensor force on few excited states in light nuclei, by using a simple interaction and a series of restricted Tamm-Dancoff approximation (TDA) calculations. Looking at the negative parity excitations of ^{16}O, described as superpositions of 1p-1h configurations, they have found that the tensor force has a large effect on the energies of the isoscalar states and this effect is attractive for the non-natural parity states 0^-, 2^- and 4^-, while it is repulsive for the natural parity states 1^- and 3^-. The absolute value of these energy shifts decreases with J, being around ≈ 4 MeV for 0^- and going down to 1 MeV or less in the case of the high J values. For the isovector states the energy shifts are significantly smaller and they are of the order of 1 MeV or less. The 1^+ (M1) states in ^{12}C have also been studied. The tensor interaction has also a noticeable attractive effect in this channel. The states come out too low with respect to experiment. However, it has been noticed that in this case a full shell-model calculation differs from the simple TDA result.

Looking at modern self-consistent calculations, one may try to disentangle the effects of the tensor force on single-particle states and on the residual interaction. The 1^+ state is, as we said, a possible benchmark for the tensor force and the effect of this latter force could be extracted from Eq. (51). Interactions like SLy5$_{\rm T}$ [55] enlarge the spin-orbit splittings in ^{48}Ca, ^{90}Zr and ^{208}Pb (as compared with the original force SLy5) and push the unperturbed 1^+ states upwards; the effect of the residual interaction is not easy to guess from simple arguments but does not tend to alter the positive sign of the shift induced by the change in spin-orbit splittings [for comparison, small residual matrix elements can also be found by using the phenomenological tensor forces that reproduce the experimental findings and that have been introduced in [49] (cf. Table III of this reference)].

The key point is that, anyway, simply adding a tunable tensor force does not automatically ensure that one can reproduce the experimental findings. In fact, one needs to start from an effective force in which the $\sigma\sigma$ and $\sigma\sigma\tau\tau$ terms are realistic. This is not the case for many microscopic interactions. For instance, the Lyon forces SLy* that are among the most modern and accurate Skyrme sets [73], have an attractive (repulsive) isovector (isoscalar) spin-spin residual force (these forces are associated, respectively, with the Landau parameters G_0 and G'_0; cf. Sec. 4 for a discussion concerning these parameters). This is at variance with the empirical findings. In fact, experimentally, the isoscalar M1 states are found at lower energies than the isovector M1 states. It is interesting to notice that the same shortcoming is associated with the D1 Gogny force [107, 41]. The calculations of the 1^+ states performed, respectively, in [101] with the SLy5 force and in [49] with the D1 force show an inversion of the isospin doublet with respect to experiment. By implicity commenting also the role of the tensor, the authors of Ref. [108] did also discuss the shortcomings of the current models as far as the prediction of M1 states are concerned. It would be interesting to check the performance of the new Skyrme set SAMi proposed in Ref. [109] for the properties of 1^+ states. Once more, we may remark that forces in which all parameters are fit on equal footing may perform better. Along this line, it has been noted in [101] that the force T44 introduced in [58] produces reasonable results for the 1^+ states.

In [49] other kind of excitations (2^- and 4^-) in ^{12}C, ^{16}O, ^{40,48}Ca, and ^{208}Pb have been considered in the framework of both phenomenological and microscopic (i.e., Gogny-based) calculations. A step forward in the microscopic approach by the same group is discussed in Ref. [110]. In this work, self-consistent RPA calculations have been performed. A tensor force of the type (49) has been added to the forces D1S [47] and D1M [60]. In both cases, the parameter b of Eq. (49) has been fitted (and the spin-orbit strength readjusted) so that the 0^- state in ^{16}O is well reproduced. This state has been identified as the most sensitive to the tensor force (not surprisingly since it carries the same quantum

numebers of the pion). The new forces have been named D1ST and D1MT. By using them, the binding energies and radii are not affected in a significant manner, while the s.p. states are affected since this attractive bare pion-like force has a positive value of β and $\alpha \approx \beta/2$ as recalled in Sec. 2.3 (O, Ca, Ni, Zr, Sn and Pb isotopes have been considered in [110]). In RPA, it has been found that the effect of the tensor force follows the trends that we have previously discussed. The natural-parity states are less affected than the spin-flip states, and among those latter the IV states undergo smaller shifts than the IS states, these shifts being also a decreasing function of J. The tensor force introduced in Ref. [110] improves the agreement with experiment of the 0^- excited states in several nuclei and not only in ^{16}O. For the states with different quantum numbers it is hard to make such a statement. From Table II in the paper one notices that, although the effect of the tensor force cannot be ignored, its inclusion sometimes improves the agreement with experiment but sometimes goes in the opposite direction. This is probably an indication that for such observables a refit of the whole Gogny force would be mandatory, including both IS and IV terms [79]. The same group considered also the magnetic states in nuclei with neutron excess in Ref. [111].

3.5 Rotation and tensor coupling constants

To study the high-spin properties of atomic nuclei is one the current subjects of mean field theories, especially because of recent advances in the experimental study of superdeformed (SD) rotational bands. Recently, the influence of the tensor terms on the high-spin properties was studied using a cranked HFB approach for different parametrization of Skyrme tensor interactions in Ref. [39] The authors separate the Skyrme EDF into two parts

$$E = \int d^3r \sum_{t=0,1} \left[\mathcal{E}_t^{\rm te} + \mathcal{E}_t^{\rm to}\right], \tag{52}$$

where the first (second) term in the bracket is the time-even (time-odd) part of the EDF and the suffix t is the isospin index ($t = 0, 1$). All densities and currents are distinguished into isoscalar ($t = 0$) and isovector ($t = 1, t_z = 0$). Detailed expressions for $\mathcal{E}_t^{te}$ and $\mathcal{E}_t^{to}$ can be found, e.g., in Ref. [40] and have been already discussed in Sec. 2.4. Some arguments are repeated here from Sec. 2.4 for the reader's convenience. The names "time-odd" and "time-even" associated to terms of the EDF refer to the properties under time reversal of the densities and currents they are built from, but not to the properties of the EDF itself which is time-even by definition. For example, the part of the EDF constructed from the density $\rho(\mathbf{r})$ or the kinetic density $\tau(\mathbf{r})$ belongs to the time-even part, while that involving the spin density $\mathbf{s}(\mathbf{r})$ belongs to the time-odd part.

The SD rotational bands are calculated by the self-consistent cranked HFB approach. The method can be seen as a semiclassical description of the collective rotation of a finite system with a constant angular velocity ω. In particular, the model takes into account the distortion of the nucleus intrinsic state by the centrifugal and Coriolis forces induced by the collective rotation. The variation of the EDF including the constraints on particle number and rotational frequency leads to the cranked HFB equations

$$\begin{pmatrix} h - \lambda - \omega J_z & \Delta \\ -\Delta & -h^* + \lambda + \omega J_z^* \end{pmatrix} \begin{pmatrix} U_\mu \\ V_\mu \end{pmatrix} = E_\mu \begin{pmatrix} U_\mu \\ V_\mu \end{pmatrix}, \tag{53}$$

where U_μ and V_μ are the two components of the quasiparticle wave functions and E_μ is the quasiparticle energy, often called Routhian in the rotating frame [112]. The effective interaction in the HFB Hamiltonian manifests itself in the mean field Hamiltonian h and the pairing field Δ. The rotational frequency ω is self-consistently adjusted to fulfill the auxiliary condition for the mean value of the projected angular momentum J_z on the rotating axis. The component J_z is chosen along the axis perpendicular to the axis of the longest elongation. At high spins and large deformations, the solution of Eq. (53) can be

seen as an approximation of a variation after the projection of angular momentum and the model is particulaly adequate for the description of SD bands.

In Ref. [39], the authors studied the dynamical moment of inertia defined by

$$J^{(2)} = \frac{d < J_z >}{d\omega} \tag{54}$$

where $< J_z >$ is the average value of the projected angular momentum on the rotation axis. This quantity is the well-established observables of SD bands, and can be also expressed through the derivative of the energy with respect to the rotational frequency as

$$J^{(2)} = \frac{1}{\omega}\frac{dE}{d\omega}, \tag{55}$$

which makes it possible to separate the contributions of time-even and time-odd terms in the EDF.

The dynamical moment of inertia of ^{194}Hg was calculated by using Skyrme forces like SLy4 and members of the TIJ family that include tensor interactions, and some results are shown in Fig. 19. In general, some of TIJ interactions give equally good or somewhat better agreement with experimental data than SLy4. Especially T22, T44 and T26 give satisfactory results, but the T62 parametrization in which tensor acts only between protons and neutrons in spherical symmetry shows an artificial enhancement of $J^{(2)}$ in very high-spin states, and does not give a satisfactory description of experimental observations. Concerning the tensor contributions, the time-even contribution to $J^{(2)}$ for T44 is small and varies between -4% at low spin and 2% at high spin. For T26, the contribution is larger at high spin going up to 4%. For the time-odd contributions, the spin dependent terms tend to cancel largely and the total contribution is less than 1%. As was pointed out in the previous studies using TIJ interactions [38], the presence of the tensor terms has an impact on the $J^{(2)}$ value mainly through the rearrangement of other coupling constants in the fit and also through the self-consistency of the HFB approach.

3.6 Tensor correlations and spin-isospin charge-exchange excitations

This section is devoted to the study of the impact of the tensor terms of the Skyrme effective interaction in the self-consistent charge-exchange RPA calculations. In particular, we will focus on the Gamow-Teller (GT) and Spin-Dipole (SD) transitions, which are expected to be significantly affected in keeping with the fact that the corresponding operator is spin-dependent. The results presented in this Section are mainly based on the recent studies of Refs. [115, 116, 117] (see also [118, 119]).

3.6.1 Gamow-Teller states

In the study of GT transitions, the quenching problem is of some relevance. The experimentally observed strength from 10 to 20 MeV excitation energy (with respect to the ground state of the target nuclei) is about 50% of the model-independent non-energy weighted sum rule (NEWSR); this percentage becomes about 70% if the whole strength in the neighbouring energy region is collected [120]. It is expected that the tensor force has an effect on the centroid of the GT resonance (GTR), in analogy with what discussed for the case of the M1 resonance in Sec. 3.4. In addition, it is interesting to study if the tensor force has an effect in producing some amount of quenching by shifting strength in the high-energy region, already at one particle-one hole (1p-1h) level. Coupling the GTR with two particle-two hole states is essential, e.g., to describe the resonance width (although it is not expected to affect strongly the position of the main GT peak) and will increase the quenching effect; the role of the tensor force in connection with the 2p-2h coupling was studied in Ref [121].

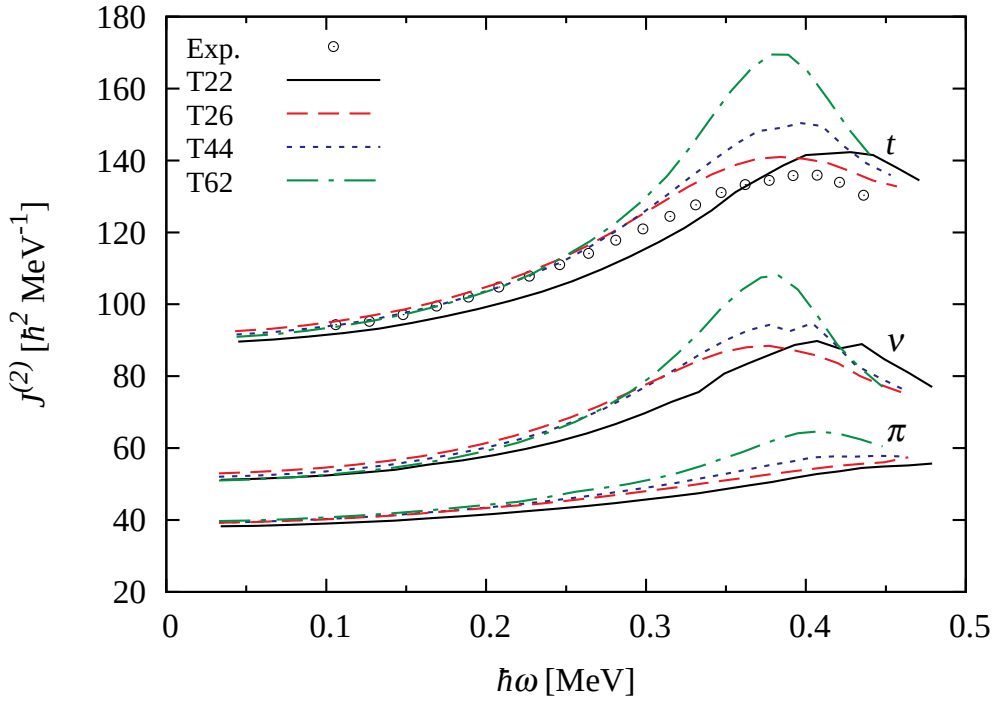

Figure 19: Proton (π), neutron (ν), and total (t) dynamical moments of inertia in ^{194}Hg as a function of the rotational frequency for the SD band in ^{194}Hg calculated with the T22, T26, the T44, and the T62 parametrization. Experimental data are taken from [113]. Figure adapted [114] from Ref. [39].

As already discussed, the spin-orbit density J_q gives essentially no contribution in the $\vec{l}\cdot\vec{s}$-saturated cases. Therefore, we will discuss the example of the nuclei ^{90}Zr and ^{208}Pb. ^{90}Zr is a proton $\vec{l}\cdot\vec{s}$-saturated nucleus, with a neutron orbit $1g_{9/2}$ contributing to J_n. ^{208}Pb is chosen as it is not saturated either in protons or neutrons. The two examples should allow elucidating separately the role of tensor-even and tensor-odd terms in the results of self-consistent charge-exchange RPA.

The operator for GT transitions is defined as

$$O_{GT\pm} = \sum_{im} t^i_{\pm}\sigma^i_m \tag{56}$$

in terms of the isospin operators, $t_{\pm} = \frac{1}{2}(t_x \pm i t_y)$. In the charge-exchange RPA, the t_- and t_+ channels are coupled and the corresponding eigenstates emerge from a single diagonalization of the RPA matrix. In the self-consistent charge-exchange HF+RPA calculations, the NEWSRs $m_{\pm}(0)$ and the Energy-Weighted Sum Rules (EWSRs) $m_{\pm}(1)$ (associated with the two different isospin channels) satisfy the following relations:

$$\begin{aligned} m_-(0) - m_+(0) &= \sum_{\nu} \left(|\langle\nu|O_-|0\rangle|^2 - |\langle\nu|O_+|0\rangle|^2\right) \\ &= \langle 0|\left[O_-, O_+\right]|0\rangle, \end{aligned} \tag{57}$$

$$\begin{aligned} m_-(1) + m_+(1) &= \sum_{\nu} \left(E_\nu|\langle\nu|O_-|0\rangle| + E_\nu|\langle\nu|O_+|0\rangle|^2\right) \\ &= \langle 0|\left[O_+, [H, O_-]\right]|0\rangle, \end{aligned} \tag{58}$$

where O_+ (O_-) is a generic charge-changing operator proportional to t_+ (t_-). In the GT case, the difference of NEWSRs (57) is model-independent and turns out to be

$$m_-(0) - m_+(0) = 3(N - Z), \tag{59}$$

whereas the sum of the EWSRs is model-dependent. This latter receives a contribution from the tensor interaction, which is obtained by replacing the total Hamiltonian H in the double commutator of (58) with V_T. If there is enough neutron excess, and the contributions from the t_+ channel to the sum rules, $m_+(0)$ and $m_+(1)$, are small, then we can estimate the effect of the tensor interaction on the GT centroid in the t_- channel by writing

$$\begin{aligned}\Delta E_{GT} &= \frac{m_-(1)}{m_-(0)} \\ &\sim \frac{m_-(1)+m_+(1)}{m_-(0)-m_+(0)} \\ &= \frac{4\pi}{3(N-Z)}\int drr^2\ [-(\frac{5}{2}U+\frac{5}{2}T)J_nJ_p-\frac{5}{3}U(J_n^2+J_p^2)], \end{aligned} \tag{60}$$

where the last line comes from a lengthy but straightforward evaluation of the double commutator [55]

As far as the calculations shown in this Section are concerned, the two-body spin-orbit residual interaction is not included in the RPA. However, this term of the residual interaction has been shown to be very small [122] in the case of the GTR; no further approximation is involved. The values reported in Table 2 are, however, calculated by dropping completely the spin-orbit contribution, both at HF and RPA level. This calculation (with the Skyrme parameter W_0 set at 0) is not supposed to be compared with the experimental findings but respects self-consistency in a strict sense. The shift in the GT centroid caused by the inclusion of tensor terms, [calculated by using either RPA or the analytical formula (60)], and the EWSR $m_-(1)$ obtained from RPA, are listed in Table 2 for the two nuclei ^{90}Zr and ^{208}Pb. One should notice the good agreement between the RPA results and the analytical results for the shift.

Table 2: Values of the EWSR $m_-(1)$ obtained from self-consistent HF plus RPA calculations, with and without the tensor terms. δE_{RPA} and δE_{DC} are the contributions of the tensor terms to the GT centroid energy calculated, respectively, by using RPA and the analytical formula (60). In the case of the numbers reported here (not for the other results in this paper), the spin-orbit term is dropped both at HF and RPA level. See also the text for details.

	$m_-(1;$ no tensor) MeV	$m_-(1;$ with tensor) MeV	δE_{RPA} MeV	δE_{DC} MeV
^{90}Zr	271.45	338.68	2.241	2.276
^{208}Pb	1854.12	2000.76	1.111	1.118

The GT$_-$ strength distributions in ^{90}Zr and ^{208}Pb are shown in Figs. 20 and 21, respectively. The tensor force affects these results in two ways. Firstly, it changes the single-particle energies in the HF calculation; secondly, it contributes to the RPA residual force. We display the results of three different kinds of calculations to analyze separately these effects. In the first one, the tensor terms are not included at all. In the second one, the tensor terms are included in HF but dropped in RPA. This calculation is not self-consistent, but it demonstrates the effects of the changes in the single-particle energies on the strength distribution. In the last one, the tensor terms are included both in HF and RPA calculations. For simplicity, results of the three categories of calculations are labeled by 00, 10 and 11, respectively.

The exhaustion of the EWSR $m_-(1)$ in the different excitation energy regions is shown in Table 3. The EWSR in the energy region below 30 MeV (where the 1p-1h transitions are located) decreases after the inclusion of the tensor term. From Table 3, we also see that an appreciable amount of EWSR is shifted from the lower energy region (0-30 MeV) to the higher energy region (30-60 MeV) by including

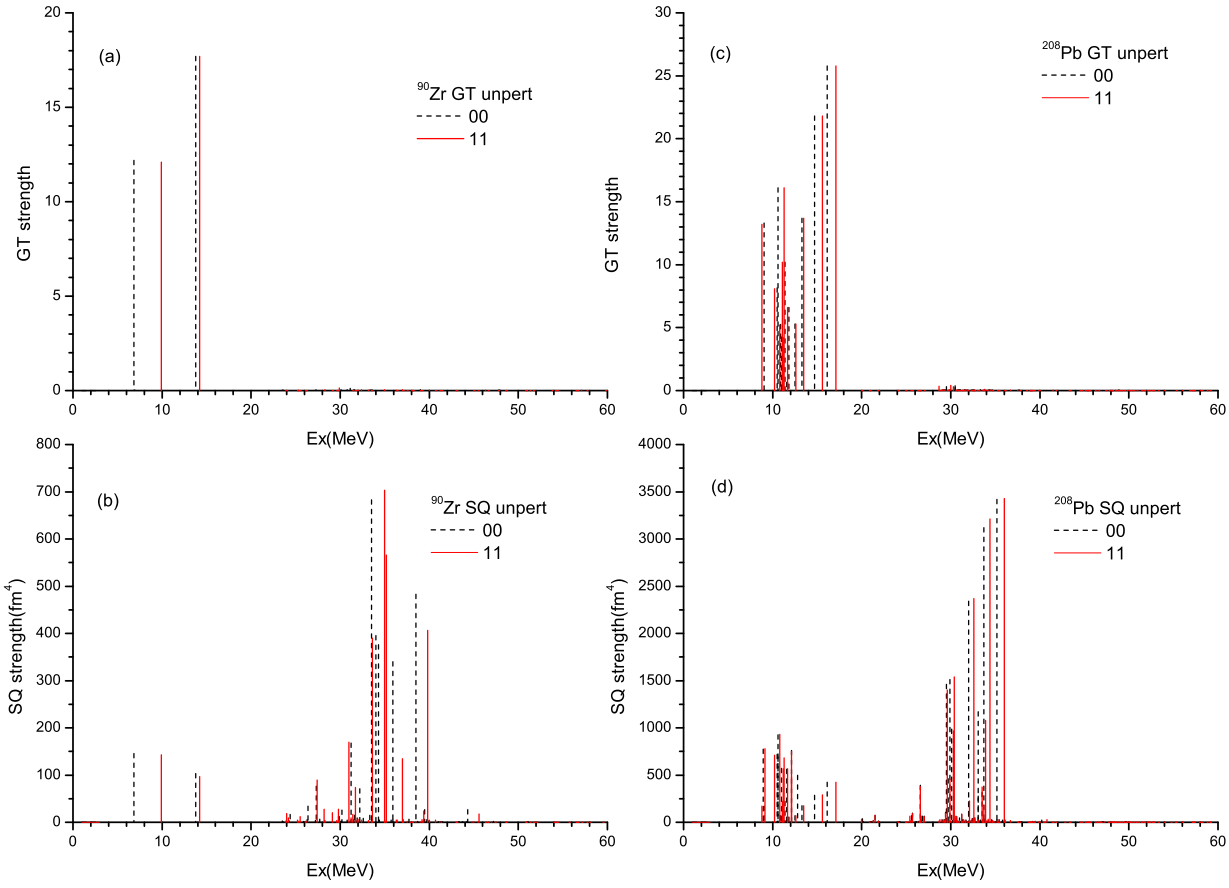

Figure 20: The unperturbed GT$_-$ and SQ$_-$ (spin-quadrupole) strength in ^{90}Zr and ^{208}Pb. The results labeled by 00 correspond to neglecting the tensor terms both in HF and RPA, while 11 corresponds to including the tensor terms both in HF and RPA. Figure taken from Ref. [115].

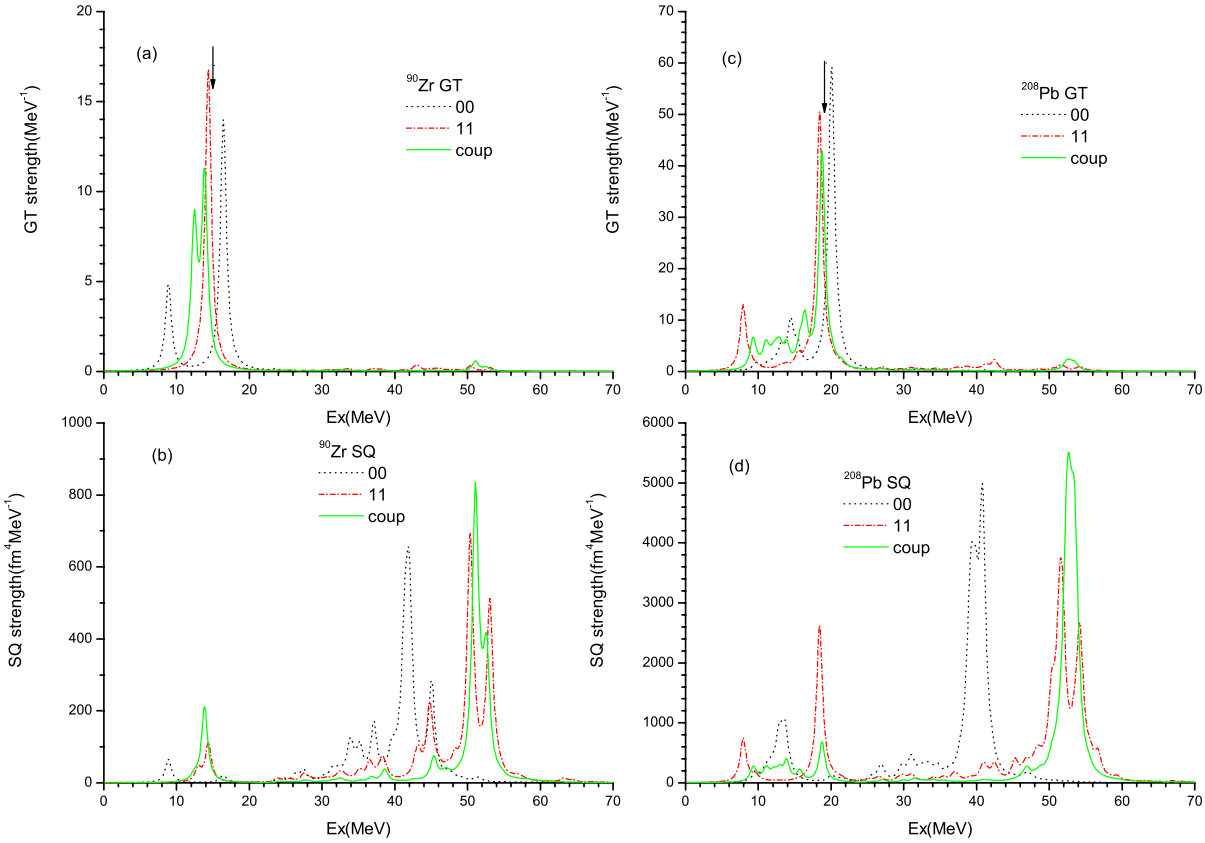

Figure 21: RPA results for the GT$_-$ and SQ$_-$ strength in ^{90}Zr and ^{208}Pb. The results labeled by 00 correspond to neglecting the tensor terms both in HF and RPA, while 11 corresponds to including the tensor terms both in HF and RPA without the coupling between GT and SQ states. The solid line includes full tensor correlations, with the coupling between GT and SQ states. The RPA results are displayed by smoothing them with Lorentzian weighting function having 1 MeV width. Figure taken from Ref. [115].

Table 3: Values of the EWSRs $m_-(1)$ for ^{90}Zr and ^{208}Pb in different excitation energy regions. The results labeled by 00 correspond to neglecting the tensor terms both in HF and RPA; 10 corresponds to including the tensor terms in HF but neglecting them in RPA; 11 corresponds to including the tensor terms both in HF and RPA. See the text for a discussion of the effects of the tensor terms.

	type of RPA calculation	$m_-(1)$ 0-30 MeV	$m_-(1)$ 30-60 MeV	$m_-(1)$ total	$m_+(1)$ total
^{90}Zr	00	395	26.2	421.8	10.1
	10	444	22	466	11.1
	11	366.9	122	493.2	10.3
^{208}Pb	00	2080	124.5	2212.8	18.8
	10	2176	93	2269	21
	11	1658	694	2370	19.3

tensor terms in HF plus RPA calculations. We can also consider the values of the NEWSR in the 0-30 MeV and 30-60 MeV energy regions for ^{90}Zr and ^{208}Pb. When the tensor is not included in the residual interaction (i.e., the calculations labeled by 00 and 10), the values of the NEWSR in the energy region between 30-60 MeV for both ^{90}Zr and ^{208}Pb are small, only few % of EWSR (see the Figs. 20(a) and 21(a)). But in the case 11, about 10% of the NEWSR is shifted from the lower energy region to the higher energy region (corresponding to 25% and 29% of the EWSR in ^{90}Zr and ^{208}Pb, respectively). Moreover, we can see that essentially no unperturbed strength appears in this region (see the Figs. 20(a) and 21(a)). This means that including tensor terms in the RPA calculations shifts about 10% of the GT strength to the energy region 30-60 MeV. While 2p-2h couplings will increase further these high energy strength, we can stress that the tensor correlations move substantial GT strength from the low energy region 0-30 MeV to the high energy region 30-60 MeV even within the 1p-1h model space. The coupling between GT and SQ states is responsible for this quenching. Without the tensor interaction, the coupling is almost nothing, but it becomes substantial when the tensor interaction is switched on. This strong coupling can be seen clearly by a decomposition of the tensor interaction into the spin-multipole couplings as will be given in Eq. (64).

In ^{90}Zr, from Fig. 20(a) one can notice that the GT strength is concentrated in two peaks in the region below 30 MeV. There there are only two important configurations involved which are $(\pi 1g_{9/2} - \nu 1g_{9/2}^{-1})$ and $(\pi 1g_{7/2} - \nu 1g_{9/2}^{-1})$ (see Fig. 20(b)). When the tensor term is included only in HF and neglected in RPA, the centroid in the energy region 0-30 MeV is moved upwards by about 1.5 MeV, and the higher energy peak at $E_x \approx 16$ MeV is moved upwards by only 0.5 MeV, as compared with the results without tensor term. When the tensor term is included both in HF and RPA, the centroid of the GT strength in the energy region 0-30 MeV is moved downwards by about 1 MeV, and the higher energy peak is also moved downwards by about 2 MeV, as compared with the results obtained without tensor term. Including tensor terms in RPA makes the two main separated peaks closer (this situation also happens for ^{48}Ca). This can be understood as a typical effect of the tensor correlations on the single-particle states (cf. Sec. 3.2). When the $\nu 1g_{9/2}$ orbit is filled by neutrons, the tensor correlations provide some quenching of the spin−orbit splitting between $\pi 1g_{9/2}$ and $\pi 1g_{7/2}$ orbits so that the unperturbed energies of the two main p-h configurations $(\pi 1g_{7/2} - \nu 1g_{9/2}^{-1})$ and $(\pi 1g_{9/2} - \nu 1g_{9/2}^{-1})$ are closer in energy. The RPA results in Fig. 20(a) labelled by (10) and (11) reflect these changes of the HF single particle energies due the tensor correlations and the energy difference between two peaks is narrower.

In ^{208}Pb, from Fig. 21(a) we see that the GT strength is concentrated in two peaks in the low energy region 0-30 MeV for all cases 00, 10 and 11. There are eleven important configurations which contribute to these peaks. When the tensor terms are only included in HF and neglected in RPA, the centroid of these peaks is moved upwards by about 0.5 MeV, and the higher energy peak at $E_x \approx 18$ MeV is also

raised by about 0.8 MeV. When the tensor terms are included in both HF and RPA, the centroid of the peaks in the energy region 0-30 MeV moves downward by about 1.5 MeV, and the higher energy peak moves also downwards by about 3.3 MeV, compared with the result obtained without tensor terms. By including tensor terms in the RPA calculation, the GT strengths in the energy region 30-60 MeV are increased substantially by the shift of the strength in the energy region of 0-30 MeV through the tensor force.

The tensor interaction is spin-dependent, so we expect that it can have important effects not only on the GT transitions, but also on spin-dipole and other spin-dependent excitation modes as well. These issues will be discussed in the next subsection.

3.6.2 Spin-Dipole states

The study of the charge-exchange spin-dipole (SD) excitations of ^{208}Pb (inspired by recent accurate measurements [123]) and of ^{90}Zr will be shown to elucidate in a quite specific way the effect of tensor correlations. To get an unambiguous signature of the effect of the tensor force, which is strongly spin-dependent, one can expect that the separation of the strength distributions of the $\lambda^\pi = 0^-$, 1^- and 2^- components is of great relevance.

We will discuss here calculations that employ two different Skyrme parameter sets, namely the set T43 of Ref. [58] the set SLy5+T$_w$ that is a set in which the tensor terms are added on top of the existing force SLy5, in a perturbative way [116]. One should notice that the tensor part of SLy5+T$_w$ is different from that of SLy5+T which was introduced in Ref. [55] and discussed in the previous Sections. In Ref. [117], results obtained with the other forces T11, T22, T33, and T44 were also studied. The values of T, U, α and β for the adopted interactions are listed in Table 4.

Table 4: The tensor strength parameters T and U of Eq. (15) as well as the α and β values of Eq. (19). All values are in MeV·fm^5.

Force	T	U	α_T	β_T	α_C	β_C
SLy5+T$_w$	820.0	323.4	134.76	238.2	80.2	-48.9
T43	590.6	-147.5	-61.5	92.3	121.5	27.7

Table 5: The SD sum rules $m_-(0)$ and $m_-(1)$ for ^{208}Pb with and without the tensor terms. ΔE is the difference between the values of $m_-(1)/m_-(0)$ calculated with and without tensor.

		without tensor			with tensor			
force	λ^π	$m_-(0)$	$m_-(1)$	$m_-(1)\ /m_-(0)$	$m_-(0)$	$m_-(1)$	$m_-(1)/m_-(0)$	ΔE
SLy5 +T$_w$	0^-	158.6	4718	29.7	171.9	5138	29.9	0.2
	1^-	432.0	11746	27.2	440.0	10111	23.0	−4.2
	2^-	646.0	13742	21.3	657.4	14008	21.3	0
	sum	1236.6	30206	24.4	1269.3	29256	23.0	−1.4
T43	0^-	154.8	4693	30.3	164.0	6170	37.5	7.2
	1^-	440.3	12138	27.6	444.1	10366	23.3	−4.3
	2^-	645.5	14067	21.8	649.4	14675	22.6	0.8
	sum	1240.6	30898	24.9	1257.5	31211	24.8	−0.1

The charge-exchange SD operator is defined as

$$O^\lambda_\pm = \sum_i t^i_\pm r_i \left[Y_1(\hat{r}_i) \otimes \sigma^i\right]_\lambda . \tag{61}$$

The $n-$th energy weighted sum rules m_n for the λ-pole SD operator are defined as

$$m_n^\lambda(t_\pm) = \sum_i E_i^n |\langle i|O_\pm^\lambda|0\rangle|^2, \tag{62}$$

and the model-independent sum rule which is known to hold is

$$m_0^\lambda(t_-) - m_0^\lambda(t_+) = \frac{2\lambda+1}{4\pi}(N\langle r^2\rangle_n - Z\langle r^2\rangle_p), \tag{63}$$

where $\langle r^2\rangle_n(\langle r^2\rangle_p)$ is the mean square radius of neutrons (protons).

As above, we will discuss two kinds of calculations. In the first one, the tensor terms are neither included in HF nor in RPA. In the second one, the tensor terms are included both in HF and in RPA. In Section 3.6.1, it has been found that the effect of tensor correlations in HF is large for the Gamow-Teller mode. This is largely due to the fact that the unperturbed GT transitions are exactly those among spin-orbit partners. On the other hand, this is not the case for the SD transitions: the average unperturbed energies are not much affected by the spin-orbit splittings since they are $1\hbar\omega$-type excitations. The numerical results of the HF+RPA calculations with the forces T43 and SLy5+T$_w$ are shown in Fig. 22. They are compared with experimental data obtained by multipole decomposition analysis of the (p,n) reaction data and extraction of the strength functions by means of Distorted Wave Impulse Approximation (DWIA) calculations [123]. From Fig. 22(a) and (b) one can see that in the case of the T43 interaction the main peaks of the 0^- and 1^- strength distributions are shifted upwards by about 7.5 MeV and downwards by about 5 MeV, respectively, due to the tensor correlations. There are several 2^- peaks (cf. Fig.22(c)). The peak at excitation energy $E_x \approx 17.7$ MeV is moved upwards by about 2 MeV by including tensor forces, and comes close to an experimental peak, while another peak at $E_x \approx 3.9$ MeV is shifted downwards by about 0.6 MeV and is also eventually close to the observed low energy peak. For the total SD strength in Fig. 22(d), it is remarkable that the main peak at 26 MeV is shifted to 21 MeV when tensor is included, and this provides good agreement with the experimental data.

In the same figure, the SD strength distributions in ^{208}Pb calculated by using the set SLy5+T$_w$ are also shown. From Fig. 22(e), we see that the calculated 0^- strength is concentrated in one peak which is shifted upwards by about 1.3 MeV by the tensor correlations. In Fig. 22(f), the RPA tensor correlations move the 1^- peak downwards and split it into three peaks, in qualitative agreement with the bump-like experimental strength. In the case of the 2^- component [Fig. 22(g)], the main peaks in the high energy region are rather near to the experimental main peak. Therefore, as shown in Fig. 22(h), the inclusion of the tensor terms in HF+RPA can make the calculated main peak of the total SD strength coincide with the main measured peak. However, in the low energy region the agreement is not good compared with the experimental result in the case of SLy5+T$_w$. The sum rule analysis of the SD excitations can be seen in Table 5. The general trends of the excitation energies of the SD peaks are also reflected in the average energies $m_-(1)/m_-(0)$ as one can deduce from the values of ΔE in the last column of the Table. The absolute values $m_-(0)$ and $m_-(1)$ are also affected by the tensor interaction, but at most at the one or few % level.

We would like at this stage to obtain a better understanding of this peculiar role of tensor interactions. The diagonal matrix element of their triplet-even (TE) term on a state with multipolarity λ can be expressed as [124]

$$\begin{aligned} V_{TE}^{(\lambda)} &= \frac{5T}{4}\sum_{\ell,k,k'} \frac{(-)^{k+k'+\lambda+\ell+1}\hat{k}\hat{k'}}{2\lambda+1} \left\{ \begin{array}{ccc} k & k' & 2 \\ 1 & 1 & \ell \end{array} \right\} \\ &\times \left\{ \begin{array}{ccc} 1 & 1 & 2 \\ k' & k & \lambda \end{array} \right\} \langle p||\hat{O}_{k',\lambda}||h\rangle\langle p||\hat{O}_{k,\lambda}||h\rangle^*, \end{aligned} \tag{64}$$

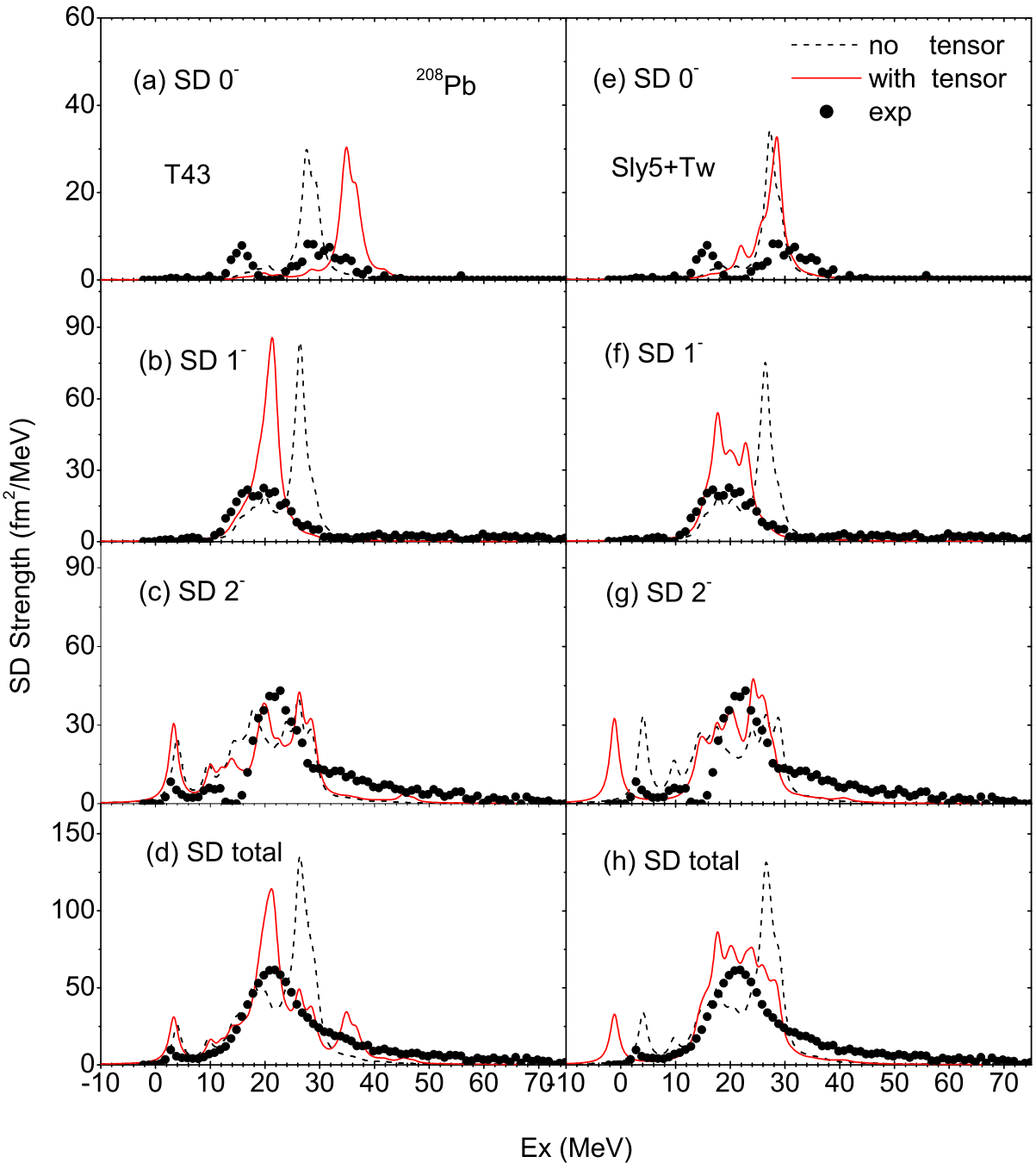

Figure 22: Charge-exchange SD$_-$ strength distributions in ^{208}Pb. In the panels (a), (b), and (c) the RPA results obtained by employing the interaction SLy5+T$_w$ for the multipoles 0^-, 1^-, 2^- are displayed. In panel (d) we show the total strength distribution. Panels (e), (f), (g) and (h) correspond to similar results when the parameter set T43 is employed. All these discrete RPA results have been smoothed by using a Lorentzian averaging with a width of 2 MeV and compared with experimental findings. The excitation energy is with respect to the ground state of ^{208}Bi. The experimental data are taken from Ref. [123]. See the text for details and discussion. Figure taken from Ref. [116].

in terms of the reduced matrix elements of the operator $\hat{O}_{k,\lambda} = \sum_i [\sigma_i \otimes (\nabla_i \otimes Y_\ell(i))^{(k)}]^{(\lambda)}$ and $6j$ symbols. In Eq. (64), the notation $\hat{k} \equiv \sqrt{2k+1}$ is used. For GT case with $\lambda = 1$, there are the ph matrix elements not only with k=k'=0, but also with k=0 (2) and k'=2(0). The latter makes possible the coupling between GT and SQ states which are not connected directly by other terms of the Skyrme interactions. For the SD excitations, taking $\ell = 0$ and k=k'=1, Eq. (64) gives

$$V_{TE}^{(\lambda)} = -\frac{5}{12} T \left\{ \begin{array}{c} 1 \\ -1/6 \\ 1/50 \end{array} \right\} |\langle p||\hat{O}_{1,\lambda}||h\rangle|^2 \text{ for } \lambda = \left\{ \begin{array}{c} 0^- \\ 1^- \\ 2^- \end{array} \right\}. \tag{65}$$

The TO tensor part is also expressed in a similar way as

$$V_{TO}^{(\lambda)} = \frac{5}{12} U \left\{ \begin{array}{c} 1 \\ -1/6 \\ 1/50 \end{array} \right\} |\langle p||\hat{O}_{1,\lambda}||h\rangle|^2 \text{ for } \lambda = \left\{ \begin{array}{c} 0^- \\ 1^- \\ 2^- \end{array} \right\}. \tag{66}$$

We can see in Eqs. (65) and (66) that the diagonal p-h matrix element in the 0^- case is the largest, and that for 1^- is the next. The effect on 2^- is rather small. It should be noticed that these relative strengths of the Skyrme tensor interactions on each multipole are similar to those obtained from the finite-range tensor interactions both in magnitude and in sign [125]. We can sum the TE and TO direct matrix elements as

$$V_T^{(\lambda)} = V_{TE}^{(\lambda)} + V_{TO}^{(\lambda)} \equiv a_\lambda T + b_\lambda U. \tag{67}$$

The proper antisymmetrization is easy to obtain for contact interactions and gives, in the isovector channel,

$$V_{T,AS}^{(\lambda)} = [-\frac{1}{2} a_\lambda T + \frac{1}{2} b_\lambda U] \langle \vec{\tau}_1 \cdot \vec{\tau}_2 \rangle. \tag{68}$$

Since the coupling constant T is positive for the interactions we considered, $V_{TE}^{(\lambda)}$ is repulsive for the 0^- and 2^- case, while it is attractive for 1^- . The $V_{TO}^{(\lambda)}$ part may contribute with the same sign as the $V_{TE}^{(\lambda)}$ one if the value of U is negative. For the TIJ family, the value of U is negative or small positive, so that the $V_{TO}^{(\lambda)}$ contributions have the same multipole dependence or almost negligible. All together, the tensor correlations are strongly repulsive for 0^- and weakly repulsive for 2^- in general. For 1^-, the net effect will be attractive. For SLy5+T$_w$, the value of U is positive and will give opposite contributions to those of T. However, the T value is much larger than the value of U so that the same argument given for the TIJ family will hold. One can see from Table 5 that Eq. (68) provides a very effective guideline for interpreting the numerical results of microscopic RPA.

In conclusion, in the case of the charge-exchange t_- SD excitations of ^{208}Pb it has been clearly demonstrated that tensor correlations have a specific multipole dependence, that is, they produce a strong hardening effect on the 0^-mode and a softening effect on the 1^- mode. A weak hardening effect is also observed on the 2^- mode. These characteristic effects of the tensor force can be understood by using analytic formulas based on the multipole expansion of the contact tensor interaction, and are confirmed by the favourable comparison with the experimental data.

In Ref. [117], the constraints set on the tensor force by both GT and SD excitations are summarized. It is found that T and U can be restricted in a range that has a reasonable overlap with the values discussed in Sec. 3.2, namely β positive and α negative (cf. Fig. 4 of Ref. [117] and corresponding discussion).

3.7 β-decay

Quite recently, the impact of the tensor correlations on β-decay has been discussed in Ref. [126]. In keeping with our previous discussion about Gamow-Teller transitions, a significant effect can be expected. However, no study has been performed earlier despite the difficulty that mean-field calculations

have in reproducing the experimental data for β-decay. Using Skyrme interactions, the work of Ref. [127] was the first to demonstrate that a fully self-consistent Quasiparticle RPA (QRPA) calculation of β-decay tends to overestimate the experimental half-lives. The proton-neutron ($T = 0$) pairing residual force can produce an additional attractive effect and bring the half-lives in agreement with data. In fact, the proton-neutron $T = 0$ pairing cannot be constrained by ground-state data and escapes, strictly speaking, the philosophy of self-consistent mean-field: its strength is a free parameter. It is of obvious interest to assess if the agreement with β-decay data can also be improved by including tensor correlations, whose parameters can be checked by using all observables that we have discussed so far in the present review paper. Moreover, one should add that the effect of proton-neutron pairing is expected to weaken going towards drip-line nuclei, and among the nuclei that undergo β-decay there are magic nuclei in which pairing is negligible anyway.

The authors of Ref. [126] have studied the effect of tensor on β-decay based on forces with reasonable values of the Landau parameters, that is, of the spin and spin-isospin residual forces, in order to avoid the shortcomings that we have described in connection with the M1 resonance in Sec. 3.4. However, they have used tensor forces that are added perturbatively on top, respectively, of the Skyrme sets SkO [83] and SkX [71].

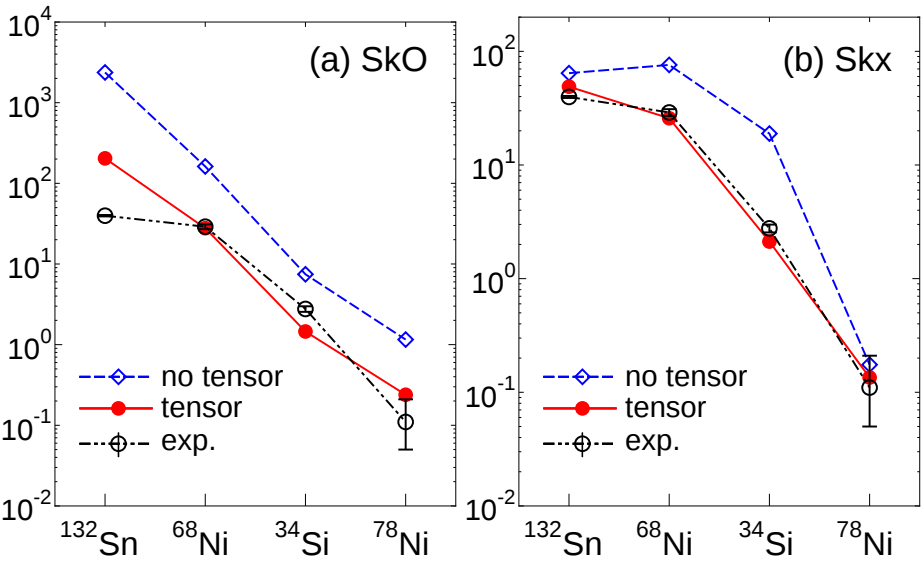

Figure 23: Half-lives of several nuclei obtained in QRPA with the SkO and SkX interactions, with and without tensor added. Figure taken from [126].

Some of the results obtained in Ref. [126] are displayed in Figs. 23 and 24. The strong effect of the tensor correlations on the half-lives is visible and quite remarkable in case of both Skyrme sets considered. In particular, in the case of SkX plus tensor, the result with tensor included can reproduce the experimental values of the half-life in all the nuclei shown in Fig. 23. These nuclei are not amenable to a description including pairing, and their half-lives span about three orders of magnitude. As is well known, both matrix elements and Q-values play a role in such kind of calculations. Fig. 24 demonstrates that both for the Q-value and $\log(ft)$ values it is crucial to take into account tensor correlations both in the HF mean-field and residual interaction.

4 Instabilities

Recently, there has been much interest in detecting possible instabilities associated with the widely used energy density functionals. Instabilities could manifest themselves in several possible ways but

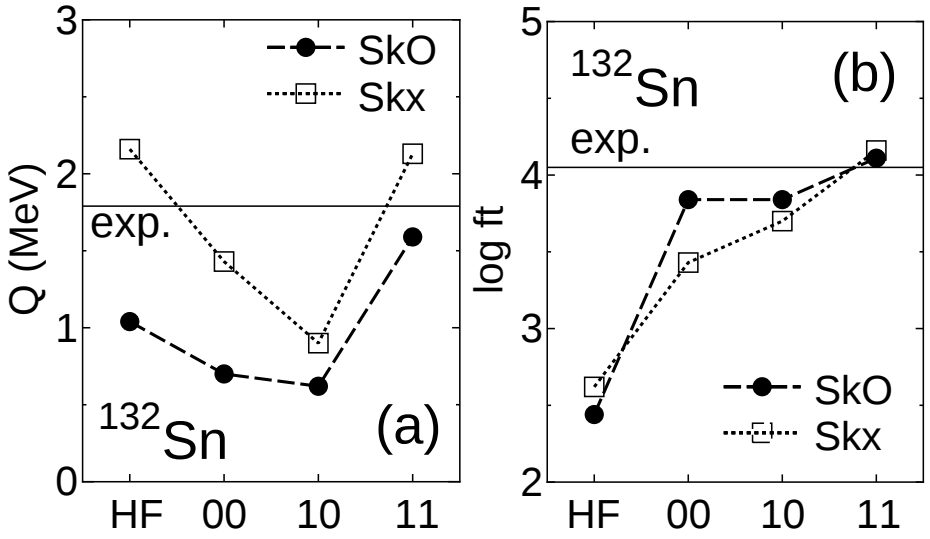

Figure 24: Q-values and log(ft) values of ^{132}Sn obtained within the same framework as in the previous figure. Figure taken from [126].

in all cases the system must be subject to an external perturbing field if one wishes to detect those instabilities.

If the perturbation brings zero momentum ($\vec{q} = 0$), or infinite wavelength, we are in the so-called Landau limit. This case has been studied within the Landau's theory of Fermi liquids, that has been extended by Migdal and collaborators to the case of finite Fermi systems like atomic nuclei [128]. In the Landau-Migdal's theory the key quantity is the interaction V acting among quasiparticles around the Fermi surface, whose matrix elements are written in the momentum space as

$$\langle \vec{k}_1 \vec{k}_2 | V | \vec{k}_1 \vec{k}_2 \rangle = N_0^{-1} (F(\vec{k}_1 \vec{k}_2) + F'(\vec{k}_1 \vec{k}_2)\tau_1\tau_2 + G(\vec{k}_1 \vec{k}_2)\sigma_1\sigma_2 + G'(\vec{k}_1 \vec{k}_2)\tau_1\tau_2\sigma_1\sigma_2), \tag{69}$$

where $N_0 = 2k_F m^*/\hbar^2\pi^2$ is the density of states per energy at the Fermi surface and m^* is the effective mass. The single-particle momenta $\vec{k_1}$ and $\vec{k_2}$ are, in fact, taken exactly at the Fermi surface: then, in homogeneous matter, the so-called Landau parameters F, F', G and G' are only functions of the angle θ between $\vec{k_1}$ and $\vec{k_2}$ and can be consequently expanded in Legendre polynomials:

$$F = \sum_l F_l P_l(cos\theta), \tag{70}$$

and likewise for F', G and G'. In order for a spherical Fermi surface to be stable against any deformation, the parameters must satisfy the criterion

$$F_l > -(2l+1), \tag{71}$$

and analogous criteria for all the other parameters. We remind that the Landau parameters defined in this way have no dimension: the units are chosen so that the change $F_l/(2l+1)$ in the potential energy is accompanied by a change 1 in the kinetic energy. For any given interaction, like the Skyrme or Gogny interaction, the Landau parameters can be estimated by calculating matrix elements on a plane wave basis and by comparing with Eq. (69). As we stress again, all states are considered at the Fermi surface and the initial and final relative momenta $\vec{k}$ and $\vec{k}'$ are equal in Eq. (69); therefore, the momentum transfer $\vec{q} \equiv \vec{k} - \vec{k}'$ vanishes as we mentioned at the start of this paragraph. The inequality (71) ensures that the system is free from zero-momentum or long-wavelength instabilities. This equality must be satisfied by the Landau parameters for every value of l. For the Skyrme force, only $l = 0, 1$ Landau

parameters do not vanish and have to be considered. This is not the case for the Gogny interaction (see below).

Tensor components can be added to V and Eq. (69) has to be modified accordingly. The effects of tensor forces within the Landau-Migdal framework has been considered for the first time in Ref. [129] (see also [130, 131]). Using the convention of Ref. [129], the tensor terms

$$\Big(\frac{q_k^2}{k_F^2}H(cos\theta) + \frac{q_k^2}{k_F^2}H'(cos\theta)\vec{\tau}_1\vec{\tau}_2\Big)S_{12}(\hat{q}_k) \tag{72}$$

are added to the interaction (69). Here $\vec{q}_k = \vec{k}_1 - \vec{k}_2$ with $\vec{k}_1$ and $\vec{k}_2$ again lying at the Fermi surface, and

$$S_{12}(\hat{q}_k) = 3\vec{\sigma}_1 \cdot \hat{q}_k\vec{\sigma}_2 \cdot \hat{q}_k - \vec{\sigma}_1 \cdot \vec{\sigma}_2, \tag{73}$$

where $\hat{q}_k$ denotes the unit vector in the direction of $\vec{k}_1 - \vec{k}_2$. H and H' can be expanded in principle on the Legendre polynomials in the same way as in Eq. (70). The stability conditions of nuclear matter in the spin and spin-isospin channels will be affected by the tensor interaction. One must consider spin and isospin degrees of freedom, and impose that the Fermi surface is stable under generalized deformations. The resulting stability conditions have been studied (see, e.g., Ref. [130]). The associated equations, that generalize Eq. (71), can be found in Refs. [130, 124] and will not be reported here for the sake of brevity. However, it is useful to remind that since the tensor force couples $\vec{l}$ and $\vec{s}$ (the spin-orbit force does not act in uniform matter), the deformations of the Fermi surface have J^π as quantum numbers. For $l = 1$, one has three independent deformations associated with $0^-, 1^-$ and 2^-. For 1^+ one has two coupled equations associated with $l = 0$ and $l = 2$. All these equations that guarantee stability must be checked separately for the isoscalar and isovector case.

In Ref. [124] a very careful study of the stability of a large set of Skyrme forces plus tensor has been performed. The main conclusions of this work are: (i) instabilities occur for all the considered sets at some value of critical density ρ_C; (ii) if applications for finite nuclei are envisaged (excluding systems like neutron stars), pushing the value of the critical density above ≈ 1.5 or 2 times the saturation density may be satisfactory enough, and this can be obtained for some limited values of the parameters in (α, β) plane; (iii) a full variational procedure to determine the Skyrme parameters is preferable to a perturbative adding of the tensor terms also from the point of view of avoiding instabilities.

Later, the question has been raised above the finite-$\vec{q}$ instabilities. This sort of discussion has been initially driven by some sparse findings that are not, at first sight, easy to be cast in a unifying picture. One of such findings has been that in HF calculations with some Skyrme forces, even when performed for standard double magic nuclei, after a sufficiently long number of iterations the system converges to an unphysical state in which proton densities and neutron densities are separated apart [132]. Another case of instability occurred in cranked-HFB calculations performed in ^{194}Hf, where it has been found that in certain cases the system was converging to a polarised state, namely a spin phase-transition was taking place [39]. One may be tempted to associate these situations with the instabilities that manifest themselves through imaginary eigenvalues in the response of the system to an external field, although no formal proof exist, to our best knowledge, of a relationship between the aforementioned situations and the imaginary eigenvalues.

In order to explore systematically the finite-$\vec{q}$ instabilities, thanks to the Lyon group [100], a general response function formalism has been developed for a Skyrme force including central, spin-orbit and tensor terms. This formalism has been applied to symmetric unpolarised nuclear matter with the purpose of detecting the appearance of imaginary eigenvalues. This work has generalised the previous works of Refs. [133, 134]. The response function of uniform matter is labelled by the indices corresponding to the total spin and isospin (S and I) as well as by those corresponding to their projection on the quantisation axis (M and Q). The quantisation axis is chosen in the direction of the transferred

momentum $\vec{q}$. The label α denotes the set (S, M; I, Q). To find the response function $\chi^{(\alpha)}(q,\omega)$ one starts by solving the Bethe-Salpeter equation,

$$G^{(\alpha)}_{\rm RPA}(q,\omega,\vec{k}_1) = G^{(\alpha)}_{\rm HF}(q,\omega,\vec{k}_1) + G^{(\alpha)}_{\rm HF}(q,\omega,\vec{k}_1)\sum_{\alpha'}\int \frac{d^3k_2}{(2\pi)^3} V^{(\alpha,\alpha')}_{\rm ph}(q,\vec{k}_1,\vec{k}_2) G^{(\alpha')}_{\rm RPA}(q,\omega,\vec{k}_2). \tag{74}$$

This equation is written in terms of the HF Green's function $G_{\rm HF}$ and of the particle-hole interaction $V_{\rm ph}$ derived consistently from the starting Skyrme force. Once this is solved and the RPA Green's function $G_{\rm RPA}$ is known, the response function can be easily found as

$$\chi^{(\alpha)}_{\rm RPA}(q,\omega) = g\int \frac{d^3k_1}{(2\pi)^3} G^{(\alpha)}_{\rm RPA}(q,\omega,\vec{k}_1), \tag{75}$$

where g is the degeneracy factor (4 in the case of symmetric unpolarised nuclear matter). Finally, the main quantity of interest is the strength function defined as

$$S^{(\alpha)}(q,\omega) = -\frac{1}{\pi}\, Im\ \chi^{(\alpha)}(q,\omega). \tag{76}$$

The main finding of Ref. [100] has been that the tensor force significantly affects the $S=1$ strength functions. At a critical density ρ_c, the strength function is found to diverge for finite values of q. This critical density may be lower than the critical density at which the strength function diverges for $q=0$ (this latter divergence coincides, at zero momentum, with the instability defined in terms of the Landau parameters and discussed in the first part of this Section). Intuitively, while the strength function divergence (*viz.* instability) at zero momentum can be thought to concern the whole uniform medium, the same phenomenon at finite q can be associated with a finite size instability taking place in a domain whose scale is $\Delta R \approx 2\pi/q$. On a principle basis, this could be tolerable if the momentum scale (the real space scale) are much larger (much smaller) than that which matters for low-energy nuclear physics. However, for practical purposes, it may be of great advantage to dispose of functionals that are free from those pathologies.

The work of Ref. [100] has been extended to a functional (not necessarily derived from an Hamiltonian) in Ref. [135]. One of the main goals of this paper is also to find an efficient way to detect the instabilities. It has been found that the poles in the response function manifest themselves in the inverse energy-weighted sum rule m_{-1}. We remind that, given the strength function $S(\omega)$, the sum rule m_k is defined as

$$m_k = \int d\omega\ \omega^k S(\omega).$$

Thus, if instabilities manifest themselves as eigenvalues that become zero or imaginary, the associated inverse-energy weighted sum rule will have a pole. The advantage of seeking a pole by directly analyzing the inverse energy-weighted sum rule is that this has an analytical expression which can be calculated quite fast. Using this method, in Ref. [135] a thoroughly analysis of the poles revealing instabilities in the known Skyrme functionals, has been undertaken. We display in Figs. 25 and 26 some results obtained with the method of Ref. [135], in the case of the Skyrme forces SGII [104], SLy5 [73], T43 and T44 [58]. In symmetric nuclear matter, one finds the previously known spinoidal (i.e., mechanical) instability that corresponds to the $S=0, M=0, I=0$ channel. The presence of tensor terms favours the rise of instabilities, as is visible in Fig. 25 by comparing T43 and T44 (that have been discussed in the previous Sections) with SLy5 and SGII. This feature remains true if we look at the case of neutron matter. Thus, the functionals TIJ are, generally speaking, very much plagued by instabilities. The Lyon group is presently working to include in the fitting protocol of a Skyrme functional the requirement that no instability should manifest at least at a density smaller than ≈ 1.2 times the saturation density. Probably the question about a maximum q to be considered should be raised.

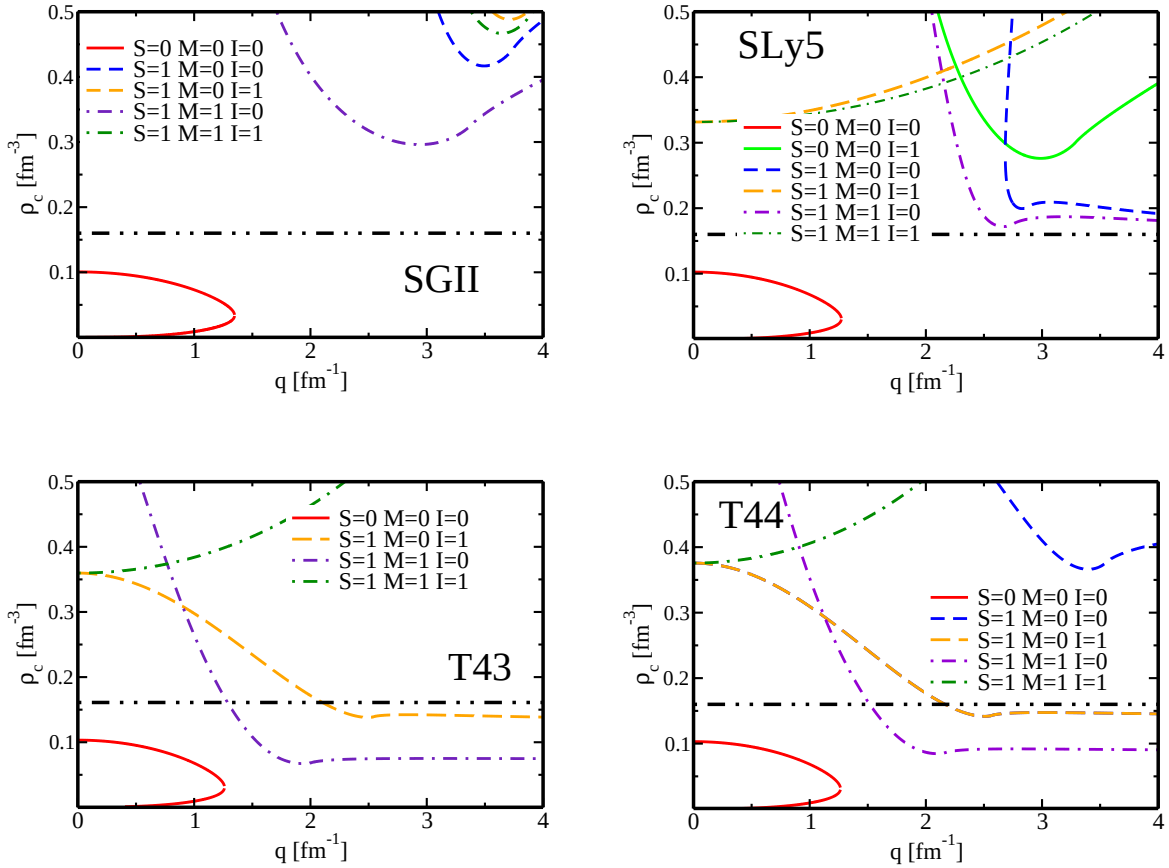

Figure 25: Critical densities ρ_C as functions of the transferred momentum q, in symmetric nuclear matter. These critical densities have been extracted from the poles of the inverse energy-weighted sum rule. They are displayed for different channels, and compared with the saturation density (horizontal line). This figure [136] is analogous to Figs. 6 and 7 of Ref. [135]. See the text for a short discussion.

In the work of Ref. [13] an interesting comparison between instabilities induced by zero-range and finite-range interactions is carried out. It has been shown that in the case of zero-range interactions the addition of tensor terms favours the appearance of instablities but this is not the case for the finite-range forces. For instance, the force M3Y-P2 [51] is quite free from instabilities although containing a genuine tensor part. Another interesting point of Ref. [13] is that the authors have shown that instabilities manifest themselves in another quantity that is easier to calculate than the full response function, namely the spin susceptibility that is obtained as a proper limit to zero energy and momentum transfer of Eq. (75). The spin susceptibility can be written as $\chi_{\rm RPA}(0)$. Its values, as a function of the density, are displayed in Fig. 27 in the case of neutron matter. Given that realistic interactions can be employed to perform reliable *ab-initio* calculations of neutron matter, and these calculations do not show any trace of ferromagnetic instablities, it is interesting to compare the associated values of spin susceptibility with those exracted from effective interactions that can also include tensor terms. The values of spin susceptibility from realistic interactions have still some error bar, as it is evident from Fig. 27; however, the trend of the spin susceptibility is better followed by finite-range forces like M3Y-P2 and D1MT.

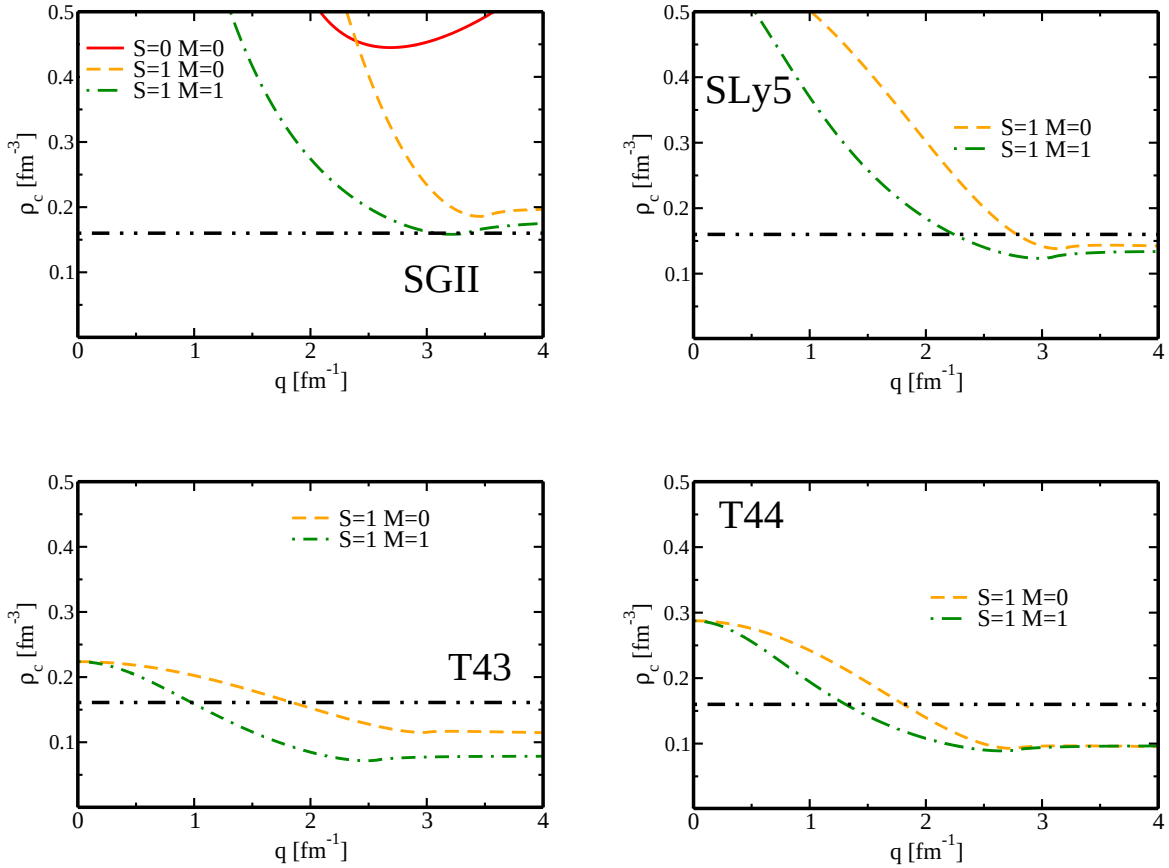

Figure 26: The same as Fig. 25 in the case of pure neutron matter [136].

5 Conclusions and future perspectives

There has been a lively debate on the role of the tensor force in nuclear structure. While in light nuclei the tensor force manifests itself in the form of the bare force, which is well known from textbooks in the deuteron case, the situation is less clear in medium-mass or heavy nuclei. The question about the role of the tensor force in the effective theories for medium-heavy nuclei, like self-consistent mean-field or DFT, has been raised because of the suggestion that the tensor force plays a crucial role for the shell evolution far from the valley of stability, towards the proton or neutron drip lines. At the same time, it is expected that the tensor force is also important for spin and spin-isospin states. In this review article, we discussed extensively the role of tensor interactions not only on the ground state properties (the binding energies, the single-particle states and the deformations), but also on the excited states (M1 states, GT states, SD states and the rotational bands). We compared also several different approaches to disentangle the effect of tensor correlations on nuclear structure problems, i.e., Skyrme Hamiltonians, Skyrme EDFs, RHF and finite-range Gogny tensor interactions.

Several groups have attacked the problem of the tensor force. In some cases, the characteristic feature of the bare proton-neutron tensor force has been used as a guideline for the tensor interaction in the nuclear medium: we refer to its attractive (repulsive) character in the case in which the spins are aligned with (perpendicular to) the relative distance. In other cases, the philosophy has been completely different: based on the idea that in complex nuclei, the major effect of the tensor force is often taken care of by central terms, the parameters of the tensor force have been treated as completely free. We have tried, in the present review paper, to discuss with some care the relationships between the bare tensor

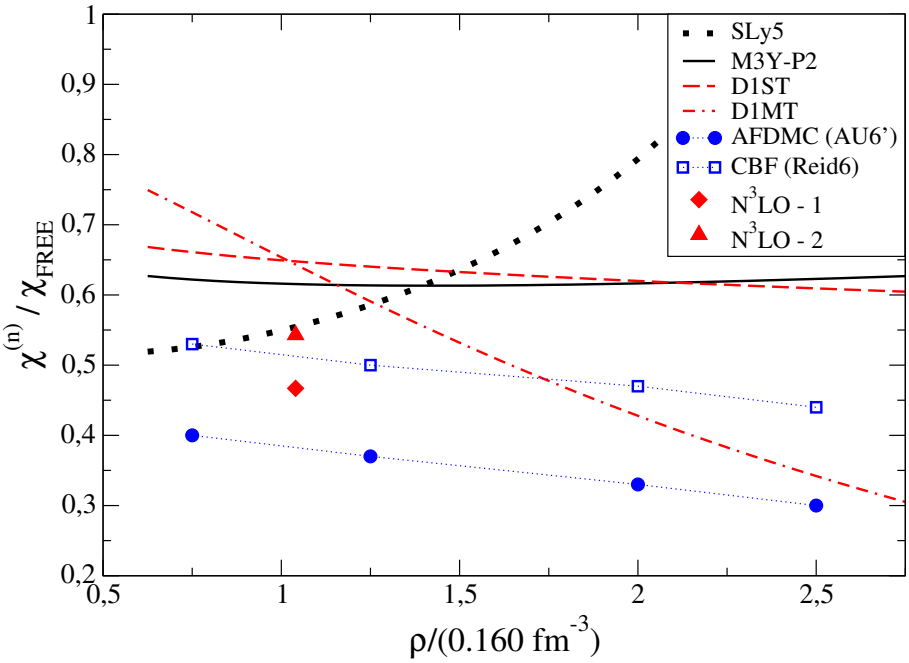

Figure 27: Spin susceptibility of neutron matter (expressed as a ratio of the free susceptibility) as a function of the density. Results for both phenomenological and realistic interactions are shown. All of them include tensor terms. Figure taken from Ref. [13].

force, and the effective tensor implemented either in relativistic Hartree-Fock or in the non-relativistic zero-range and finite-range frameworks.

The main difficulty faced by the works of many authors has been that of finding unambiguous signatures of the tensor force. In fact, in self-consistent mean-field or DFT, strictly speaking all parameters are coupled and the specific effects of e.g. the tensor terms are not at all easy to disentangle.

Based on the work of Ref. [10], many papers have tried to find a signature of the tensor force in the evolution of the single-particle states along isotopic or isotonic chains. We have reviewed all these activities, that has led to two main conclusions. In most of the cases, evidence has been found of a strong attraction between neutrons and protons lying respectively in $j = l + \frac{1}{2}$ and $j = l - \frac{1}{2}$ orbits; this interaction becomes instead repulsive when the neutron and the proton lie both in the same $j = l + \frac{1}{2}$ orbit, or in the same $j = l - \frac{1}{2}$ orbit. The interaction between equal particles is far less clearly established, although it seems that it has the opposite sign. If one tries to explain systematically the single-particle spectra based on this picture, however, many contradictions show up. It is not completely clear to which extent these contradictions depend on the specific ansatz (e.g., the Skyrme ansatz), and to which extent they point to more general problems.

Certainly, the single-particle states do not belong, strictly speaking, to the DFT framework, i.e., beyond mean field effects such as the particle-vibration coupling could be very important. Therefore, several groups have tried to pay attention to excited states like spin or spin-isospin modes. The unnatural parity modes, like excited 0^- states, are quite sensitive to the tensor force. Also the 1^+ (M1) resonance and the charge-exchange Gamow-Teller resonance are significantly affected by the tensor force, although these effects cannot be easily separated from other effects. In other words, one could pin down precise values of the tensor force parameters provided the uncertainty on the other terms is much smaller. A very specific signature of the tensor force is the splitting between the different components (0^-, 1^- and 2^-) of the spin-dipole charge-exchange resonance, which has been recently measured in ^{208}Pb and which has to be mainly attributed to the tensor force. Recently, also the β-decay in exotic magic nuclei has been highlighted. These charge-exchange transitions point to values of the tensor force parameters

that turn out to be in reasonable agreement with what extracted from the single-particle states (see the previous paragraph).

In the language which is familiar to Skyrme practitioners, the overall conclusion seems to be that the parameter β [see Eq. (21)] should be definitely positive. The conclusion on α [see Eq. (21)] is less clear although a negative value may be preferable. These signs can be also extracted from Gogny or other finite-range forces as well as from RHF Lagrangians. So far, the isovector-type pion tensor and the ρ tensor interactions are introduced in RHF Lagrangians. It was found that the strength of these tensor interactions are strongly suppressed in the nuclear media to obtain good binding energy systematics and the shell structure of heavy nuclei. It is a challenge to include the isoscalar-type ω tensor interaction to improve further the RHF model [138].

Unfortunately, although there is a general consensus on the fact that a tensor component should be added to all parameter sets, attention has been drawn on the fact that some implementation of the tensor force lead to instabilities of the energy functionals. Spin and spin-isospin instabilities (i.e., transitions to configurations that display spontaneous ferromagnetization) plague many paramatrizations of EDFs that include the tensor force. This is especially true for the Skyrme EDFs. Care should be taken to avoid this.

Ultimately, the introduction of the tensor force has opened several new lines of investigation. The tensor terms in the EDFs cannot be discarded but further analysis of the instabilities, of the properties of spin-isospin transitions and of the correlations associated with single-particle states are called for.

Acknowledgments

This work stems from several previous papers and collaborations and it is our pleasure to acknowledge these collaborations here, in particular with C.L. Bai, P.F. Bortignon, L. G. Cao, S. Fracasso, A. Li, Z.Y. Ma, L. Sciacchitano, F.R. Xu, H.Q. Zhang, X.Z. Zhang, X.R. Zhou and W. Zou. We also acknowledge fruitful discussions with D. M. Brink, G. Co', T. Duguet, M. Grasso, M. Ichimura, H.Z. Liang, W.H. Long, T. Otsuka, H. Sakai, T. Suzuki, N. Van Giai, K. Yako and T. Wakasa. We would also like to warmly thank all those who helped by providing or preparing figures for this paper, namely T. Abe, M. Anguiano, C.L. Bai, G. Co', T. Duguet, M. Grasso, T. Lesinski, W.H. Long, F. Minato, H. Nakada, J. Navarro, T. Otsuka, A. Pastore, A. Polls, and V. Hellemans.

References

[1] H.A. Bethe, Phys. Rev. 57, 390 (1940).

[2] W. Rarita and J. Schwinger, Phys. Rev. 59, 436 (1941).

[3] W. Rarita and J. Schwinger, Phys. Rev. 59, 556 (1941).

[4] J.M. Blatt and V.F. Weisskopf, *Theoretical Nuclear Physics* (Wiley, New York, 1952).

[5] E. Epelbaum, H.-W. Hammer, U.-G. Meissner, Rev. Mod. Phys. 81, 1773 (2009); R. Machleidt and D.R. Entem, Phys. Rep. 503, 1 (2011).

[6] M. Bender, P.-H. Heenen, P.-G. Reinhard, Rev. Mod. Phys. 75, (2003) 121.

[7] I. Tanihata *et al.*, Phys. Rev. Lett. 55, 2676 (1985); P.G. Hansen and B. Jonson, Europhys. Lett. 4, 409 (1987); K. Hagino, I Tanihata and H. Sagawa, "Exotic Nuclei far from the Stability Line" in *100 Years of Subatomic Physics* (edited by E. M. Henley and S. D. Ellis, World Scientific, 2013).

[8] A. Ozawa, T. Kobayashi, T. Suzuki, K. Yoshida and I. Tanihata, Phys. Rev. Lett. 84, 5493 (2000).

[9] N. Paar, D. Vretenar, E. Khan, G. Colò, Rep. Progr. Phys. 70 (2007) 691; D. Savran, T. Aumann, A. Zilges, Prog. Part. Nucl. Phys. 70, 210 (2013).

[10] T. Otsuka *et al.*, Phys. Rev. Lett. 95, 232502 (2005).

[11] F. Osterfeld, Rev. Mod. Phys. 64, 491 (1992).

[12] M. Ichimura, H. Sakai, and T. Wakasa, Prog. Part. Nucl. Phys. 56, 446 (2006).

[13] J. Navarro and A. Polls, Phys. Rev C87, 044329 (2013).

[14] H. Yukawa, Proc. Phys. Math. Soc. Japan 17, 48 (1935).

[15] A. Bouyssy *et al.*, Phys. Rev. C36, 380 (1987).

[16] W.H. Long *et al.*, Phys. Lett. B640, 150 (2006).

[17] W.H. Long *et al.*, Phys. Rev. C76, 034314 (2007).

[18] W.H. Long, private communication.

[19] W.H. Long, N. Van Giai, and J. Meng, Phys. Lett. B640, 156 (2006).

[20] W.H. Long, J. Meng, N. Van Giai, and S.-G. Zhou, Phys. Rev. C69, 034319 (2004).

[21] G.A. Lalazissis, T. Nikšić, D. Vretenar, and P. Ring, Phys. Rev. C71, 024312 (2005).

[22] A.M. Oros, Ph.D. thesis, University of Köln (1996).

[23] H. Liang, N. Van Giai, and J. Meng, Phys. Rev. Lett. 101, 122502 (2008).

[24] T.H.R. Skyrme, Philos. Mag. 1, 1043 (1956).

[25] J.S. Bell and T.H.R. Skyrme 1, 1055 (1956).

[26] T.H.R. Skyrme, Nucl. Phys. 9 (1959) 615.

[27] D. Vautherin and D.M. Brink, Phys. Rev. C5, 626 (1972).

[28] F. Stancu, D.M. Brink, and H. Flocard, Phys. Lett. B68, 108 (1977).

[29] J. Dudek *et al.*, Nucl. Phys. A341, 253 (1980).

[30] M. Ploszajczak and M.E. Faber, Zeit. Phys. A299, 119 (1981).

[31] F. Tondeur, Phys. Lett. B123, 139 (1983).

[32] K.-F. Liu, H. Luo, Z.Y. Ma, Q. Shen, and S.A. Moszkowski, Nucl. Phys. A534, 1 (1991); K-.F. Liu, H. Luo, Z.Y. Ma, Q. Shen, Nucl. Phys. A534, 25 (1991).

[33] M. Moreno-Torres, M. Grasso, H. Liang, V. De Donno, M. Anguiano, and N. Van Giai, Phys. Rev. C81, 064327 (2010).

[34] J.W. Negele and D. Vautherin, Phys. Rev. C5, 1472 (1972).

[35] D.M. Brink and Fl. Stancu, Phys. Rev. C75, 064311 (2007).

[36] T. Neff and H. Feldmeier, Nucl. Phys. A713, 311 (2003); R. Roth, H. Hergert, and P. Papakonstantinou, T. Neff and H. Feldmeier, Phys. Rev. C72, 034002 (2005); R. Roth, P. Papakonstantinou, N. Paar, H. Hergert, T. Neff, and H. Feldmeier, Phys. Rev. C73, 044312 (2006).

[37] T. Myo, Y. Kikuchi, K. Kato, H. Toki and K. Ikeda, Prog. Theor. Phys. 119, 561 (2008); T. Myo, H. Toki and K. Ikeda, Prog. Theor. Phys. 121, 511 (2009); T. Myo, A. Umeya, H. Toki, and K. Ikeda Phys. Rev. C86, 024318 (2012).

[38] M. Bender, K. Bennaceur, T. Duguet, P.-H. Heenen, T. Lesinski, and J. Meyer, Phys. Rev. C80, 064302 (2009).

[39] V. Hellemans, P.-H. Heenen, and M. Bender, Phys. Rev. C85, 014326 (2012).

[40] E. Perlińska, S.G. Rohoziński1, J. Dobaczewski, and W. Nazarewicz, Phys. Rev. C69, 014316 (2004).

[41] J. Decharge and D. Gogny, Phys. Rev. C21, 1568 (1980).

[42] D. Gogny, Nucl. Phys. A237, 399 (1975).

[43] R. Blümel and K. Dietrich, Nucl. Phys. A471, 453 (1987).

[44] N. Onishi and J.W. Negele, Nucl. Phys. A301, 336 (1978).

[45] T. Otsuka, T. Matsuo, and D. Abe, Phys. Rev. Lett. 97, 162501 (2006).

[46] B.S. Pudliner *et al.*, Phys. Rev. C56, 1720 (1997).

[47] J.F. Berger, M. Girod, and D. Gogny, Nucl. Phys. A428, 23 (1984); Comput. Phys. Commun. 63, 365 (1991).

[48] F. Arias de Saavedra, C. Bisconti, G. Co', and A. Fabrocini, Phys. Rep. 450, 1 (2007).

[49] V. De Donno, G. Co', C. Maieron, M. Anguiano, A.M. Lallena, and M. Moreno Torres, Phys. Rev. C79, 044311 (2009).

[50] G. Co', private communication.

[51] H. Nakada, Phys. Rev. C68, 014316 (2003).

[52] H. Nakada, Phys. Rev. C78, 054301 (2008); C82, 029903(E).

[53] H. Nakada, K. Sugiura, and J. Margueron, Phys. Rev. C87, 067305 (2013).

[54] G.F. Bertsch, J. Borysowicz, H. McManus, and W.G. Love, Nucl. Phys. A284, 399 (1977).

[55] G. Colò, H. Sagawa, S. Fracasso, P.F. Bortignon, Phys. Lett. B646, 227 (2007) [erratum, Phys. Lett. B668 (2008) 457].

[56] J. Dobaczewski, in Proceedings of the Third ANL/MSU/JINA/INT RIA Workshop, edited by T. Duguet, H. Esbensen, K. M. Nollett, and C. D. Roberts (World Scientific, Singapore, 2006).

[57] D. Lunney, J.M. Peason, C. Thibault, Rev. Mod. Phys. 75, 1021 (2003),

[58] T. Lesinski, M. Bender, K. Bennaceur, T. Duguet, and J. Meyer, Phys. Rev. C76, 014312 (2007).

[59] G.A. Lalazissis, S. Karatzikos, M. Serra, T. Otsuka, and P. Ring, Phys. Rev. C80, 041301(R) (2009).

[60] S. Goriely, S. Hilaire, M. Girod, and S. Péru, Phys. Rev. Lett. 102, 242501 (2009).

[61] C.W. Wong, Nucl. Phys. A108, 481 (1968).

[62] R.R. Scheerbaum, Phys. Lett. B61, 151 (1976).

[63] R.R. Scheerbaum, Phys. Lett. B63, 381 (1976).

[64] A.L. Goodman and J. Borysowicz, Nucl. Phys. A295, 333 (1978).

[65] M. Beiner, H. Flocard, N. Van Giai, and Ph. Quentin, Nucl. Phys. A238, 29 (1975).

[66] B.A. Brown, T. Duguet, T. Otsuka, D. Abe, and T. Suzuki, Phys. Rev. C74, 061303 (2006).

[67] W. Zou, G. Colò, Z.Y. Ma, H. Sagawa and P.F. Bortignon, Phys. Rev. C77, 014314 (2008).

[68] T. Otsuka, R. Fujimoto, Y. Utsuno, B.A. Brown, M. Honma, and T. Mizusaki, Phys. Rev. Lett. 87, 082502 (2001).

[69] B. Fornal *et al.*, Phys. Rev. C70, 064304 (2004).

[70] D.-C. Dinca *et al.*, Phys. Rev. C71, 041302 (2005).

[71] B.A. Brown, Phys. Rev. C58, 220 (1998).

[72] A. Hosaka, K.I. Kubo, and H. Toki, Nucl. Phys. A444, 76 (1985).

[73] E. Chabanat, P. Bonche, P. Haensel, J. Meyer, and R. Schaeffer, Nucl. Phys. A627, 710 (1997).

[74] J.P. Schiffer *et al.*, Phys. Rev. Lett. 92, 162501 (2004).

[75] R.B. Firestone *et al.*, *Table of Isotopes. 8th edition* (John Wiley & Sons, New York, 1996).

[76] L. Gaudefroy *et al.*, Phys. Rev. Lett. 97, 092501 (2006).

[77] M. Grasso, Z.Y. Ma, E. Khan, J. Margueron, and N. Van Giai, Phys. Rev. C76, 044319 (2007).

[78] O. Sorlin and M.-G. Porquet, Prog. Part. Nucl. Phys. 61, 602 (2008).

[79] M. Anguiano *et al.* (to be published).

[80] D. Tarpanov, H. Liang, N. Van Giai, and Ch. Stoyanov, Phys. Rev, C77, 054316 (2008).

[81] M. Zalewski, J. Dobaczewski, W. Satula, and T.R. Werner, Phys. Rev. C77, 024316 (2008).

[82] J. Dobaczewski, H. Flocard, and J. Treiner, Nucl. Phys. A422, 103 (1984).

[83] P.-G. Reinhard, D.J. Dean, W. Nazarewicz, J. Dobaczewski, J.A. Maruhn, and M.R. Strayer, Phys. Rev. C60, 014316 (1999).

[84] R. Satchler, *Direct nuclear reactions* (Oxford University Press, Oxford, 1983).

[85] C. Mahaux, P. F. Bortignon, R. A. Broglia, C. H. Dasso, Phys. Rep. 120, 1 (1985).

[86] G. Colò, H. Sagawa, and P.F. Bortignon, Phys. Rev. C82, 064307 (2010).

[87] P.F. Bortignon, G. Colò, and H. Sagawa, J. Phys. G: Nucl. Part. Phys. 37 (2010) 064013.

[88] L. Cao *et al.* (to be published).

[89] J.K. Hwang, A.V. Ramayya, J.H. Hamilton, J.O. Rasmussen, Y.X. Luo, D. Fong, K. Li, C. Goodin, S.J. Zhu, S.C. Wu, M.A. Stoyer, R. Donangelo, X.-R. Zhu, and H. Sagawa, Phys. Rev. C 74, 017303 (2006); J.K. Hwang, A.V. Ramayya, J.H. Hamilton, Y.X. Luo, A.V. Daniel, G.M. Ter-Akopian, J.D. Cole, and S.J. Zhu, Phys. Rev. C 73, 044316 (2006); H. Mach, M. Moszyǹski, R.L. Gill, G. Molnár, F.K. Wohn, J.A. Winger, and J.C. Hill, Phys. Rev. C41, 350 (1990).

[90] A. Li, X.R. Zhou, and H. Sagawa, Prog. Theor. Exp. Phys., 063D03 (2013).

[91] T.R. Werner *et al.*, Nucl. Phys. A597, 327 (1996).

[92] R.W. Ibbotson *et al.*, Phys. Rev. Lett. 80, 2081 (1998).

[93] D. Vautherin, Phys. Rev. C7, 296 (1973).

[94] H. Sagawa, X.R. Zhou, X.Z. Zhang, and T. Suzuki, Phys. Rev. C70, 054316 (2004).

[95] X.R. Zhou, H.-J. Schulze, H. Sagawa, C.X. Wu, and E.G. Zhao, Phys. Rev. C76, 034312 (2007).

[96] Ang Li, X.-R. Zhou, H. Sagawa, Prog. Theor. Exp. Phys. 063D03 (2013).

[97] Z.P. Li, J.M. Yao, D. Vretenar, T. Nikšić, H. Chen, and J. Meng, Phys. Rev. C84, 054304 (2011).

[98] E.B. Suckling and P.D. Stevenson, Eur. Phys. Lett. 90, 12001 (2010).

[99] X.R. Zhou and H. Sagawa, J. Phys. G39, 085104 (2012).

[100] D. Davesne, M. Martini, K. Bennaceur, and J. Meyer, Phys. Rev. C80, 024314 (2011) [Erratum-*ibid.* C84, 059904 (2011)]

[101] L. G. Cao, G. Colò, H. Sagawa, P.F. Bortignon, and L. Sciacchitano, Phys. Rev. C80 (2009) 064304.

[102] G. Colò, L. G. Cao, N. Van Giai, L. Capelli, Comp. Phys. Comm. 184, 142 (2013).

[103] L. G. Cao, H. Sagawa, and G. Colò, Phys. Rev. C83, 034324 (2011).

[104] N. Van Giai and H. Sagawa, Phys. Lett. B106, 379 (1981).

[105] J. Blomqvist and A. Molinari, Nucl. Phys. A106, 545 (1968).

[106] D.C. Zheng and L. Zamick, Ann. Phys. (N.Y.) 206, 106 (1991).

[107] J.P. Blaizot, D. Gogny, Nucl. Phys. A284, 429 (1977).

[108] P. Vesely, J. Kvasil, V.O. Nesterenko, W. Kleinig, P.-G. Reinhard, and V.Yu. Ponomarev, Phys. Rev. C80, 031302(R) (2009).

[109] X. Roca-Maza, G. Colò, and H. Sagawa, Phys. Rev. C86, 031306 (2012).

[110] M. Anguiano, G. Co', V. De Donno, and A.M. Lallena, Phys. Rev. C83, 064306 (2011).

[111] M. Anguiano, M. Grasso, G. Co', V. De Donno, and A.M. Lallena, Phys. Rev. C86, 054302 (2012).

[112] For general arguments on HFB and cranking model, see: P. Ring and P. Schuck, *The nuclear many-body problem* (Springer-Verlag, New York-Berlin, 1980)

[113] R.V.F. Janssens and T.L. Khoo, Annu. Rev. Nucl. Part. Sci. 41, 321 (1991); R. Wadsworth and P.J. Nolan, Rep. Prog. Phys. 65, 1079 (2002).

[114] V. Hellemans, private communication.

[115] C.L. Bai *et al.*, Phys. Lett. B675, 28 (2009).

[116] C.L. Bai *et al.*, Phys. Rev. Lett. 105, 072501 (2010).

[117] C.L. Bai, H.Q. Zhang, H. Sagawa, X.Z. Zhang, G. Colò, and F.R. Xu, Phys. Rev. C83, 054316 (2011).

[118] C.L. Bai, H.Q. Zhang, X.Z. Zhang, F.R. Xu, H. Sagawa, and G. Colò, Phys. Rev. C79 (2009) 041301(R).

[119] C.L. Bai, H. Sagawa, G. Colò, H.Q. Zhang, X.Z. Zhang, Phys. Rev. C84, 044329 (2011).

[120] J. Rapaport *et al.*, Nucl. Phys. A410, 371 (1983); C. Gaarde, in *Proceedings of the Niels Bohr Centennial Conference on Nuclear Structure* (North-Holland, Amsterdam, 1985), p. 449c.

[121] G.F. Bertsch and I. Hamamoto, Phys. Rev. C26, 1323 (1982).

[122] S. Fracasso and G. Colò, Phys. Rev. C76, 044307 (2007).

[123] T. Wakasa, arXiv:1004.5220[nucl-ex]; T. Wakasa *et al.*, Phys. Rev. C85, 064606 (2012).

[124] L. G. Cao, G. Colò and H. Sagawa, Phys. Rev. C81, 044302 (2010).

[125] H. Sagawa and B.A. Brown, Phys. Lett. 143B, 283 (1984); H. Sagawa and B. Castel, Nucl. Phys. A435, 1 (1985).

[126] F. Minato and C.L. Bai, Phys. Rev. Lett. 110, 122501 (2013).

[127] J. Engel, M. Bender, J. Dobaczewski, W. Nazarewicz, and R. Surman, Phys. Rev. C 60, 014302 (1999).

[128] A.B. Migdal, *Theory of Finite Fermi Systems and Applications to Atomic Nuclei* (Interscience, London, 1967).

[129] J. Dabrowski and P. Haensel, Ann. Phys. 97, 452 (1976).

[130] S.-O. Bäckman, O. Sjöberg and A.D. Jackson, Nucl. Phys. A321, 10 (1979).

[131] E. Olsson, P. Haensel and C.J. Pethick, Phys. Rev. C70, 025804 (2004).

[132] T. Lesinski, K. Bennaceur, T. Duguet, and J. Meyer, Phys. Rev. C74, 044315 (2006).

[133] C. Garcia-Recio, J. Mavarro, N. Van Giai, and L.L. Salcedo, Ann. Phys. (N.Y.) 214, 293 (1992).

[134] J. Margueron, J. Navarro, and N. Van Giai, Phys. Rev. C74, 015805 (2006).

[135] A. Pastore, D. Davesne, Y. Lallouet, M. Martini, K. Bennaceur, and J. Meyer, Phys. Rev. C85, 054317 (2012).

[136] A. Pastore, private communication.

[137] A. Pastore, M. Martini, V. Buridon, D. Davesne, K. Bennaceur, and J. Meyer, Phys. Rev. C86, 044308 (2012).

[138] W. L. Long, private communications.